

# **Probing the binding mechanism of a solid-binding peptide**

by

**Rachit Bansal**

A thesis submitted in fulfilment of the requirements for the degree of  
**Doctor of Philosophy**

Supervisors:

A/Prof. Anwar Sunna

Dr. Andrew Care



**MACQUARIE**  
University

Department of Molecular Sciences

Macquarie University

Sydney, Australia

December 2019

# Table of contents

<b>Abstract .....</b>	<b>iii</b>
<b>Statement of originality .....</b>	<b>v</b>
<b>Acknowledgements .....</b>	<b>vi</b>
<b>Presentations and awards .....</b>	<b>ix</b>
<b>Poster presentations.....</b>	<b>ix</b>
<b>Oral presentations.....</b>	<b>ix</b>
<b>Awards .....</b>	<b>ix</b>
<b>List of publications .....</b>	<b>x</b>
<b>List of abbreviations.....</b>	<b>xi</b>
<b>Chapter 1</b>	
Experimental and theoretical tools to elucidate the binding mechanisms of solid-binding peptides .....	14
<b>1.1 Introduction.....</b>	<b>15</b>
<b>1.2 Manuscript 1.....</b>	<b>16</b>
<b>1.3 Aims and scope of this thesis .....</b>	<b>26</b>
<b>Chapter 2</b>	
Elucidating the binding mechanism of a novel silica-binding peptide.....	28
<b>2.1 Introduction .....</b>	<b>29</b>
<b>2.2 Contribution to manuscript 2.....</b>	<b>30</b>
<b>2.3 Manuscript 2.....</b>	<b>31</b>
<b>Chapter 3</b>	
Effect of solid-binding peptide multimerization on its binding to silica-based materials.....	51
<b>3.1 Introduction .....</b>	<b>52</b>
<b>3.2 Contribution to manuscript 3.....</b>	<b>53</b>
<b>3.3 Manuscript 3.....</b>	<b>54</b>
<b>Chapter 4</b>	
Solid-binding peptide-based biosensor for efficient detection of HER2.....	82
<b>Chapter 5</b>	
Summary and future perspectives.....	94
<b>Appendix Biosafety Approvals .....</b>	<b>101</b>

# Abstract

The interactions between biomolecules and solid surfaces play an important role in designing new materials and applications which mimic nature. Recently, solid-binding peptides (SBPs) have emerged as potential molecular building blocks in nanobiotechnology. SBPs are short amino acid sequences (7-12 amino acids) that have the distinctive ability to recognize and bind to the surfaces of specific solid materials, such as metals and metal oxides, semiconductors, carbon-based materials, and polymers. These peptides act as ‘molecular linkers’ that mediate the simple and controlled attachment of biomolecules onto solid surfaces to confer biological functionality. SBP-solid interactions rely primarily on the peptide adopting structural conformations that maximize the contact between the reactive side chains of its amino acid residues and the solid surface. However, due to the high level of complexity of the SBP-solid interface within the surrounding solution, the exact mechanism that determines the SBP recognition, selectivity, and strong binding affinity remain ill-defined.

We have engineered a bifunctional fusion protein composed of a solid-binding peptide (referred to as the ‘linker’), which is a tetra-repeat of 21 amino acid sequence with unique binding affinity to silica-based materials, and a Streptococcus protein G, which binds antibodies. Linker protein G (LPG) acts as an anchor for the rapid and oriented immobilization of antibodies onto silica surfaces without using any complex conjugation chemistry. Although we have used this linker technology in biotechnology and biomedicine applications, there is still a lack of knowledge and understanding about the interaction mechanism which facilitates the binding of this SBP to the surface of silica.

In this work, different biophysical characterization techniques, namely quartz crystal microbalance for dissipation monitoring (QCM-D), surface plasmon resonance (SPR), circular dichroism spectrometry (CD) and fluorescence spectrometry, were used to study the binding of LPG to silica surfaces and compared to protein G (PG) without the linker. LPG displayed high binding affinity to silica surface ( $K_D=34.77\pm11.8$  nM) with a standing-up orientation in comparison to parent PG, which exhibited no measurable binding affinity. Incorporation of the linker in the fusion protein LPG had no effect on the antibody binding function of PG, which retained its secondary structure and displayed no alteration of its chemical stability.

We also engineered several truncated derivatives (1xLPG, 2xLPG, 3xLPG) from LPG to determine the effect of SBP multimerization on the silica binding function of LPG.

The quantitative binding analysis for the different truncated derivatives were compared to that of LPG and PG (without linker) using various biophysical characterization techniques. Out of these truncated derivatives, 1xLPG (single linker sequence) displayed no binding to silica surface while the 2xLPG (two linker sequences) displayed minimal binding. Although the three-repeat derivative (3xLPG) binds to silica with a binding affinity ( $K_D$ ) of  $53.23 \pm 4.5$  nM, it was 1.5 times lower than that of the four-repeat sequence (LPG). Spectroscopic techniques like circular dichroism (CD) spectroscopy and fluorescence spectroscopy studies indicated that the SBP degree of multimerization has no effect on the secondary structure and chemical stability of the parent protein G. However, the data from quartz crystal microbalance with dissipation monitoring (QCM-D) showed that multimerization was an important parameter for a strong and stable silica binding. The effect of peptide length on silica binding was evaluated by replacing the 3 sequence repeats by a (GGGGS)<sub>12</sub> glycine-rich spacer. The results indicated that the overall length rather than the SBP multimerization mediated the effective binding to silica.

A preliminary investigation was performed to assess the linker-protein G (LPG) as a suitable system for potential use in nanomedicine applications. We took advantage of the ability of the LPG bifunctional fusion protein to bind in an end-on-end orientation on the silica surface. The sensitive, selective and efficient detection of the HER2 biomarker was also investigated in the presence of biological fluids. This preliminary work showed that LPG mediates the functionalization of silica-coated nanoparticles with the anti-HER2 antibody trastuzumab easily and under mild conditions. The system was able to detect the HER2 biomarker in the presence of biological fluids demonstrating its potential suitability in nanomedicine applications e.g., nanoparticle-based drug delivery systems and efficient detection of disease biomarkers.

This work provides the first insights into the binding mechanism of the aforementioned silica binding SBP. It also highlights the advantage of the LPG as a milder, facile and faster affinity immobilization technique of biomolecules to inorganic surfaces compared to traditional chemical coupling techniques.



# Statement of originality

This submission is the result of my own work and to the best of my knowledge includes nothing which is previously published or written by another individual, or substantial proportions of work which have been accepted for the award of any other degree or diploma at Macquarie University or any other educational institution, except for where due acknowledgement is made in the thesis. Any contribution made to the research by others, with whom I have worked at Macquarie University or elsewhere, has been explicitly acknowledged in the thesis. I also declare that the intellectual content of this thesis is the product of my own work, except to the extent that assistance from others in the project's design and conception or in style, presentation and linguistic expression is acknowledged.

Rachit Bansal

December 2019

# Acknowledgements

This thesis comprises three years of full-time research conducted in the Department of Molecular Sciences at Macquarie University from November 2016 to December 2019.

Although writing up a thesis might be the effort of one person, but the research conducted in this thesis would have taken far longer to complete without the encouragement from many others. It is a delight to acknowledge all those who have supported me over the course of these three years of my PhD.

First of all, I would like to thank my supervisors A/Prof. Anwar Sunna and Dr. Andrew Care for the immense support during my time as a PhD candidate.

Anwar, I express my deepest gratitude to you for accepting me as a PhD student and motivating me all through this time. I highly appreciate your great commitment and enthusiasm for the project and honour your style of guidance in creating space for creativity and self-development. I highly value your patience in reading and correcting my work as well as bearing my childish behaviour (sometimes!!!). Knowing the fact that I did not have a background in biology, you always supported me by pushing me towards new experiences, the outcome of which now everyone knows in the form of this successfully completed PhD thesis. I hope after all this time, I am able to match your high level of standards and expectations.

Andrew, I am very grateful for your invaluable scientific advice in many research questions, whether it is experimental designing, biochemistry, or experimental approach. I appreciate your critical feedback on my project as well as my poster and oral presentations and improving my English writing skills. My thesis would not have gotten this far without your help. Thank you for always putting up a positive and pro-active attitude and teaching me very valuable lessons scientifically and personally. I will never forget your words – “QUALITY comes before QUANTITY” ...

I would like to thank A/Prof. Megan Lord from University of New South Wales (UNSW) for allowing me to work in her lab and helping me out in my experimental designing, data

analysis and writing. I also thank her research staff and students, especially Ha Na and Lu for helping me out whenever in need and made me feel comfortable.

I sincerely thank Dr. Zehra Elgundi from University of New South Wales (UNSW) for her endless support and guidance which made it possible for this project to reach its destination. Although being from other university, she always made me feel acceptable and helped me to put a smile back on my face whenever I went through a rough patch. She taught me everything from scratch and was readily available for my help despite having works of her own. Her knowledge and expertise of her field of research, her enthusiastic approach to problems, keen and skillful observation and interpretation of data, dedication towards her work and her students, ability of multitasking, and extraordinary level of patience inspired me to work hard and broaden my perspective towards life.

I also want to thank Professor Alison Rodger for allowing me to work in her lab and giving valuable input for my data analysis. Special thanks to Dr. Sophie Goodchild for helping me out in spectroscopy analysis and giving her time for my data analysis and also valuable feedback and corrections in my manuscripts.

I also acknowledge the international Macquarie University Research Excellence Scholarship (iMQRES) and Centre for Nanoscale Biophotonics (CNBP) for financially supporting me over the course of this project.

Special thanks to Kalpesh, Sarita, Minakshi, Pankaj, Kabir, Rashmi, Sujish, Shreyash and Adéla for their massive support, inspiring conversations, countless discussions, strong commitment, great food and most importantly being my family away from home. I am grateful to have you all in my life.

Thanks to all amazing peers in the lab/office and your great company, Dennis, Kaitlin, Sandra, India, Kerstin, Vinoth, Dominik, Manuel and Alex. Thanks also to Rashika, Monica, Heinrich, Briardo, Atul, Ehsaan, Irene, Shalini, Karthik, Shivani, Liisa, Ravi, Elsa, Elizabeth, Lynda, Sameera, Wisam, and all other people that I have worked and become friends with over the three years for your support and encouragement.

I also want to thank the people in my personal life. Great thanks go to my friend Ashish,

Swapnil, Bhomik, Prakhar, Gautam, Rati, Shweta, Jagrity, Raunak, Rajat and Animesh for their never-ending support and encouragement to pursue this career.

Finally, my greatest thanks and love goes to my family, who has always been there for me and supported me in every way they possibly could.

# Presentations and awards

## Poster presentations

**Bansal, R.,** Care, A., Elgundi, Z., Lord, M.S., Sunna, A. (2018). Chemical-free bioconjugation of antibodies onto silica surfaces using a novel fusion protein. Poster presented at the 9<sup>th</sup> International Nanomedicine Conference, Sydney, Australia.

**Bansal, R.,** Care, A., Elgundi, Z., Lord, M.S., Sunna, A. (2018). Probing the silica-binding mechanisms of a novel fusion protein. Poster presented at the Bionetwork Symposium, Sydney, Australia.

**Bansal, R.,** Care, A., Elgundi, Z., Lord, M.S., Sunna, A. (2018). Chemical-free bioconjugation of antibodies onto silica surfaces. Poster presented at the 5<sup>th</sup> CNBP Annual Conference, Lorne, Australia.

## Oral presentations

**Bansal, R.,** Care, A., Elgundi, Z., Lord, M.S., Sunna, A. (2018). Using SPR to study the effect of a solid-binding peptide on a fusion protein. Oral presentation at Sydney Surfaces and Soft Stuff meeting (Sassy) Symposium, Sydney, Australia.

## Awards

**2016 Three-year international Macquarie University Research Excellence Scholarship, (iMQRES).** Approx. value: 200,000 AUD.

# List of publications

This thesis include three manuscripts for publication (Chapter 1, 2 and 3).

- 1) **Bansal, R.**, Care, A., Lord, M.S., Walsh, T.R., Sunna, A. (2019). Experimental and theoretical tools to elucidate the binding mechanisms of solid-binding peptides. Invited review article published in *New Biotechnology*, 52:9-18.
- 2) **Bansal, R.**, Elgundi, Z., Care, A., Goodchild, S.C., Lord, M.S., Rodger, A., Sunna, A. (2019). Elucidating the binding mechanism of a novel silica-binding peptide. *Biomolecules*,10:4.
- 3) **Bansal, R.**, Elgundi, Z., Goodchild, S.C., Care, A., Lord, M.S., Rodger, A., Sunna, A. (2019). Effect of solid-binding peptide multimerization on its binding to silica-based materials. Prepared for submission to *ACS Biomacromolecules*.

# List of abbreviations

APTES	3-aminopropyl-triethoxysilane
ABP	aluminium-binding peptide
AFM	atomic force microscopy
BSA	bovine serum albumin
CI	confidence interval
CD	circular dichroism
CPMAS	cross polarized magic angle spinning
D.I.T	digital integration time
DFT	density functional theory
DMEM	Dulbecco's modified eagle medium
$\Delta D$	dissipation change
EDC	1-ethyl-3-(3-dimethylaminopropyl)carbodiimide
ELISA	enzyme linked immunosorbent assay
EDTA	ethylenediaminetetraacetic acid
FTIR	Fourier-transform infrared spectroscopy
FBS	fetal bovine serum
FF	force-fields
$\Delta f$	frequency shift
GrBP	graphene-binding peptide
GFET	graphene field effect transistor
GA	glutaraldehyde
GrSP	graphene specific peptide
GCE	glass carbon electrode
GBP	gold-binding peptide
GRAVY	grand average of hydropathy
GdnHCl	guanidinium hydrochloride
HER2	human epidermal growth factor receptor 2
HBS	HEPES-buffered saline
HOPG	highly oriented pyrolytic graphite
HEPES	4-(2-hydroxyethyl)-1-piperazineethanesulfonic acid

ITC	isothermal titration calorimetry
IgG	immunoglobulin G
$k_a$	association rate constant
$k_d$	dissociation rate constant
$K_D$	binding affinity/equilibrium dissociation constant
LPG	linker-protein G
LOD	limit of detection
LOQ	limit of quantification
MES	2-(N-morpholino) ethanesulfonic acid
MM	molecular mechanics
MetaD	metadynamics
MD	molecular dynamics
NHS	N-hydroxysuccinimide
NaCl	sodium chloride
NMR	nuclear magnetic resonance
NOESY	nuclear Overhauser effect spectroscopy
pI	isoelectric point
PG	protein G
PAH	polycyclic aromatic hydrocarbon
PPV	poly(phenylene vinylene)
PBS	phosphate-buffered saline
PEI	polyetherimide
PtNP	platinum nanoparticles
PLLA	poly (L-lactide)
QCM-D	quartz crystal microbalance with dissipation monitoring
QM	quantum mechanical
REST	replica exchange with solute tempering
RGO	reduced graphene oxide
RU	response unit
SBP	solid-binding peptide
SDS-PAGE	sodium dodecyl sulfate-polyacrylamide gel electrophoresis
SA	streptavidin
SPR	surface plasmon resonance
TOCSY	total correlation spectroscopy



TFE	2,2,2-trifluoroethanol
TBP	titanium-binding peptide
$t_{1/2}$	half-life
$[\theta_M]$	mean residual ellipticity
$\chi^2$	chi-square (measure of fitting reliability)
ZBP	zinc oxide-binding peptide

# **Chapter 1**

Experimental and theoretical  
tools to elucidate the binding  
mechanisms of solid-binding  
peptides

## 1.1 Introduction

The self-assembly, binding and molecular recognition of biomolecules to solid surfaces plays an important role in molecular biomimetics. Traditionally, these biomolecules are chemically conjugated to inorganic surfaces by creating various self-assembled monolayers (SAMs) linkages on the solid surfaces, the most common being thiol or silane chemistry. However, one of the major drawback of this approach is that SAMs are highly complex and require harsh chemical reagents such as organic solvents and high temperatures, which may reduce the stability of biomolecules and the biocompatibility of the nanomaterial surfaces. An interesting alternative to this approach is the use of combinatorially selected peptides, known as solid-binding peptides (SBPs), as molecular linker and assemblers. SBPs are short amino acid sequences that specially bind to the surfaces of various solid materials. In doing so, they mediate the simple and controlled attachment of biomolecules onto solid surfaces, conferring biological functionality or as material synthesizers in binding, erecting and linking of solid nanostructures. Although many of these SBPs have been demonstrated for their potential use in the fields of biotechnology and biomedicine, there is still a lack of knowledge and understanding about the interaction mechanism that governs the binding of these peptides to inorganic surfaces.

In the following review, various experimental (biophysical characterization techniques) and theoretical (algorithm-based approach, like computer modelling and simulation) tools are described, which can be used individually or in combination to characterize and study these SBP-surface interactions, and how these approaches will further contribute to rationally design new peptides for tailored binding.

This chapter was an invited review article and has already been published in the peer-review journal *New Biotechnology*.

## 1.2 Manuscript 1

New BIOTECHNOLOGY 52 (2019) 9–18



Contents lists available at ScienceDirect

New BIOTECHNOLOGY

journal homepage: [www.elsevier.com/locate/nbt](http://www.elsevier.com/locate/nbt)

## Review Article

## Experimental and theoretical tools to elucidate the binding mechanisms of solid-binding peptides

Rachit Bansal<sup>a,b</sup>, Andrew Care<sup>a,b</sup>, Megan S. Lord<sup>c</sup>, Tiffany R. Walsh<sup>d</sup>, Anwar Sunna<sup>a,b,e,\*</sup><sup>a</sup> Department of Molecular Sciences, Macquarie University, Sydney, NSW 2109, Australia<sup>b</sup> ARC Centre of Excellence for Nanoscale Biophotonics, Macquarie University, Sydney, NSW 2109, Australia<sup>c</sup> Graduate School of Biomedical Engineering, University of New South Wales, Sydney, NSW 2052, Australia<sup>d</sup> Institute for Frontier Materials, Deakin University, Geelong, Victoria 3216, Australia<sup>e</sup> Biomolecular Discovery and Design Research Centre, Macquarie University, Sydney, NSW 2109, Australia

## ARTICLE INFO

## Keywords:

Solid-binding peptides

Binding affinity

Binding mechanisms

Molecular modelling

Biosensors

## ABSTRACT

The interactions between biomolecules and solid surfaces play an important role in designing new materials and applications which mimic nature. Recently, solid-binding peptides (SBPs) have emerged as potential molecular building blocks in nanobiotechnology. SBPs exhibit high selectivity and binding affinity towards a wide range of inorganic and organic materials. Although these peptides have been widely used in various applications, there is a need to understand the interaction mechanism between the peptide and its material substrate, which is challenging both experimentally and theoretically. This review describes the main characterisation techniques currently available to study SBP-surface interactions and their contribution to gain a better insight for designing new peptides for tailored binding.

## Introduction

Solid-binding peptides (SBPs) are short amino acid sequences (7–12 amino acids) that have the distinctive ability to recognise and bind to the surfaces of specific solid materials, such as metals and metal oxides, semiconductors, carbon-based materials and polymers [1–3]. These peptides have been shown to act as ‘molecular linkers’ that mediate the simple and controlled attachment of biomolecules onto solid surfaces to confer biological functionality [4] or as ‘material synthesisers’ that activate and modulate the synthesis of materials, e.g. metal-based nanoparticles [5]. As a result, SBPs have been extensively developed for a diverse range of applications in the areas of biotechnology (e.g. bio-sensing, biocatalysis and bioremediation) and biomedicine (e.g. drug delivery, vaccine development and biomedical implants) [6].

In general, SBPs bind to solid surfaces via a combination of non-covalent interactions (e.g. electrostatic, van der Waals, hydrophobic,

dipole-dipole and hydrogen bonding), which together result in strong binding constants ( $K_T$ ) in the nM to sub- $\mu$ M range [6]. SBP-solid interactions rely primarily on the peptide adopting structural conformations that maximise the contact between the reactive side chains of its amino acid residues and the solid surface [6,7]. However, due to the high level of complexity of the SBP-solid interface within the surrounding solution, the exact mechanisms that determine SBP recognition, selectivity and strong binding affinity remain ill-defined [5].

For accurate characterisation of an SBP's binding mechanism, a number of properties must be carefully considered and potentially investigated: (i) the SBP and its composition, sequence, structural conformation and charge; (ii) the solid surface and its chemistry, charge, and architecture (e.g. size and topography); (iii) the surrounding solution (e.g. water and solvent) and its condition (e.g. pH and ionic strength); and (iv) the molecular dynamics of the peptide-solid interface, where SBPs exhibit a constant state of motion, in which they

**Abbreviations:** SBP, solid-binding peptide; SPR, surface plasmon resonance; PAH, polycyclic aromatic hydrocarbon; PPV, poly(phenylene vinylene); PEI, poly-etherimide; SA, streptavidin; QCM-D, quartz crystal microbalance with dissipation monitoring; ITC, isothermal titration calorimetry; ZBP, zinc oxide-binding peptide; AFM, atomic force microscopy; GrBP, graphene-binding peptide; HOPG, highly oriented pyrolytic graphite; CD, circular dichroism; GBP, gold-binding peptide; TFE, 2,2,2-trifluoroethanol; NMR, nuclear magnetic resonance; TBP, titanium-binding peptide; NOESY, nuclear overhauser effect spectroscopy; TOCSY, total correlation spectroscopy; CPMAS, cross polarized magic angle spinning; FTIR, Fourier-transform infrared spectroscopy; ABP, aluminium-binding peptide; QM, quantum mechanical; MM, molecular mechanics; FF, force-fields; REST, replica exchange with solute tempering; MetaD, metadynamics; MD, molecular dynamics; DFT, density functional theory; GFET, graphene field effect transistor; GrSP, graphene specific peptide; RGO, reduced graphene oxide; PtNP, platinum nanoparticles; GCE, glass carbon electrode

\*Corresponding author at: Department of Molecular Sciences, Macquarie University, North Ryde, NSW 2109, Australia.

E-mail address: [anwar.sunna@mq.edu.au](mailto:anwar.sunna@mq.edu.au) (A. Sunna).

<https://doi.org/10.1016/j.nbt.2019.04.001>

Available online 05 April 2019

1871-6784/ © 2019 Elsevier B.V. All rights reserved.

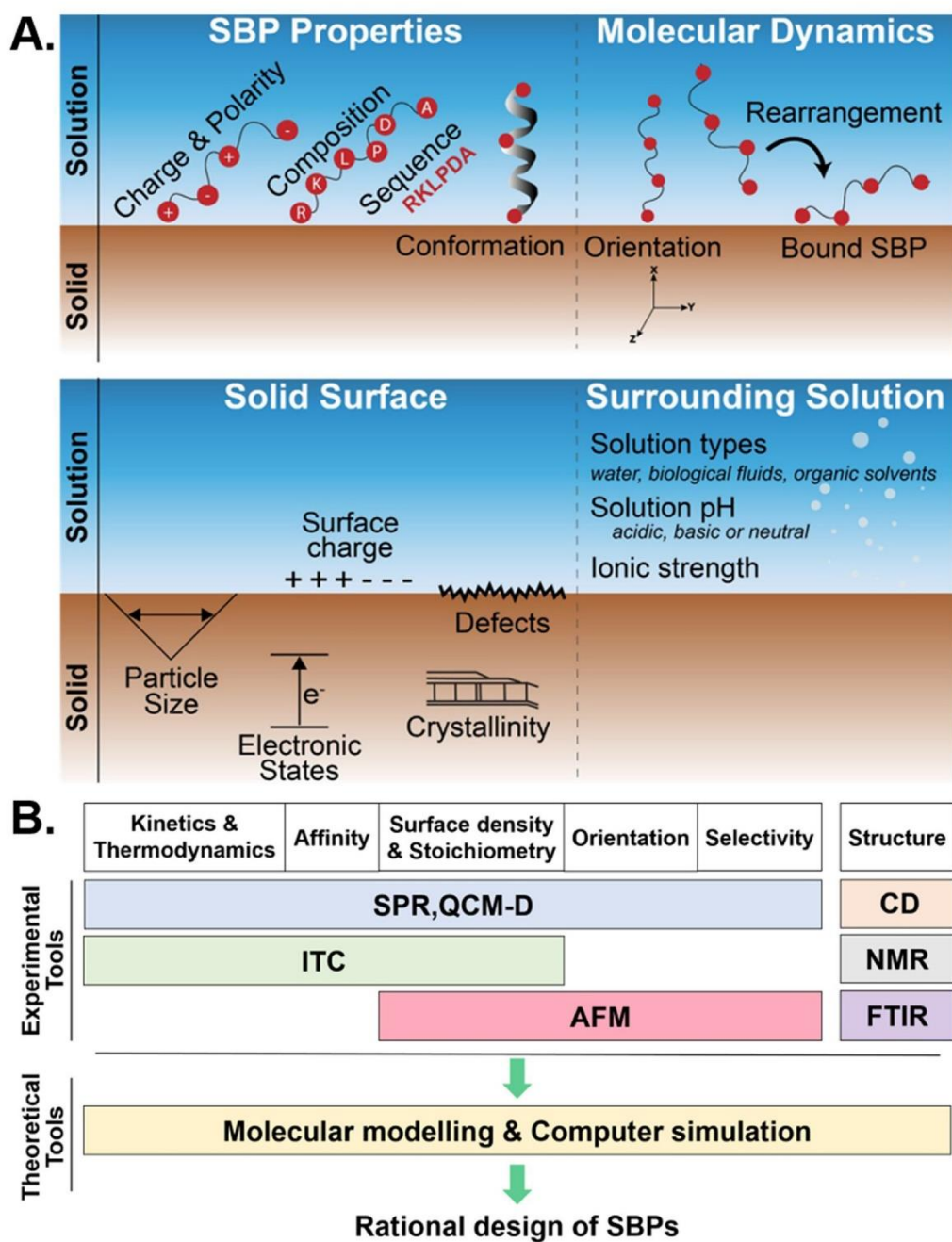


**Fig. 1.** Top panel, (A) Various parameters affecting SBP-solid interactions. These include physical and chemical properties of SBPs, their molecular dynamics, surface morphology and the effect of surrounding environment. Middle panel, (B) Experimental and theoretical tools available for efficient characterisation of SBPs binding mechanisms to rationally design SBPs for enhanced functionality.

diffuse, reorient and adopt their lowest-energy conformations [5,8] (Fig. 1A).

A suite of experimental and theoretical tools is currently available for the in-depth analysis of biophysical interactions. In this review, we address how these tools, including real-time label-free detection (e.g. surface plasmon resonance) and computational modelling and simulations, can be used individually and in combination to characterise and/or predict SBP-solid interactions (Fig. 1B). We also highlight the functional application of SBPs in the construction of biosensing devices for the sensitive detection of pathogenic bacteria and other relevant analytes. Lastly, we comment on how continuing efforts to understand the fundamental mechanisms that drive SBP binding will lead to the rational/tailored design of functional SBPs, expediting their development and practical application.

### Experimental techniques to characterise SBP-solid interactions

The isolation of solid-binding peptides (SBPs) is usually performed using combinatorial display techniques such as phage display and surface display (cell, bacterial, yeast, mRNA) [9,10]. Although screening techniques are the best source to identify high-affinity SBPs, they yield no information on their binding mechanism. Several biophysical characterisation techniques are currently available to study the binding mechanism of SBPs. They are summarised in Table 1 and are described in more detail below.

### Surface plasmon resonance (SPR)

SPR is an optical technique that allows the real-time, label-free analysis of biomolecular interactions at the solid-liquid interface by monitoring the adsorption and desorption kinetics [11]. This technique is regularly used to monitor the binding affinity and selectivity of SBPs towards solid substrates.

Gold is the most widely studied surface for understanding the adsorption characteristics of SBPs. Accordingly, SPR has been used to measure the kinetics and thermodynamics of SBP-gold surface interactions. For example, it was found that the adsorption of a three-repeat gold-binding peptide (MHGKTQATSGTIQS)<sub>3</sub> (3R-GBP1) on the surface of gold was the result of both a fast and a slow adsorption owing to structural irregularities of the gold surface [12]. Although the association rate of the fast binding ( $k_a = 1.01 \times 10^4 \text{ M}^{-1}\text{s}^{-1}$ ) was about 20 times higher than the slow binding ( $k_a = 5.87 \times 10^2 \text{ M}^{-1}\text{s}^{-1}$ ), the peptide dissociated at nearly similar rates ( $k_d = 10^{-3} \text{ s}^{-1}$ ) and resulted in equilibrium association constants ( $K_A$ ) of  $2.54 \times 10^6 \text{ M}^{-1}$  and  $4.51 \times 10^5 \text{ M}^{-1}$ , respectively. The standard Gibbs free energy of adsorption ( $\Delta G_{\text{ads}}$ ) for the two binding processes was calculated to be  $-36.80 \text{ kJ/mol}$  and  $-32.48 \text{ kJ/mol}$ , respectively, suggesting a strong and exothermic binding.

Many SBPs are highly selective and capable of discriminating between the surfaces of similar solid materials. Selectivity of an SBP towards different solid materials, including those with analogous

**Table 1**  
Comparison of different biophysical characterisation techniques to understand SBP-solid interactions.

Experimental Tools for SBPs characterisation					SBPs characterised <sup>a</sup>			Ref.
Technique	Property characterised	Mode of operation	Advantage	Disadvantage	Name	Sequence	Target Solid	
SPR	Kinetics; affinity; specificity; thermodynamics; stoichiometry; surface density	Shifting of plasmon resonance	Real-time, label-free, less sample volume, high sensitivity	Gold is the only preferred sensor surface, mass transfer limitation	Nap01 3R-GBP1 LBP <sup>b</sup> p1-B	HFTFPQQQPPRP (MHGKTQATSGTIQS) <sub>3</sub> HFPSPIFQRHSH TGADLNT	Naphthalene Gold Lignin Polyetherimide (PEI)	[12,13,15,16]
QCM-D	Kinetics; affinity; viscoelasticity; mass; specificity; surface density	Mass deposited	Real-time, label-free, high sensitivity, choice of different sensor surfaces, viscoelasticity measurement	Not possible to determine the absolute value of a molecule's mass	MoS2-P15 MoS2-P28 HA	GVIHRNDQWTPAGGG DRWVARDPASIFGGG SVSVGMKPSRP	Molybdenite Hydroxyapatite	[23–25]
ITC	Affinity; Thermodynamics; stoichiometry	Heat gradient	Flexibility of using nanoparticles	Large sample amount, buffer limitations, unable to model multiple binding sites	G-12 1xZBP 3xZBP	GLHVMHKVAPRP RPHRKGGA 3x RPHRKGGA	ZnO microparticles ZnO nanoparticles	[31,40]
AFM	Orientation; surface coverage; binding force; surface density	Force	High sensitivity and resolution	Difficult experimental design, risk of sample damage, prone to mechanical stress	GrBP Amphipathic peptide	AGSWLRDIWTWLQSAL AGSWLRDIWTWLQSAL	Graphene Hydrophilic Surfaces	[35,36]
CD	Structure	Vibrational frequencies	Fast data collection and analysis, small sample amount	Samples should be highly pure and does not form aggregates	Nap01 1-GBP1 3I-GBP1	HFTFPQQQPPRP MHGKTQATSGTIQS (MHGKTQATSGTIQS) <sub>3</sub>	Naphthalene Gold	[13,40]
NMR	Structure and dynamics	Chemical shift	Direct structural analysis, can analyse non-crystalline peptides	Large amount of samples if they are not labelled isotopically	TBP Pif80-11 Pif80-22	RKLPGA DDRKDDRKGKK (DDRKDDRKGKK) <sub>2</sub>	TiO <sub>2</sub> /SiO <sub>2</sub> Aragonite	[46–48]
FTIR	Structure and conformation	Vibrational frequencies	Quick spectra generation, sample turbidity does not cause light scattering, solvent flexibility	Unable to characterise in complex media	ABP EM-12	VPSSGQDTRIT EAHVMHKVAPRP	Aluminium ZnO	[51,52]

<sup>a</sup> Selected SBPs mentioned in this review.

<sup>b</sup> LBP; Lignin-binding peptide.



structures and chemistries, can be investigated by altering the SPR sensing surface. For example, the selectivity of a naphthalene-binding peptide HFTFPQQPPRP (Nap01) was investigated by comparing its binding affinity to SPR surfaces modified with different polycyclic aromatic hydrocarbons (PAHs) [13]. Nap01 exhibited strong binding to naphthalene, but significantly weaker binding to smaller (benzene) and larger (pyrene and anthracene) PAHs, despite all of them containing highly similar benzene-ring structures and identical functional groups. Similarly, SPR was used to quantify the binding of two poly(phenylene vinylene) (PPV)-binding peptides, Lin01 (ELWSIDTSAHRK) and Hyp01 (HTDWRLGTWHHS), towards PPV substrates with linear or hyper-branched structures [14]. Lin01 showed a 2.1-fold higher binding affinity to linear PPV than the hyper-branched form. In contrast, Hyp01 displayed reverse selectivity for hyper-branched PPV with a 15-fold higher binding affinity for it than towards the linear form.

SBP binding is primarily dependent upon amino acid composition and sequence. To analyse how each amino acid residue contributes to the binding affinity of an SBP, single-residue-substituted mutants (e.g. by alanine scanning techniques) can be synthesised and their affinities measured by SPR. For example, SPR analysis of a lignin-binding peptide (HFPSPFIQRHSH) revealed an almost complete loss of binding functionality after Phe2 was substituted by Ile (HIPSPIQRHSH), suggesting that  $\pi$ - $\pi$  stacking interactions via the phenyl group of Phe2 were primarily responsible for lignin binding [15]. Interestingly, the substitution of Phe7 with Ile (HFPSPFIQRHSH) caused a decrease in the peptide's affinity to softwood lignin without affecting its affinity to hardwood lignin, indicating that Phe7 plays a role in the recognition and selectivity properties of the lignin-binding peptide [15].

SPR data can be used to investigate the density, coverage and orientation of an SBP on a solid surface. SPR was used to investigate the ability of a biotinylated polyetherimide (PEI)-binding peptide TGADLNT (p1-B) to mediate the immobilisation of streptavidin (SA) onto PEI films [16]. The authors showed that the quantity of SA bound changed with the surface density of immobilised p1-B. Specifically, it increased with an increasing p1-B density and reached a maximum at a p1-B density of  $19.8 \text{ pmol cm}^{-2}$ . At this maximum, the amount of p1-B involved in SA immobilisation was only 11% and probably the result of poor peptide orientation which inhibited the accessibility of SA to the biotin moieties present on the PEI films. In addition, the quantity of bound SA was shown to decrease at higher p1-B densities, indicating that p1-B forms clusters at higher densities, further inhibiting SA binding. The bound SA was used to immobilise biotinylated DNA probes with up to 95% efficiency, indicating that at the right surface density, p1-B was able to direct the oriented immobilisation of SA without affecting its functionality.

Despite its widespread use, the measurement of SBP-solid binding interactions using SPR has some limitations. A drawback is the mass transfer limitation which should be considered when designing experiments and calculating the kinetic parameters [17]. Gold is the most reliable SPR surface alongside other noble metals such as silver. However, sensing surfaces are frequently modified with polymers, ceramics and inorganic glasses [18] which result in non-uniform surface coverage and roughness, with the formation of a very thin layer on the sensor surface [19,20].

#### Quartz crystal microbalance with dissipation monitoring (QCM-D)

QCM-D is a piezoelectric sensor which, like SPR, measures biomolecule-surface interactions in a real-time, label-free environment and can detect mass changes on a sensor surface with a sensitivity of  $\text{ng/cm}^2$  [21,22]. One of the major advantages of QCM-D over SPR is the flexibility of choosing a variety of substrates other than gold.

Recently, phage display was used to isolate two peptides, MoS2-P15 (GVHRNDQWTAPGGG) and MoS2-P28 (DRWVARDPASIFGGG), that bound strongly to molybdenite, a mineral of molybdenum disulphide ( $\text{MoS}_2$ ) [23]. Binding measurements performed by QCM-D showed that

MoS2-P15 had an 80% higher binding affinity ( $K_{\text{eq}} = 1.87 \times 10^5 \text{ M}^{-1}$ ) to molybdenite than MoS2-P28 ( $K_{\text{eq}} = 1.09 \times 10^5 \text{ M}^{-1}$ ). The calculated negative free energy values ( $\Delta G$ ) of MoS2-P15 and MoS2-P28 were  $-29.91 \text{ kJ/mol}$  and  $-28.58 \text{ kJ/mol}$ , respectively, further suggesting a slightly more favourable molybdenite binding by MoS2-P15 than MoS2-P28.

Molecules can be modified to display multiple copies (multivalency) of an SBP to enhance its immobilisation onto a solid surface. For example, dendrons, capable of carrying proteins or small-molecules, were modified to display different numbers of an hydroxyapatite (HA)-binding peptide (SVSGMKPSRP) and QCM-D then used to monitor the effect that this multivalency had on each dendron's affinity towards an HA surface [24,25]. A tetravalent dendron displaying four evenly spaced copies of the HA-binding peptide had a 100-fold higher binding affinity to the HA-surface than a monovalent dendron displaying only one HA-binding peptide [25].

QCM-D data can be used to understand how SBPs are able to mediate the assembly of simple and complex nanomaterials. For example, QCM-D was applied to monitoring the process of SBP-mediated assembly of a silica/gold nanocomposite [26]. First, a bifunctional peptide comprising both a silica- and gold-binding peptide (SSKSGS-YSGSGSKRRIL-GSGSG-MHGKTQATSGTIQS) was shown to display  $\mu\text{M}$  binding affinity and good surface coverage on both silica and gold surfaces. The changes in dissipation observed during peptide binding showed that the peptide layers formed on each surface were rigid and tightly packed. Next, the bifunctional peptide was used to mediate the assembly of gold nanoparticles onto a silica-coated QCM sensor chip. Using the QCM-D data in conjunction with viscoelastic modelling, the thickness of the peptide film on the silica surface was calculated to be  $\sim 2 \text{ nm}$ , and that of the gold nanoparticle film formed on top was  $\sim 34 \text{ nm}$ .

The composition (e.g. ionic strength, pH) of the surrounding solution (water, buffer, solvent) can have a significant effect on SBP binding, including orientation, density, packing and spatial arrangement on a solid surface. QCM-D studies have been performed in different solvents ( $\text{H}_2\text{O}$  and saline solution) with two titanium-binding peptides, Ti-1 (QPYLFATDSLK) and Ti-2 (GHYHYAVRTQT), of different overall charge and number of hydrophobic residues [27]. QCM-D analysis performed in water showed a significant and measurable increase in dissipation energy for both peptides. This represented the formation of viscoelastic multilayers on the titanium surface, owing to water entrapment between the layers, and was most likely due to the hydrophobic nature of the peptides. In contrast, the QCM-D analysis performed in saline (0.15 M NaCl) showed almost negligible energy dissipation for both peptides implying the formation of a rigid monolayer on the surface. These results suggest that the ionic strength of solvents affect the formation and structure of adsorbed peptide layers.

Although QCM-D measures the hydrated mass of adsorbed layers, it cannot determine the absolute value of a molecule's mass without the hydration shell. However, the QCM-D can be paired with optical techniques, such as SPR, to analyse the hydration shell associated with the adsorbed molecules [28].

#### Isothermal titration calorimetry (ITC)

ITC is a highly sensitive method to determine interactions between micro- and nanoparticles and biomolecules, biomolecules-biomolecules, and cell-biomolecules in solution and in a label-free environment. The binding interactions are measured by changes in heat during binding events. Unlike SPR and QCM-D, ITC allows the study of the interactions between SBPs and nanoparticles in solution, enabling the stoichiometry, binding constant, enthalpy, free energy and entropy change of binding interactions to be determined [29–31].

ITC has been used to measure binding between ZnO microparticles and ZnO-binding peptides [31]. Analysis revealed favourable binding interactions from the high binding-affinity and negative free energy of

binding values. Furthermore, the interaction of the peptides with ZnO displayed a biphasic process, involving both exothermic events, indicating peptide-surface and peptide-peptide interactions, and endothermic events, indicating peptide conformational change and displacement of water molecules. Also, the presence of negative enthalpy values (between -25 and -67 kJ/mol) indicated non-covalent binding interactions between the peptides and the ZnO surface.

Analysis of the effect of SBP multimerisation on binding has been explored by ITC comparing the binding interactions of a monomeric ZnO-binding peptide RPHRKGDDA (1xZBP) and a trimeric variant (RPHRKGDDA)<sub>3</sub> (3xZBP) with optically active ZnO-coated nanoparticles [32]. These experiments showed that the binding affinity of 3xZBP towards the ZnO nanoparticles was nearly twice as strong as that of 1xZBP. However, the calculated binding stoichiometry of each ZBP per ZnO nanoparticle was higher for 1xZBP (~3.9 molecules) when compared to 3xZBP (~2.3 molecules). This difference was most likely the result of the small tethered length of 1xZBP which allowed for a denser packing (~3–10 pmol of peptide per µg of nanoparticle) of the peptide due to the comparative availability of more free binding sites on the surface of ZnO nanoparticles.

The main drawback of ITC is that it requires a large amount of sample for measurement of binding interactions, in addition to the sensitivity of the instrument which is insufficient at lower concentrations. In addition, it becomes difficult to model ITC data in those cases where multiple binding sites are involved, leading to limitations in stoichiometry calculations.

#### Atomic force microscopy (AFM)

AFM enables imaging of protein coated surfaces with sub-nm resolution [33]. Due to its excellent ability to measure interaction forces in the (pN range [34], AFM can be used to study adhesion forces at a single-molecule level, and thus offers a deeper insight into the selectivity and binding mechanism of SBPs. For example, a combination of AFM and QCM-D was used to assess the selective adhesion properties of an SBP (AGSWLRDIWTWLQSAL) that binds to hydrophilic surfaces [35]. The AFM tip was functionalised with the SBP and the tip was then placed in contact with Au, TiO<sub>2</sub>, SiO<sub>2</sub>, and Al<sub>2</sub>O<sub>3</sub> surfaces and found only to bind to Au. The selectivity towards Au was also supported by a higher mean adhesion force (290 pN) compared to TiO<sub>2</sub> and Al<sub>2</sub>O<sub>3</sub> (120–140 pN) and SiO<sub>2</sub> (70 pN), possibly due to the presence of a large number of polar amino acids. The AFM results correlated with those obtained from QCM-D which also indicated that the peptide interacted with Au and only weakly with the oxide surfaces.

AFM imaging also provides insight into the selectivity, orientation, conformation and surface aggregation of adsorbed peptides. Thus, AFM revealed that a graphene-binding peptide (GrBP) AGSWLRDIWTWLQSAL formed aggregates near the edges of highly oriented pyrolytic graphite (HOPG), while a carbon-nanotube binding peptide settled uniformly on the same surface [36]. This shows that a GrBP can selectively discriminate between different facets of HOPG which can modulate the electronic properties of graphene.

Few studies have used AFM to measure SBP binding, which may be due to difficulties in optimisation of the experimental parameters, tip-induced movement of the proteins during analysis and interpretation of the results [37].

#### Circular dichroism (CD) spectroscopy

CD spectroscopy is an optical technique for the determination of the secondary structures of proteins and peptides [38,39]. The structure and conformation of SBPs affects their binding properties and can be readily altered by the surrounding solution. CD spectroscopy analysis performed in [40] indicated that a gold-binding peptide 1-GBP1 (MHGKTQATSGTIQS) and a trimeric variant 3l-GBP1

(MHGKTQATSGTIQS)<sub>3</sub> both adopted a mixture of random coil and nonrandom coil conformations in a standard buffered solution at pH 7.5. However, when exposed to the organic solvent 2,2,2-trifluoroethanol (TFE), the trimeric 3l-GBP1 underwent conformational changes in which it adopted both β-strand and α-helical secondary structures, whereas the shorter monomeric 1-GBP1 did not fold. Unlike 1-GBP1, the binding of 3l-GBP1 to gold was improved by adopting secondary structures in the presence of TFE. Increased length and multimerisation were attributed to 3l-GBP1 possessing different folding properties to 1-GBP1, which enabled the trimer to adapt its structure to bind gold surfaces more strongly.

The binding mechanisms of SBPs can be better understood by identifying the amino acid residues that maintain or alter their structure and conformation. CD spectroscopy provides an overall view of SBP structure but does not reveal the influence of each amino acid residue on its secondary structure. However, in combination with amino acid substitution techniques (such as site-directed alanine mutagenesis), it is possible to define structural differences induced by individual residues. CD spectroscopy has been used with site-directed Ala mutagenesis to study the influence that secondary structure had on the binding of a naphthalene-binding peptide Nap01 (HFTFPQQPPRP) [13]. In its native form, Nap01 has a β-turn structure and displays high affinity towards naphthalene. In contrast, a Nap01 variant (HFTF**A**QQ**A**ARP) in which 3 out of 4 of the rigid Pro residues were substituted with more flexible Ala residues, displayed a random coiled structure and a significantly reduced affinity for naphthalene (approximately 6-fold reduction was observed in bound peptide per ng cm<sup>-2</sup> naphthalene). These results indicated that the secondary β-turn structure of Nap01 induced by its Pro residues was essential for binding to naphthalene.

While CD is a rapid technique to analyse protein structure, it cannot resolve structures for proteins that are not in pure form or form aggregates in solution [38,41].

#### Nuclear magnetic resonance (NMR) spectroscopy

NMR can be used to investigate the structure, dynamics and kinetics of proteins and peptides in solution [42–45]. The structure and dynamics of a Ti-binding peptide (TBP) RKLPGA to TiO<sub>2</sub> and SiO<sub>2</sub> nanoparticles were studied in solution [46,47]. The broadening of TBP peaks in the nuclear Overhauser effect spectroscopy (NOESY) and total correlation spectroscopy (TOCSY) spectra indicated that the positively charged amino group of Lys and negatively charged carboxyl group of Asp residues determined the selective affinity of TBP to the surface of TiO<sub>2</sub> and SiO<sub>2</sub> nanoparticles, respectively. The binding of TBP to negatively charged TiO<sub>2</sub> was attributed to interaction of positively charged residues Arg1 and Lys2 while the binding to SiO<sub>2</sub> was mediated by the presence of both positive (Arg1) and negative (Asp5) charged residues.

The amino acid sequence of SBPs and the surface properties play a role in determining the structural arrangement of the SBP once adsorbed. Solid state (ss)NMR experiments performed revealed that basic residues acted as anchors for SBP-solid interactions [48]. It was reported that the backbones of two aragonite binding peptides, Pif80-11 (DDRKDDRKGK) and Pif80-22 (DDRKDDRKGK)<sub>2</sub>, adopted a random coiled conformation on aragonite which was evident from their <sup>13</sup>C-<sup>13</sup>C correlation spectra and <sup>13</sup>C CPMAS spectra, respectively [48]. Although the overall 3-D structure of Pif80-22 and Pif80-11 was disordered, binding to the aragonite surface gave structural ordering to the positively charged basic residues (Arg and Lys), which supports the oriented binding of peptides to the surface. The presence of narrow signals in the NMR spectra indicated that Pif80-22/aragonite interactions were not governed by electrostatic attractions.

A limitation of NMR is that it requires a large amount of sample if it is not isotopically labelled with either <sup>13</sup>C or <sup>15</sup>N [49].



### Fourier-transform infrared spectroscopy (FTIR)

FTIR is used for conformational analysis of peptides in a wide range of solvents [50]. It has a better time scale than NMR spectroscopy ( $10^{-5}$  s versus  $10^{-12}$  s) for screening peptide structures and unlike CD spectroscopy, it is not limited by light scattering introduced by the turbidity of samples and spectra generation is quick.

FTIR can be used to study the effect of an SBP on its fusion protein partner. Thus, an aluminium-binding peptide (ABP) VPSSGPQDTRTT was fused with an antifreeze protein isolated from the Antarctic marine diatom, *Chaetoceros neogracile* (Cn-AFP) [51]. The high intensities of the protein-specific FTIR peaks corresponding to N–H stretching, amide C=O stretching, and amide C–N stretching indicated effective binding of ABP-fused Cn-AFP to the aluminium surface without denaturation of the fusion protein (Cn-AFP).

SBPs can act as a ‘material synthesiser’ and the effect of certain amino acid residues in an SBP can affect the crystal formation, which can be monitored by FTIR spectroscopy. The influence was studied of a ZnO-binding peptide EM-12 (EAHVMMHKVAPRP) on ZnO crystal formation and how it is affected by a mutant peptide EC-12 (EAHVCHKVAPRP) in which Met of EM-12 was substituted with Cys [52]. FTIR data showed that although both the peptides affected the crystal formation process, EC-12 had a higher effect on crystal formation by moderating the amount of  $\text{Zn}^{2+}$  ions in solution. Furthermore, EC-12 changed the morphology of the ZnO crystals via reversible adsorption onto the crystal surface, due to the presence of the Cys substitution in the mutant peptide.

One limitation of FTIR is that it is unable to characterise samples in complex media [53].

### In-silico molecular modelling and computer simulation

Computational methods are emerging as a complementary tool to investigate SBP-substrate interactions, in addition to providing a detailed analysis of the direct relationship between the bio-interface structure and its properties. Methods such as molecular modelling have the potential to provide deeper insights into these interfaces at the atomic level [54,55]. One key advantage of computational approaches is the possibility to test hypotheses *in silico* which might be inconclusive, costly or intractable to test in the laboratory. In principle, molecular modelling can predict not only the complex ensemble of peptide conformations that give rise to the functionality of the bio-interface, but also predict and capture the effects of peptide sequence mutations. It provides a way to explore systematically structural/thermodynamic/dynamical phenomena, to test and develop assumptions of the basic principles that govern molecular structure, flexibility, and function [56]. Improvements in modelling theories and approaches are vital contributions to progressing this field, alongside technical innovations such as improved algorithms, faster computer hardware and improved force fields.

The different approaches used to model SBP-surface interactions range from sub-atomic quantum mechanical (QM) through classical atomic levels to mesoscopic descriptions and continuum descriptions on a macroscopic scale. Simulations at the QM level are usually applied to small nanoparticle-peptide systems [57] and typically do not capture time-dependent (i.e. dynamic) information. While the permanent interactions are associated with strong binding affinities (in the nM range), weak or dynamic interactions usually fall in the  $\mu\text{M}$  range. The all-atom molecular mechanics (MM) simulation approach has been widely used to investigate the dynamics and thermodynamic properties of peptide adsorption [57,58] while coarse-grained and multiscale approach are more commonly employed to capture the time and length scale of a complete adsorption process [59,60]. However, the potential energy of the SBPs in contact with inorganic surfaces is typically modelled using classical force-fields (FF) which can be orders of magnitude faster to compute than QM *ab initio* methods.

### Prediction of SBP-solid surface interactions using molecular simulation

The adsorption free energy of SBPs can be predicted via molecular simulation together with their specific interaction with the solid surface. The facet-dependent adsorption free energies for peptide-gold interactions were revealed by predicting the free energy of adsorption of an Au-binding peptide (AuBP1) [2] at three aqueous gold interfaces [Au(111), Au(100)( $1 \times 1$ ) and Au(100)( $5 \times 1$ )] using *in situ* combination of Replica Exchange with Solute Tempering and Metadynamics (REST + MetaD) simulations [61]. The modelling data showed the critical influence of interfacial solvation structure for selective peptide adsorption on the Au surface, which mediated binding in two ways: (i) direct contact between peptide and gold surface atoms, and (ii) interfacial water molecules tightly bound between gold and peptide. Accordingly, the adsorption of AuBP1 on Au(111) was found to be stronger ( $-51.8 \pm 18.1$  kJ/mol) and thermodynamically favoured over Au(100) ( $-21.3 \pm 4.2$  kJ/mol). The predicted [61] and experimental [2,6] free energies were found to be consistent and suggested the significance of surface hydration as a key factor in determining peptide-surface recognition.

The influence of amino acid sequence and functionality was studied on the binding process of the Au-binding peptide, A3 (AYSSGAPPMPPF) [62] and other similar peptides (e.g., AYASGAPPMPPF, AYAAGAPPMPPF, AYPGAPPMPPF, AYSSPPMPPF) [63] on Au(111) interface by employing the AMBER10 suite of programs to run molecular dynamics (MD) simulation studies [63]. The simulation data suggested that the peptide binding was a four-step process: diffusion, anchoring, crawling and binding. The process was reliant on amino acid composition and sequence which indicated that the individual amino acid residues Tyr, Met and Phe acted as strong binding residues while Ser was responsible for the effective anchoring of the peptide to the gold surface. Pro served as dynamic anchoring while Gly and Ala provided more flexibility to the peptide backbone [63].

The binding mechanism was investigated of a phage-display-derived hydroxyapatite (HAP)-binding sequence, H12 (VTKHLNQISQSY) [65] and its three mutants [64–66] to HAP(100) surface using a combination of bioinformatics, MD and metadynamics. The data indicated that the sequence and composition of residues was the governing factor for the peptide conformation, with H12 having an  $\alpha$ -helical conformation as predicted by *RosettaSurface* and subsequently investigated using classical MD simulations. The charge density of the peptide was identified as the primary factor responsible for the binding of the peptide, which was slightly affected by secondary structure. Basic and acidic residues in the sequence were suggested to be the primary factors facilitating peptide-HAP binding by forming hydrogen bonds with the phosphate ions in HAP. Binding energies calculated using parallel-tempering metadynamics (between  $-62$  and  $-147$  kJ/mol) were qualitatively consistent with the experimental data [66].

The binding affinity of a SBP in addition to its adhesion behaviour can be quantified by using a combination of MD simulations with spectroscopic techniques. The adsorption behaviour of a positively charged pentapeptide, RTHRK [67] and its two analogues to mica surface was studied by using AFM in combination with MD simulations [68]. The topological data demonstrated that although Coulomb interactions support peptide adsorption to the mica surface, it was the formation of salt bridges and hydrogen bonds which influenced the binding affinity of the peptide to the surface lattice. Desorption free energies ( $\sim 100$  kJ/mol), calculated by umbrella sampling, illustrated the importance of the Lys residue for strong binding to mica surface. The phenomenon of salt bridges in mediating SBP-solid binding was also recently highlighted [69], in an MD simulation study of titanium-binding peptides in the presence of calcium ions.

Pristine graphene is a two-dimensional material made solely from carbon, with potential applications in nanotechnology, nanomedicine and biomedical engineering. Graphene oxide (GO) and reduced GO are



related materials, which are chemically-modified forms of graphene. Specifically, GO features oxygen-bearing functional groups. The adsorption and surface-mediated self-assembly were studied of a graphene (graphite)-binding peptide sequence (GrBP5-WT) IMVTESDYSSY and its mutants, M1 (IMVTESDASSA), M2 (IMVTESDWSW), M4 (TQTESDYSSY) and M5 (LIATESDYSSY) [70,71], to aqueous graphene interfaces, via the use of advanced conformational sampling using REST-MD simulations in combination with polarisable FFs. The computational analyses correlated well with the experimental data [71] and showed that the adsorption of GrBP5-WT in addition to M2 and M5, was mediated by the aromatic amino acid residues present in the C-terminal subdomain, SD3 (-YSSY) of GrBP5-WT, whereas the hydrophilic and hydrophobic subdomains, SD2 (-TESSD) and SD1 (IMV-), respectively, were involved in weak (between -2 and -8 kJ/mol) aqueous graphene surface interactions. The aggregation of peptide chains on the graphene surface was a result of hydrogen-bonding and charge-charge interactions between hydrophobic and hydrophilic subdomains, in contrast to hydrophobic-hydrophobic subdomains as suggested previously [72].

The specificity of an SBP for different crystallographic structures of the same material can be deduced from computational modelling. MD simulations were employed [73] to study the facet-specific binding of two phage display isolated platinum-binding peptides, S7 (SSFPQPN) and T7 (TLTILT) [74], having affinity and specificity to two different crystallographic planes of platinum, Pt(100) and Pt(111), respectively. Computational analysis revealed that differential adsorption of an SBP's amino acids was the reason for their surface recognising property [73], which was evident from the fact that the peptides S7 (-615 kJ/mol) and T7 (-368 kJ/mol) bound both surfaces with comparable strengths but displayed higher affinity towards Pt(111) than Pt(100). The peptide-surface mediation was favoured by the presence of ions or water which was inferred by high adsorption energies of S7 and T7. The main driving factor which decides the degree of an SBP binding was suggested to be the presence of reactive residue groups (polar and amine) and peptide composition near the facets. Phe, Gln, Pro, and Asn were found to be responsible for binding the Pt(111) facet while the binding on Pt(100) facet was specifically driven by Leu and Thr.

Peptide residues play a key role in the affinity of SBPs to semimetals and semiconductors. Computer simulation techniques such as density functional theory (DFT) and classical MD simulations were used [75] to investigate the adsorption mechanism of three 12-mer Si-binding peptide sequences, P1 (SVSVGMKPSRP), P2 (LLADTTHRPWT) and P3 (SPGLSLVSHMQT) [76], on  $n^+$ -type Si and  $p^+$ -type Si. Their simulation results agreed with the experimental data [76] which showed the selective binding of P1 and P2 to  $n^+$ -type Si relative to P3, with P2 exhibiting the best adhesion ( $-60.79 \pm 0.91$  kJ/mol) to  $n^+$ -Si. The selective binding to Si was shown to be dependent on peptide composition and residue sequence, where polar residues (Asp, Thr, His, Arg) and non-polar aromatic residues (Trp) were predicted to be the best-binding residues for P2. An increment in binding affinity was predicted by replacing non-polar (Pro) with polar (Cys) or non-polar (Met) or by introducing additional Trp in place of Thr. Surprisingly, substitution of short non-polar residues Ala and Val by Pro caused a decrease in the predicted binding affinity of P2 towards Si [75].

#### Applications of solid-binding peptides (SBPs) in the field of sensing

Biofunctionalisation involves the modification of material surfaces to impart them with a biological function by attaching biomolecules (e.g., peptides, carbohydrates, nucleic acids, and antibodies) to enhance their functionality in several nanobiotechnological applications. The attachment of biomolecules to solid surfaces is usually achieved by means of well-established chemical bioconjugation reactions [77,78]. However, these methods may be laborious or inefficient and sometimes interfere in the recognition of specific molecular/receptor partner by the

immobilised biomolecule [79]. Also, the biomolecules attached via chemical bioconjugation might be arranged non-uniformly and in a random orientation which can affect their overall biological function.

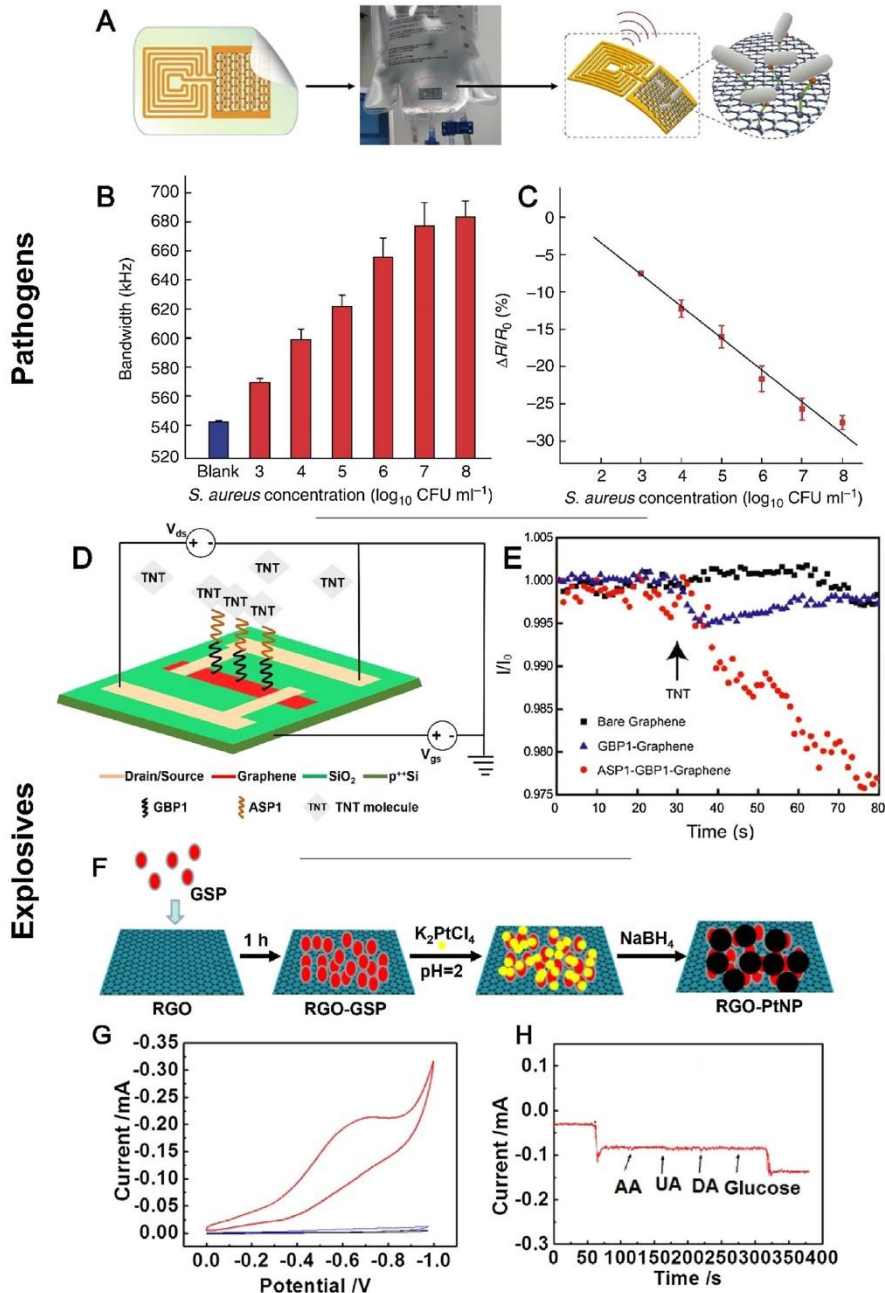
SBPs can act as “molecular linkers” to direct the facile and oriented immobilisation of biomolecules onto solid surfaces [80] or as “material synthesisers” to initiate and regulate the synthesis of composite materials [5]. These two unique properties of SBPs have been exploited in a diverse range of nanobiotechnological applications ranging from vaccine development [81], bioimaging [82], drug delivery [83,84], cell capture [80], biomedical diagnostics [85], and anti-microbial therapeutics [86] to surgical implants and biomaterials [87,88]. In recent years, the selectivity of SBPs towards defined chemical and biological targets [85] have opened new opportunities for the development of novel sensing mechanisms. Here, the combination of electronics and biology have given rise to a variety of high sensitivity sensors for applications ranging from pathogen detection to the detection of harmful chemicals and compounds [89]. One of the most studied target materials for this purpose is graphene.

Several intrinsic properties make graphene a promising material for electrochemical and biological sensing applications. They include high surface area-to-volume ratio, fast electron transfer rate, high electron and thermal conductivity at room temperature, good biocompatibility, high mechanical strength and high elasticity [90,91]. However, the functionalisation of graphene with biomolecules is difficult to achieve due to the lack of functional groups and established self-assembled monolayer chemistries. Since the covalent functionalisation of graphene leads to deterioration of its structure and loss of electronic properties [92], graphene-binding peptides have been used to mediate the non-covalent bioconjugation of unique bioactive peptide motifs to graphene in a number of sensors.

A graphene-based wireless biosensor was developed [85] which was functionalised using a bifunctional peptide comprising a graphene-binding peptide (GrBP) fused to an antimicrobial peptide (AMP) that can recognise and bind pathogenic bacteria such as *Staphylococcus aureus* and *Helicobacter pylori*. Since the graphene was printed onto thin films of water-soluble silk, the sensor was easily transferred to various surfaces. This approach was used to interface the wireless nanosensor with a hospital intravenous (IV) bag. This set up was used in the wireless monitoring of hospital sanitation and biohazard exposure (Fig. 2A). The sensor exhibited excellent resistance to mechanical stress when subjected to IV bag crumpling and was able to monitor the most common post-surgical antibiotic-resistant strain of *Staphylococcus aureus* with a detection limit of 1 bacterium  $\mu\text{L}^{-1}$  (Fig. 2B,C).

Other graphene-based electrochemical sensors have been designed using a similar approach. For example, for the detection of trinitrotoluene (TNT), a TNT-binding peptide domain (ASP1), derived from the binding pocket of the honeybee odorant-binding protein, was linked to a graphene-binding peptide (GrBP1) [93]. The resulting fusion peptide retained its bifunctionality when immobilised on a hybrid graphene field effect transistor (GFET)-based sensor device (Fig. 2D). The device detected vapour phase TNT with a concentration limit as low as parts per billion (ppb) (Fig. 2E).

The detection of  $\text{H}_2\text{O}_2$  in the environment is important because it acts as an explosive at high concentration and may also cause damage to the human respiratory system and skin burns. The design of a non-enzymatic electrochemical  $\text{H}_2\text{O}_2$  sensor based on a graphene (graphite)-specific peptide (GrSP) has been proposed [94]. The GrSP displayed high affinity towards reduced graphene oxide (RGO) and acted as a biomolecular template for the synthesis of RGO-platinum nanoparticles (PtNPs) nanohybrids (Fig. 2F). The PtNPs were used to modify a glass carbon electrode (GCE) for electrochemical detection of  $\text{H}_2\text{O}_2$ . The fabricated GCE exhibited enhanced electrocatalytic activity and high selectivity towards  $\text{H}_2\text{O}_2$  (Figs. 2G, H) with a mM detection limit and a linear range between 0.2–15 mM. This sensor could be used repeatedly for at least 7 times and was stable for at least 9 days when stored at 4 °C.



(caption on next page)



**Fig. 2.** Application of SBPs in the field of sensing. *Top panel*, (A) Schematic of a graphene-binding peptide (GrBP)-based wireless nanosensor for the detection of pathogenic bacteria. The graphene-based sensing element with wireless readout coil was printed on the surface of a water-soluble silk film and was biotransferred onto the surface of an intravenous (IV) bag used in hospitals. The wireless readouts indicated the binding of pathogenic bacteria to the self-assembled peptides on the graphene nanotransducer. (B) Bandwidth of the sensor resonance corresponding to various concentrations of *S. aureus* cells incubated on the sensor surface. (C) Plot of the average percentage change in graphene resistance against concentration of *S. aureus*. Adapted with permission of [85]. *Middle panel*, (D) Schematic representation of a GFET device and self-assemble bifunctional GrBP1 nanosensors fabricated on heavily doped Si wafers containing an insulating SiO<sub>2</sub> layer. (E) Electrical responses of bare (black), GrBP1-functionalised (blue) and GrBP1-ASP1 functionalised (red) graphene sensors to 12 ppb of TNT injected at 30 s. Adapted with permission of [93]. *Bottom Panel*, (F) Schematic for the synthesis of RGO-PtNP nanohybrids via GrSP mediation. GrSP and RGO were mixed in water followed by the addition of K<sub>2</sub>PtCl<sub>6</sub>, centrifuged and finally addition of NaBH<sub>4</sub> produced RGO-PtNP. (G) Cyclic voltammetry (CV) results for the interaction of 2 mM H<sub>2</sub>O<sub>2</sub> with bare GCE (black), RGO/GCE (blue), and RGO-PtNP/GCE (red). (H) High selectivity of sensor towards H<sub>2</sub>O<sub>2</sub> [94].

## Conclusion

The analysis and characterisation of SBP-solid interactions using a combination of experimental and computational methods are critical to elucidating the binding mechanisms of SBPs. The ability to tailor SBPs for specific applications will facilitate their use in a broader range of biotechnological and biomedical applications. Accordingly, there is great interest in the rational design of stable and functional SBPs which can bind to a preselected material with high selectivity and affinity, and with desired orientation, surface density and surface coverage. An improved rational design of peptides will reduce the reliance on common combinatorial techniques currently used to isolate SBPs, which are time-consuming may be subjected to selection bias based on their composition, position and expression [95].

One of the main limitations of current computational models for SBP-solid interactions is their difficulty in dealing with the complexity encountered at the SBP-solid interface in addition to the surrounding environment. Moreover, simulation methods are often limited by the large size and complexity of the multimeric peptides and the computer power available to run those simulations. The introduction of existing online peptide databases (e.g., the BDB database [96]) into appropriate multi-scale modelling and simulation tools could help in building accurate models to explore more complex systems in the near future. Recent advances in computational data analysis, development of new algorithms, machine learning and powerful computer hardware can assist in elucidating the complex, non-linear relationships between peptide sequences, structural variation and dynamics. Moreover, the emergence of artificial intelligence (AI) methods like deep learning (DL), which has already been used to predict secondary structures [97,98] and protein-protein interactions [99] are exciting new developments that could be implemented in the near future for the rational design of novel SBPs with tailored functions.

## Funding

RB is supported by an international Macquarie University Research Excellence Scholarship (iMQRES). AC is supported by a Cancer Institute New South Wales Early Career Fellowship (Project Number: ECF171114). This work was supported by the Australian Research Council (CE140100003).

## References

- [1] Matsuno H, Sekine J, Yajima H, Serizawa T. Biological selection of peptides for poly (l-lactide) Substrates. *Langmuir* 2008;24:6399–403.
- [2] Hnilova M, Oren EE, Seker UOS, Wilson BR, Collino S, Evans JS. Effect of molecular conformations on the adsorption behavior of gold-binding peptides. *Langmuir* 2008;24:12440–5.
- [3] Serizawa T, Sawada T, Matsuno H. Highly specific affinities of short peptides against synthetic polymers. *Langmuir* 2007;23:11127–33.
- [4] Zheng B, Yamashita I, Uenuma M, Iwahori K, Kobayashi M, Uraoka Y. Site-directed delivery of ferritin-encapsulated gold nanoparticles. *Nanotechnology* 2010;21:045305.
- [5] Naik RR, Stringer SJ, Agarwal G, Jones SE, Stone MO. Biomimetic synthesis and patterning of silver nanoparticles. *Nat Mater* 2002;1:169–72.
- [6] Tang Z, Palafox-Hernandez JP, Law W-C, Hughes ZE, Swihart MT, Prasad PN. Biomolecular recognition principles for bionanocombinatorics: an integrated approach to elucidate enthalpic and entropic factors. *ACS Nano* 2013;7:9632–46.
- [7] Palafox-Hernandez JP, Tang Z, Hughes ZE, Li Y, Swihart MT, Prasad PN. Comparative study of materials-binding peptide interactions with gold and silver surfaces and nanostructures: A thermodynamic basis for biological selectivity of inorganic materials. *Chem Mater* 2014;26:4960–9.
- [8] Nel AE, Mädlar L, Velegol D, Xia T, Hoek EMV, Somasundaran P. Understanding biophysical/chemical interactions at the nano-bio interface. *Nat Mater* 2009;8:543–57.
- [9] Seker UOS, Demir HV. Material binding peptides for nanotechnology. *Molecules* 2011;16:1426–51.
- [10] Zahnd C, Amstutz P, Plückthun A. Ribosome display: selecting and evolving proteins in vitro that specifically bind to a target. *Nat Methods* 2007;4:269–79.
- [11] Zeng Y, Hu R, Wang L, Gu D, He J, Wu S-Y. Recent advances in surface plasmon resonance imaging: detection speed, sensitivity, and portability. *Nanophotonics* 2017;6:1017–30.
- [12] Tamerler C, Oren EE, Duman M, Venkatasubramanian E, Sarikaya M. Adsorption kinetics of an engineered gold binding peptide by surface plasmon resonance spectroscopy and a quartz crystal microbalance. *Langmuir* 2006;22:7712–8.
- [13] Sawada T, Okeya Y, Hashizume M, Serizawa T. Screening of peptides recognizing simple polycyclic aromatic hydrocarbons. *Chem Commun (Camb)* 2013;49:5088–90.
- [14] Ejima H, Matsuno H, Serizawa T. Biological identification of peptides that specifically bind to poly(phenylene vinylene) surfaces: recognition of the branched or linear structure of the conjugated polymer. *Langmuir* 2010;26:17278–85.
- [15] Yamaguchi A, Isozaki K, Nakamura M, Takaya H, Watanabe T. Discovery of 12-mer peptides that bind to wood lignin. *Sci Rep* 2016;6:21833.
- [16] Date T, Sekine J, Matsuno H, Serizawa T. Polymer-binding peptides for the non-covalent modification of polymer surfaces: effects of peptide density on the subsequent immobilization of functional proteins. *ACS Appl Mater Interfaces* 2011;3:351–9.
- [17] Schuck P, Zhao H. The role of mass transport limitation and surface heterogeneity in the biophysical characterization of macromolecular binding processes by SPR biosensing. *Methods Mol Biol* 2010;627:15–54.
- [18] Das P, Reches M. Review insights into the interactions of amino acids and peptides with inorganic materials using single molecule force spectroscopy. *Pept Sci* 2015;104:480–94.
- [19] Vaisocherová H, Yang W, Zhang Z, Cao Z, Cheng G, Pilliarik M. Ultralow fouling and functionalizable surface chemistry based on a zwitterionic polymer enabling sensitive and specific protein detection in undiluted blood plasma. *Anal Chem* 2008;80:7894–901.
- [20] Qiang W, Tobias B, Stefano A-U, Joachim D, Christian W, NA T. Protein interactions with polymer coatings and biomaterials. *Angew Chem Int Ed* 2014;53:8004–31.
- [21] Rodahl M, Höök F, Krozer A, Brzezinski P, Kasemo B. Quartz crystal microbalance setup for frequency and Q-factor measurements in gaseous and liquid environments. *Rev Sci Instrum* 1995;66:3924–30.
- [22] Rodahl M, Kasemo B. A simple setup to simultaneously measure the resonant frequency and the absolute dissipation factor of a quartz crystal microbalance. *Rev Sci Instrum* 1996;67:3238–41.
- [23] Cetinel S, Shen W-Z, Amirpour M, Bhonkar P, Wang F, Borujeny ER. Biomining of MoS<sub>2</sub> with peptide-based smart biomaterials. *Sci Rep* 2018;8:3374.
- [24] Roy MD, Stanley SK, Amis EJ, Becker ML. Identification of a highly specific hydroxyapatite-binding peptide using phase display. *Adv Mater* 2008;20:1830–6.
- [25] Tang W, Ma Y, Xie S, Guo K, Katzenmeyer B, Wesdemiotis C. Valency-dependent affinity of bioactive hydroxyapatite-binding dendrons. *Biomacromolecules* 2013;14:3304–13.
- [26] Seker UOS, Sharma VK, Akhavan S, Demir HV. Engineered peptides for nanohybrid assemblies. *Langmuir* 2014;30:2137–43.
- [27] Sultan AM, Westcott ZC, Hughes ZE, Palafox-Hernandez JP, Giesa T, Puddu V. Aqueous peptide-TiO<sub>2</sub> interfaces: isoelectric binding via either entropically or enthalpically driven mechanisms. *ACS Appl Mater Interfaces* 2016;8:18620–30.
- [28] Lord MS, Stenzel MH, Simmons A, Milthorpe BK. Lysozyme interaction with poly (HEMA)-based hydrogel. *Biomaterials* 2006;27:1341–5.
- [29] Huang R, Lau BLT. Biomolecule-nanoparticle interactions: elucidation of the thermodynamics by isothermal titration calorimetry. *Biochim Biophys Acta* 2016;1860:945–56.
- [30] Tellinghuisen J. Optimizing isothermal titration calorimetry protocols for the study of 1:1 binding: keeping it simple. *Biochim Biophys Acta* 2016;1860:861–7.
- [31] Limo MJ, Perry CC. Thermodynamic study of interactions between ZnO and ZnO binding peptides using isothermal titration calorimetry. *Langmuir* 2015;31:6814–22.
- [32] Cho N-H, Cheong T-C, Min JH, Wu JH, Lee SJ, Kim D. A multifunctional core-shell nanoparticle for dendritic cell-based cancer immunotherapy. *Nat Nanotechnol* 2011;6:675–82.



- [33] Karrasch S, Hegerl R, Hoh JH, Baumeister W, Engel A. Atomic force microscopy produces faithful high-resolution images of protein surfaces in an aqueous environment. *Proc Natl Acad Sci U S A* 1994;91:836–8.
- [34] Carvalho FA, Santos NC. Atomic force microscopy-based force spectroscopy — biological and biomedical applications. *IUBMB Life* 2012;64:465–72.
- [35] Kim S-O, Jackman JA, Mochizuki M, Yoon BK, Hayashi T, Cho N-J. Correlating single-molecule and ensemble-average measurements of peptide adsorption onto different inorganic materials. *Phys Chem Chem Phys* 2016;18:14454–9.
- [36] Kim SN, Kuang Z, Slock JM, Jones SE, Cui Y, Farmer BL. Preferential binding of peptides to graphene edges and planes. *J Am Chem Soc* 2011;133:14480–3.
- [37] Günay KA, Klok H-A. Identification of soft matter binding peptide ligands using phage display. *Bioconjug Chem* 2015;26:2002–15.
- [38] Greenfield NJ. Using circular dichroism spectra to estimate protein secondary structure. *Nat Protoc* 2007;1:2876–90.
- [39] Whitmore L, Wallace BA. Protein secondary structure analyses from circular dichroism spectroscopy: methods and reference databases. *Biopolymers* 2008;89:392–400.
- [40] Seker UOS, Wilson B, Kulp JL, Evans JS, Tamerler C, Sarikaya M. Thermodynamics of engineered gold binding peptides: establishing the structure-activity relationships. *Biomacromolecules* 2014;15:2369–77.
- [41] Miesonai A, Wien F, Kemya L, Lee Y-H, Goto Y, Réfrégiers M. Accurate secondary structure prediction and fold recognition for circular dichroism spectroscopy. *Proc Natl Acad Sci USA* 2015;112:E3095–103.
- [42] Rule GS, Hitchens TK. *Fundamentals of protein NMR spectroscopy 1*. Netherlands: Springer; 2005. p. 1–27.
- [43] Markwick PRL, Mallavin T, Nilges M. Structural biology by NMR: structure, dynamics, and interactions. *PLoS Comput Biol* 2008;4:e1600168.
- [44] Polenova T, Gupta R, Goldbourt A. Magic Angle Spinning NMR Spectroscopy: a versatile technique for structural and dynamic analysis of solid-phase systems. *Anal Chem* 2015;87:5458–69.
- [45] Ban D, Smith CA, de Groot BL, Griesinger C, Lee D. Recent advances in measuring the kinetics of biomolecules by NMR relaxation dispersion spectroscopy. *Arch Biochem Biophys* 2017;628:81–91.
- [46] Suzuki Y, Shindo H, Asakura T. Structure and dynamic properties of a Ti-binding peptide bound to TiO<sub>2</sub> nanoparticles as accessed by 1H NMR spectroscopy. *J Phys Chem B* 2016;120:4600–7.
- [47] Suzuki Y, Shindo H. Binding sites and structure of peptides bound to SiO<sub>2</sub> nanoparticles studied by solution NMR spectroscopy. *Polym J* 2018;50:989–96.
- [48] Du Y-P, Chang H-H, Yang S-Y, Huang S-J, Tsai Y-J, Huang J-T, Chan JCC. Study of binding interaction between Pif80 protein fragment and aragonite. *Sci Rep* 2016;6:30883.
- [49] Mirau PA. Interfacial structure determination. Knecht MR, Walsh TR, editors. *Bio-inspired nanotechnology*. 1. New York: Springer; 2014. p. 95–125.
- [50] Harris PI, Chapman D. The conformational analysis of peptides using Fourier transform IR spectroscopy. *Biopolymers* 1995;37:251–63.
- [51] Gwak Y, J-Park, Kim M, Kim HS, Kwon MJ, Oh SJ. Creating anti-icing surfaces via the direct immobilization of antifreeze proteins on aluminum. *Sci Rep* 2015;5:12019.
- [52] Sola-Rabada A, Liang M-K, Roe MJ, Perry CC. Peptide-directed crystal growth modification in the formation of ZnO. *J Mater Chem B* 2015;3:3777–88.
- [53] Roach P, Farrar D, Perry CC. Interpretation of protein adsorption: surface-induced conformational changes. *J Am Chem Soc* 2005;127:8168–73.
- [54] Walsh TR. Molecular modelling of peptide-based materials for biomedical applications. Sunna A, Care A, Bergquist PL, editors. *Peptides and peptide-based biomaterials and their biomedical applications*, 1. Springer International Publishing; 2017. p. 37–50.
- [55] Walsh TR, Knecht MR. Biointerface structural effects on the properties and applications of bioinspired peptide-based nanomaterials. *Chem Rev* 2017;117:12641–704.
- [56] Schlick T, Collepardo-Guevara R, Halvorsen LA, Jung S, Xiao X. Biomolecular modeling and simulation: a field coming of age. *Q Rev Biophys* 2011;44:191–228.
- [57] Mahmoudi M, Lynch I, Eftehadi MR, Monopoli MP, Bombelli FB, Laurent S. Protein–nanoparticle interactions: opportunities and challenges. *Chem Rev* 2011;111:5610–37.
- [58] Utesch T, Daminelli G, Mroglinski MA. Molecular dynamics simulations of the adsorption of bone morphogenetic Protein-2 on surfaces with medical relevance. *Langmuir* 2011;27:13144–53.
- [59] Wei T, Carignano MA, Szleifer I. Lysozyme Adsorption on polyethylene surfaces: Why are long simulations needed? *Langmuir* 2011;27:12074–81.
- [60] Gray JJ. The interaction of proteins with solid surfaces. *Curr Opin Struct Biol* 2004;14:110–5.
- [61] Wright LB, Palafox-Hernandez JP, Rodger PM, Corni S, Walsh TR. Facet selectivity in gold binding peptides: exploiting interfacial water structure. *Chem Sci* 2015;6:5204–14.
- [62] Slock JM, Stone MO, Naik RR. Synthesis of gold nanoparticles using multifunctional peptides. *Small* 2005;1:1048–52.
- [63] Yu J, Becker ML, Carri GA. The influence of amino acid sequence and functionality on the binding process of peptides onto gold surfaces. *Langmuir* 2012;28:1408–17.
- [64] Zhao W, Xu Z, Cui Q, Sahai N. Predicting the structure-activity relationship of hydroxyapatite-binding peptides by enhanced-sampling molecular simulation. *Langmuir* 2016;32:7009–22.
- [65] Segvich SJ, Smith HC, Kohn DH. The adsorption of preferential binding peptides to apatite-based materials. *Biomaterials* 2009;30:1287–98.
- [66] Addison WN, Miller SJ, Ramaswamy J, Mansouri A, Kohn DH, McKee MD. Phosphorylation-dependent mineral-type specificity for apatite-binding peptide sequences. *Biomaterials* 2010;31:9422–30.
- [67] Hassert R, Pagel M, Ming Z, Häupl T, Abel B, Braun K. Biocompatible silicon surfaces through orthogonal click chemistries and a high affinity silicon oxide binding peptide. *Bioconjug Chem* 2012;23:2129–37.
- [68] Gladysz A, John T, Gladysz T, Hassert R, Pagel M, Naumov S. Peptides@mica: from affinity to adhesion mechanism. *Phys Chem Chem Phys* 2016;18:23516–27.
- [69] Sultan AM, Hughes ZE, Walsh TR. Effect of calcium ions on peptide adsorption at the aqueous rutile titania (110) interface. *Biointerfaces* 2018;13:06D403.
- [70] Hughes ZE, Walsh TR. Probing nano-patterned peptide self-organization at the aqueous graphene interface. *Nanoscale* 2018;10:302–11.
- [71] So CR, Hayamizu Y, Yazici H, Gresswell C, Khatayevich D, Tamerler C. Controlling self-assembly of engineered peptides on graphite by rational mutation. *ACS Nano* 2012;6:1648–56.
- [72] Perna MJ, Mijalovic M, Tamerler C, Biggs MJ. Molecular-level understanding of the adsorption mechanism of a graphite-binding peptide at the water/graphite interface. *Soft Mat* 2015;11:5192–203.
- [73] Ramakrishnan SK, Martin M, Cloitre T, Firle L, Cuisinier FJG, Gergely C. Insights on the facet specific adsorption of amino acids and peptides toward platinum. *J Chem Inf Model* 2013;53:3273–9.
- [74] Chiu C-Y, Li Y, Ruan L, Ye X, Murray CB, Huang Y. Platinum nanocrystals selectively shaped using facet-specific peptide sequences. *Nat Chem* 2011;3:393–9.
- [75] Ramakrishnan SK, Martin M, Cloitre T, Firle L, Gergely C. Molecular mechanism of selective binding of peptides to silicon surface. *J Chem Inf Model* 2014;54:2117–26.
- [76] Estephan E, Saab M-B, Agarwal V, Cuisinier FJG, Larroque C, Gergely C. Peptides for the biofunctionalization of silicon for use in optical sensing with porous silicon microcavities. *Adv Funct Mater* 2011;21:2003–11.
- [77] Sapsford KE, Algar WR, Berti L, Genmill KB, Casey BJ, Oh E. Functionalizing nanoparticles with biological molecules: developing chemistries that facilitate nanotechnology. *Chem Rev* 2013;113:1904–2074.
- [78] Aubin-Tam ME, Hamad Schifferli K. Structure and function of nanoparticle–protein conjugates. *Biomed Mater* 2008;3:034001.
- [79] Care A, Bergquist PL, Sunna A. Solid-binding peptides: smart tools for nanobiotechnology. *Trends Biotechnol* 2015;33:259–68.
- [80] Care A, Chi F, Bergquist PL, Sunna. Biofunctionalization of silica-coated magnetic particles mediated by a peptide. *J Nanopart Res* 2014;16:2543.
- [81] Ha N-Y, Shin HM, Sharma P, Cho HA, Min C-K, Kim H-I. Generation of protective immunity against *Orientia tsutsugamushi* infection by immunization with a zinc oxide nanoparticle combined with ScaA antigen. *J Nanobiotech* 2016;14:76.
- [82] Sayyadi N, Care A, Connolly R, Try A, Bergquist L, Sunna A. A novel universal detection agent for time-gated luminescence bioimaging. *Sci Rep* 2016;6:27564.
- [83] Liang L, Lu Y, Zhang R, Care A, Ortega TA, Deyev SM. Deep penetrating photodynamic therapy with KillerRed mediated by upconversion nanoparticles. *Acta Biomater* 2017;51:461–70.
- [84] Kokubun K, Matsumura S, Yudasaka M, Iijima S, Shiba K. Immobilization of a carbon nanomaterial-based localized drug-release system using a bispecific material-binding peptide. *Int J Nanomed Nanosurg* 2018;13:1643–52.
- [85] Mannoor MS, Tao H, Clayton JD, Sengupta A, Kaplan DL, Naik RR. Graphene-based wireless bacteria detection on tooth enamel. *Nat Comm* 2012;3:763.
- [86] Giessen TW, Silver PA. Converting a natural protein compartment into a nanofactory for the size-constrained synthesis of antimicrobial silver nanoparticles. *ACS Synth Biol* 2016;5:1497–504.
- [87] Yazici H, O'Neill MB, Kacar T, Wilson BR, Oren EE, Sarikaya M. Engineered chimeric peptides as antimicrobial surface coating agents toward infection-free implants. *ACS Appl Mater Interfaces* 2016;8:5070–81.
- [88] Sakaguchi T, Janairo JIB, Lussier-Price M, Wada J, Omichinski JG, Sakaguchi K. Oligomerization enhances the binding affinity of a silver biomimetic peptide and catalyzes nanostructure formation. *Sci Rep* 2017;7:1400.
- [89] Cui Y, Kim SN, Naik RR, McAlpine MC. Biomimetic peptide nanosensors. *Acc Chem Res* 2012;45:696–704.
- [90] Justino CIL, Gomes AR, Freitas AC, Duarte AC, Rocha-Santos TAP. Graphene based sensors and biosensors. *Trends Anal Chem* 2017;91:53–66.
- [91] Milowska KZ, Majewski JA. Graphene-based sensors: theoretical study. *J Phys Chem C* 2014;118:17395–401.
- [92] Mann JA, Dichtel WR. Noncovalent functionalization of graphene by molecular and polymeric adsorbates. *J Phys Chem Lett* 2013;4:2649–57.
- [93] Cui Y, Kim SN, Jones SE, Wissler LL, Naik RR, McAlpine MC. Chemical functionalization of graphene enabled by phage displayed peptides. *Nano Lett* 2010;10:4559–65.
- [94] Wang L, Sun Y, Xue X, Sun Y, Li Z. Graphite-specific peptide mediated synthesis of Pt nanoparticles on reduced graphene oxide for electrochemical detection of H<sub>2</sub>O<sub>2</sub>. *Funct Mater Lett* 2016;09:1650051.
- [95] Umlauf BJ, McGuire MJ, Brown KC. Introduction of plasmid encoding for rare tRNAs reduces amplification bias in phage display biopanning. *BioTechniques* 2015;58:81–4.
- [96] He B, Jiang L, Duan Y, Chai G, Fang Y, Kang J. Biopanning data bank 2018: hugging next generation phage display. *Database (Oxford)* 2018;2018. bay032.
- [97] Heffernan R, Paliwal K, Lyons J, Dehzangi A, Sharma A, Wang J. Improving prediction of secondary structure, local backbone angles, and solvent accessible surface area of proteins by iterative deep learning. *Sci Rep* 2015;5:11476.
- [98] Wang S, Peng J, Ma J, Xu J. Protein secondary structure prediction using deep convolutional neural fields. *Sci Rep* 2016;6:18962.
- [99] Sun T, Zhou B, Lai L, Pei. Sequence-based prediction of protein protein interaction using a deep-learning algorithm. *BMC Bioinf* 2017;18:277.

### 1.3 Aims and scope of this thesis

The overall aim of this thesis was to advance the understanding of the interaction between biomolecules and inorganic compounds. More specifically, to determine the binding mechanism of a silica-binding peptide, linker-protein G (LPG), which has been used for the directed immobilization of antibodies onto a variety of silica-based materials. Silica was the material of prime focus because the linker sequence of LPG has been shown to display high binding affinity and specificity towards silica-based materials. Furthermore, our group has used LPG-silica bioconjugation in various applications including theranostics and bioimaging. As a material, silica can be tailored easily to provide large range of porous surfaces, surface functionalities and processing conditions. Also, silica shows high mechanical strength and microbial resistance, and is also highly stable against high temperatures, pressure and extreme pHs. The LPG-mediated biofunctionalization of silica surfaces was also compared to the conventional chemical conjugation of antibodies. Different truncated derivatives of this linker were designed and analyzed using various biophysical characterization techniques to gain insights into the role played by the linker multimerization in the binding affinity of LPG to silica.

In order to realize the comprehensive aim, specific steps of this study included:

- I. To express and purify various truncated derivatives of LPG.
- II. To characterize the kinetics, binding and structure of the purified samples
- III. To study the effect of the linker on the directed immobilization of antibodies.
- IV. To study the role of multimerization and linker length on silica-binding.
- V. A preliminary application study to assess the suitability of the LPG system to detect a disease relevant biomarker in biological fluids.

The main work of this thesis is divided in to three chapters (**chapters 1-3**), which are either published, accepted or prepared for submission to peer-reviewed journals.

**Chapter 1** include an extensive review of various biophysical techniques (experimental approach) currently available for the characterization of solid-binding peptides. The review

also including molecular modelling and artificial intelligence (theoretical approach) which are used to study various binding mechanisms involved in peptide-surface interactions. This chapter provides an overview of the field and set the scene for the following experimental chapters.

**Chapter 2** describes the study of the binding mechanism of a bifunctional silica-binding peptide, linker protein G (LPG) and investigate the possible effect of the linker on the function and stability of the parental protein G. Some of the biophysical characterization techniques presented in **Chapter 1** were used here to characterize and quantitatively analyze the effect of the linker on the overall binding of LPG to silica. The mode of binding as well as the effect of the linker on the structural and chemical function of PG were also investigated. **Chapter 3** describes the potential effect of linker multimerization on the binding affinity LPG. Several truncated derivatives of LPG were designed, and biophysical characterization techniques were used to compare their binding properties on silica. The potential role of the overall linker length on the effective silica-binding was also investigated in this chapter by partial replacement of the linker region with a synthetic glycine-rich sequence .

**Chapter 4** describes a preliminary study for a proof-of-application, Here, LPG was used for the specific and efficient detection of a cancer biomarker, HER2, in complex biological fluids.

A summary and perspectives on future research including the optimization of linker sequence using spacers is described in **Chapter 5**.

## **Chapter 2**

Elucidating the binding  
mechanism of a novel  
silica-binding peptide



## 2.1 Introduction

The previous chapter highlighted the different tools available to study the binding mechanism of solid-binding peptides onto solid surfaces. This chapter introduces the bifunctional fusion protein, linker protein G (LPG) which displays binding affinity to silica-based materials. This fusion protein consists of a silica-binding peptide (referred as ‘linker’) and an antibody binding module, protein G (PG). The original sequence of the silica binding peptide was reported by Nygaard et al. The peptide sequence was only characterised using two types of specific synthetic zeolites, Faujasite and EMT. There were no previous characterization studies performed to determine the binding affinity and also no rational, combinatorial or computational optimization was done to improve the affinity of this peptide. The linker was introduced to PG as a fusion protein by Sunna et al. This fusion protein (LPG) has been used to bio-functionalize several materials for biomedical and biotechnological applications. Despite many LPG applications already established by our group, no studies have been performed to establish its binding mechanism.

The binding characteristics of LPG were quantitatively studied and was compared to the parent protein, PG. The results showed that LPG binds to silica surface in a standing-up orientation, with a strong binding affinity ( $K_D$ ), as high as  $34.77 \pm 11.8$  nM. In comparison, PG displayed no measurable affinity to silica. Further experiments indicated that the fusion of linker to PG has no major effect on PG antibody-binding function. Spectroscopic analysis confirmed that the linker neither affects the secondary structure nor does it alter the chemical stability of parent, PG. Finally, it was shown that in comparison to traditional approach of chemically conjugating biomolecules onto solid surfaces which may result in non-specific orientation of biomolecules, the linker mediated bioconjugation displayed a facile and rapid technique of protein immobilization, without compromising biological function.

This chapter has already been published in the peer-reviewed journal *Biomolecules*.

## 2.2 Contribution to manuscript 2

The concept of this publication was developed together with my main supervisor A/Prof Anwar Sunna and my co-supervisor Dr. Andrew Care. They were also involved in experimental designing and troubleshooting. I designed and performed all the experimental work including data collection and analysis. The initial draft of the manuscript was written by me and was reviewed by all authors. The contributions of each author are given in Table 2.1

Table 2.1 Author contributions for manuscript 2

	Conceptualization	Methodology	Data collection	Data analysis	Manuscript
Rachit Bansal	✓	✓	✓	✓	✓
Zehra Elgundi		✓	✓	✓	✓
Andrew Care	✓	✓			✓
Sophia C. Goodchild		✓	✓	✓	✓
Megan S. Lord		✓		✓	✓
Alison Rodger		✓		✓	✓
Anwar Sunna	✓	✓			✓

## 2.3 Manuscript 2



Article

# Elucidating the Binding Mechanism of a Novel Silica-Binding Peptide

Rachit Bansal <sup>1,2</sup>, Zehra Elgundi <sup>3</sup>, Andrew Care <sup>1,2</sup>, Sophia C. Goodchild <sup>1</sup>, Megan S. Lord <sup>3</sup>, Alison Rodger <sup>1</sup> and Anwar Sunna <sup>1,2,4,\*</sup>

<sup>1</sup> Department of Molecular Sciences, Macquarie University, Sydney NSW 2109, Australia; rachit.bansal@hdr.mq.edu.au (R.B.); andrew.care@mq.edu.au (A.C.); sophie.goodchild@mq.edu.au (S.C.G.); alison.rodger@mq.edu.au (A.R.)

<sup>2</sup> ARC Centre of Excellence for Nanoscale Biophotonics, Macquarie University, Sydney NSW 2109, Australia

<sup>3</sup> Graduate School of Biomedical Engineering, University of New South Wales, Sydney NSW 2052, Australia; z.elgundi@unsw.edu.au (Z.E.); m.lord@unsw.edu.au (M.S.L.)

<sup>4</sup> Biomolecular Discovery and Design Research Centre, Macquarie University, Sydney NSW 2109, Australia

\* Correspondence: anwar.sunna@mq.edu.au; Tel.: +612-9850-4220

Received: 17 November 2019; Accepted: 16 December 2019; Published: 18 December 2019



**Abstract:** Linker-protein G (LPG) is a bifunctional fusion protein composed of a solid-binding peptide (SBP, referred as the “linker”) with high affinity to silica-based compounds and a *Streptococcus* protein G (PG), which binds antibodies. The binding mechanisms of LPG to silica-based materials was studied using different biophysical techniques and compared to that of PG without the linker. LPG displayed high binding affinity to a silica surface ( $K_D = 34.77 \pm 11.8$  nM), with a vertical orientation, in comparison to parent PG, which exhibited no measurable binding affinity. Incorporation of the linker in the fusion protein, LPG, had no effect on the antibody-binding function of PG, which retained its secondary structure and displayed no alteration of its chemical stability. The LPG system provided a milder, easier, and faster affinity-driven immobilization of antibodies to inorganic surfaces when compared to traditional chemical coupling techniques.

**Keywords:** solid-binding peptides (SBPs); linker-protein G (LPG); surface plasmon resonance (SPR); quartz crystal microbalance with dissipation monitoring (QCM-D); circular dichroism (CD) spectrometry; equilibrium dissociation constant ( $K_D$ )

## 1. Introduction

The immobilization of proteins to solid surfaces is a key factor for many biological applications, including the development of biosensors and biocompatible materials. It is primarily achieved through a firm linkage between the functional protein and the solid surface. Protein immobilization onto solid supports is a very laborious task owing to the heterogeneous nature of proteins and their structural dynamics. A successful immobilization should involve mild physical and chemical conditions for the binding of biomolecules with very little or no non-specific binding in order to maintain the protein's biological functionality. Traditionally, the most widely used immobilization method is covalent attachment of proteins to the reactive groups of solid matrices via the protein's primary amines and carboxylic acids [1,2]. One of the major drawbacks of this coupling method is the potential attachment of biomolecules in a random orientation, which may limit or cause complete loss of the protein's biological function [3].

Solid-binding peptides (SBPs) are short amino acid sequences that display binding affinity towards the surface of a variety of materials such as metals, semiconductors, carbon materials, polymers, and minerals [4–7]. Unlike conventional bioconjugation methods (e.g., covalent attachment), SBPs can

act as molecular binders to direct the immobilization and orientation of proteins onto solid supports without impeding their functionality.

A number of factors play an important role in determining the exact binding mechanism of SBPs onto a solid surface. These include (i) the charge, composition, sequence, and structural conformation of the SBP; (ii) the physical and chemical properties of the solid surface of interest such as its chemistry, charge, size, and topography; (iii) the nature and condition of the surrounding media; and (iv) molecular dynamics of the SBP–solid interface. Based on all these parameters, an SBP diffuses and reorients on a solid surface to attain its lowest energy conformation(s) [8,9].

Several SBPs have been studied as a function of the above physical and chemical properties using various biophysical characterization techniques. For example, Seker et al. [10] showed that the adsorption and structural features of SBPs can be adjusted by the presence or absence of molecular constraints. Based on the data obtained from surface plasmon resonance (SPR) and circular dichroism (CD) spectroscopy, it was found that the binding and conformation of a platinum (Pt)-binding septapeptide in its linear and cyclic forms were purely dependent on the cysteine–cysteine (C–C) residues in the peptide sequence. SPR studies performed by Matsuno et al. [4] showed for the first time that a poly (L-lactide) (PLLA)-binding heptapeptide distinguished between the 3D arrangement of functional groups in the crystal lattice of PLLA polymorphs. It was also found that the binding of the peptide to the PLLA surface was primarily due to the proton-donor amino acids histidine (H), lysine (K), arginine (R), and aspartic acid (D) that formed H-bonds with the ester groups of the PLLA backbones. The binding specificity was largely due to the hydrophobic interactions between alanine (A) and leucine (L) residues of the peptide and the methyl and methine groups of the PLLA. Sultan et al. [11] demonstrated that the binding of peptides to the solid surface was mediated by the ionic strength of the solvents, which further determined the nature and structure of the adsorbed peptide layer. Quartz crystal microbalance with dissipation monitoring (QCM-D) analysis performed on two distinct titanium (Ti)-binding peptides of different overall charge and hydrophobic residues showed that while water as the solvent leads to the formation of viscoelastic multilayers on the surface, a 0.15 M NaCl saline solution directed the formation of a rigid monolayer on the surface for both the peptides studied.

The amino acid sequence and surrounding chemical environment of any peptide determine its secondary structure. By using CD spectroscopy in combination with site-directed alanine (A) scanning, Sawada and co-workers found that the proline (P) residues present in the native state of a naphthalene-binding peptide (Nap01) gives the peptide a  $\beta$ -turn structure and that these residues were necessary for strong naphthalene binding [12]. We previously developed an SBP-based bioconjugation platform using a genetically engineered fusion protein, linker-protein G (LPG) [13]. LPG was designed to contain two functionally distinctive regions—a silica-binding SBP (referred to as the “linker”) and an antibody-binding protein (protein G, PG) [13]. The linker was made of a  $4 \times 21$  amino acid sequence repeat ((VKTQATSREEPPRLPSKHRPG)<sub>4</sub>VKTQTAS) that displayed high binding affinity towards silica-based materials. In this platform technology, LPG acts as an anchor for the rapid and oriented immobilization of antibodies onto silica surfaces, thereby ensuring the functional display of conjugated antibodies without the need for complex conjugation chemistry. Although this linker technology has been widely used in several biotechnology and biomedical applications [14–17], there is still a lack of understanding about the interaction mechanism which facilitates the binding of this SBP to the silica surface.

In this work, different biophysical characterization techniques, namely QCM-D, SPR, CD, and fluorescence spectrometry, were used for a detailed study of the binding of LPG to silica. In addition, the effects of the linker on the stability and antibody-binding function of the parental PG were also investigated using CD and fluorescence spectrometry.



## 2. Materials and Methods

### 2.1. Materials and Chemicals

SiO<sub>2</sub>-coated crystals for QCM-D were purchased from ATA Scientific (Taren Point, NSW, Australia). CM5 chips were purchased from GE Healthcare (Parramatta, NSW, Australia). Recombinant PG from *Streptococcus* sp., fetal bovine serum (FBS), and human serum were purchased from Sigma-Aldrich (Castle Hill, NSW, Australia). Humanized anti-HER2 monoclonal antibody trastuzumab was obtained from Jomar Life Research (Melbourne, Australia) and the human HER2/ErbB2 protein (His-Tag) was ordered from Sino Biological Inc. (Beijing, China). All biological assays were performed at room temperature with standard phosphate-buffered saline (1 × PBS) at pH 7.4 containing 10 mM Na<sub>2</sub>HPO<sub>4</sub>, 1.8 mM KH<sub>2</sub>PO<sub>4</sub>, 137 mM NaCl, and 2.7 mM KCl. All other chemicals were purchased from Sigma-Aldrich unless otherwise stated. Murine monoclonal antibody, G203 (IgG1), was purchased from BTF Pty Ltd. (Macquarie Park, NSW, Australia). Purified LPG was obtained as described previously [13]. The 21-single peptide LP1 (VKTQATSREEPPRLPSKHRPG) was synthesized by Mimotopes (Mulgrave, VIC, Australia).

### 2.2. Circular Dichroism (CD) Spectroscopy

CD spectra were collected at room temperature (approximately 25 °C) on a JASCO J-1500 spectropolarimeter (JASCO Corporation, Tokyo, Japan). PBS absorbs strongly at wavelengths below approximately 200 nm, which precludes collection of CD data at these wavelengths. Hence, all CD data were collected in water. LPG and PG were buffer exchanged to Milli-Q water using Amicon Ultra-10K 0.5 mL centrifugal filters (Merck Millipore, Bayswater, VIC, Australia). Stock solutions of each protein were then further diluted in Milli-Q water to a final concentration of 0.1 mg/mL for CD spectroscopy. Wavelength scans were performed between 180 and 350 nm in a rectangular, 1 mm pathlength, quartz cuvette (Starna Scientific Ltd., Ilford, UK). For each sample, three accumulations were recorded using a 2 nm bandwidth, a scan speed of 100 nm/min, and a digital integration time (DIT) of 2 s. The data are reported in terms of mean residue ellipticity ( $\theta_M$ ), expressed in deg·cm<sup>2</sup>·dmol<sup>−1</sup>·residue<sup>−1</sup>.

### 2.3. Fluorescence Spectroscopy

LPG and PG were dissolved to a final concentration of 2 µM in 1 × PBS containing various concentrations (0–7 M) of guanidinium hydrochloride (GdnHCl). Fluorescence spectra were recorded on a JASCO FP-8500 spectrofluorometer (JASCO Corporation, Tokyo, Japan). All measurements were recorded at room temperature (approximately 25 °C) in a micro-volume fluorescence cuvette with 3 mm pathlength (Starna Scientific Ltd., Ilford, UK). Fluorescence emission spectra were collected between 300 and 550 nm using a 295 nm excitation wavelength, 2.5 nm excitation bandwidth, 5 nm emission bandwidth, and scan speed of 100 nm/min.

### 2.4. Surface Plasmon Resonance (SPR)

Surface plasmon resonance (SPR) experiments were conducted on a BIAcore 2000 instrument (GE Healthcare, Uppsala, Sweden) using the most common, versatile, and commercially available sensor chips (i.e., CM5 sensor chips) covered with a carboxymethylated dextran layer. Measurements were performed in filtered and degassed HEPES-buffered saline, HBS-P buffer (10 mM HEPES pH 7.4, 150 mM NaCl, 0.005% (*v/v*) surfactant P20); the same running buffer was used for protein dilutions. In the first step, the surface of the CM5 chip was activated by suitable amine coupling chemistry, using 1-ethyl-3-(3-dimethyl-aminopropyl)-1-carbodiimide hydrochloride (EDC) and *N*-hydroxysulfosuccinimide (EDC/NHS) and ethanolamine to deactivate unreacted NHS-esters. A maximum response level of 2750 RU was achieved by diluting the G203 (IgG1) in 10 mM CH<sub>3</sub>COONa (pH 4.0) to a final concentration of 10 µg/mL. For kinetic studies, both PG and LPG were serially diluted in HBS-P buffer to a final concentration range of 1.45–23.1 nM. The system was equilibrated with running buffer until a stable baseline was obtained, after which the samples were automatically

injected in duplicates for 3 min (association) at a flow rate of 20  $\mu\text{L}/\text{min}$  at room temperature, followed by a 5 min dissociation. The sensor surface was regenerated by injecting glycine-HCl pH 2.0 for 30 sec at 20  $\mu\text{L}/\text{min}$ . Between each sample injection, a re-equilibrium was established between the sensor surface and running buffer by a 90 s pre-run phase. A similar experiment was performed with LP1 to determine any non-specific interaction with the antibody. Global fitting of the resulting sensorgrams at five different concentrations was done using BIAevaluation software version 4.1 (GE Healthcare, Uppsala, Sweden), which simultaneously fits all sensorgrams and evaluates both the association ( $k_a$ ) ( $\text{M}^{-1}\text{s}^{-1}$ ) and dissociation ( $k_d$ ) ( $\text{s}^{-1}$ ) rate constants. The binding affinity ( $K_D$ ) (M) was calculated by the equation  $K_D = k_d/k_a$ . A similar procedure and experimental setup were adopted for the interaction of PG and LPG with anti-HER2 monoclonal antibody trastuzumab. Data were collected by performing each experiment in triplicate and the final values were reported as the mean of all three experiments.

## 2.5. Quartz Crystal Microbalance with Dissipation Monitoring (QCM-D)

A QSense E4 system (Biolin Scientific AB, Gothenburg, Sweden) was used to quantify the adsorption and binding strength of LPG to silica. AT-cut  $\text{SiO}_2$ -coated QCM-D quartz crystal sensors were excited at a fundamental frequency of 5 MHz as well as 3rd, 5th, 7th, 9th, 11th, and 13th overtones, and changes in frequency ( $\Delta f$ ), and dissipation ( $\Delta D$ ) were recorded. Additionally,  $1 \times \text{PBS}$  buffer pH 7.4 at room temperature was used as the flow medium and to prepare the samples. Before starting the measurements, the sensors were first treated in a UV-ozone chamber (Diener Electronic GmbH, Ebhausen, Germany) for 15 min followed by immersion in a solution of 2% ( $w/v$ ) SDS and then incubated in a water bath for 20 min at 60  $^\circ\text{C}$ . The sensors were moved to another beaker with fresh Milli-Q ultra-pure water (Merck Millipore, Bayswater, VIC, Australia) and incubated further for 20 min. The sensors were carefully rinsed with Milli-Q water, dried under  $\text{N}_2$  stream, and treated with UV-ozone for 15 min. The sensors were mounted in the modules provided in the Q-Sense instrument and  $1 \times \text{PBS}$  buffer was flowed (150  $\mu\text{L}/\text{min}$ ) over the bare sensor surface until a flat baseline was obtained. The protein solutions were made in  $1 \times \text{PBS}$  buffer and injected over the sensors through the flow cell at the same flow rate. The protein samples were made to flow until the system reached equilibrium, or until no change was observed in  $\Delta f$ . Finally,  $1 \times \text{PBS}$  was injected again to wash the sensor surface as well as any unbound proteins. Several protein concentrations (3.27–654 nM) were prepared in  $1 \times \text{PBS}$ , and their  $\Delta f$  was measured to determine the dissociation constant or binding affinity ( $K_D$ ). The values obtained were fitted using the Langmuir adsorption model. Data were collected from three independent measurements under the same conditions and parameters.

## 2.6. Adsorption Isotherms

The equilibrium binding constant ( $K_D$ ) and binding affinity of the proteins to silica were obtained using the GraphPad Prism 7 software (GraphPad Software, La Jolla, CA, USA). The one-site-specific binding model was used to fit the adsorption isotherm of the binding interactions between LPG and the  $\text{SiO}_2$ -coated QCM-D sensor crystals. The one-site binding (hyperbola) was defined by the following:

$$\Delta m = (B_{\max} \times C)/(K_d + C), \quad (1)$$

where  $\Delta m$  is the amount of adsorbed analyte,  $C$  is the concentration of the analyte solution,  $B_{\max}$  is the maximum adsorption of analyte onto the surface, and  $K_d$  is the apparent dissociation constant.

## 2.7. Viscoelastic Properties of Adsorbed Proteins

The  $\Delta f$  measurements obtained from the QCM-D are related to the binding of molecules to the sensor surface. However, a linear relationship between  $\Delta f$  and mass is only valid for rigid layers. In this case, the adsorbed area mass ( $\Delta m$ ) is proportional to the  $\Delta f$  in the case of a rigid film, where  $\Delta D < 1 \times 10^{-6}$  per 10 Hz. In such cases, the Sauerbrey equation ( $\Delta m = -C \bullet \Delta f_n/n$ ) can be applied, where  $C$  is the constant of mass sensitivity (17.7 ng  $\text{Hz}^{-1} \text{cm}^{-2}$ ) for a crystal with 5 MHz fundamental

frequency and  $n$  is the number of frequency overtones ( $n = 3$  was used in this work). However, biological systems usually display viscoelastic properties that are measured by  $\Delta D$  and will result in the Sauerbrey equation underestimating the adsorbed mass. Capturing  $\Delta f$  and  $\Delta D$  measurements at multiple harmonics enables modelling of the data with the Voigt viscoelastic model incorporated in QSense software's QTools (Biolin Scientific AB, Gothenburg, Sweden) to obtain parameters including mass, thickness, density, viscosity, and storage modulus [18]. In our work,  $\Delta D > 1 \times 10^{-6}$  per 10 Hz, indicating a viscoelastic layer, hence the Voigt model was used [19–21] to calculate the viscoelastic properties as well as the adsorbed mass of the peptide on the sensor surface.

### 2.8. Chemical Biofunctionalization

Prior to silanization, the QCM-D sensor crystals were cleaned and treated with oxygen plasma at a maximum power for 3 min in a Pico Plasma system (Diener Electronic GmbH, Ebhausen, Germany). The silanization solution was prepared by the addition of 3-aminopropyl-triethoxysilane (APTES) to 95% ethanol to obtain a solution concentration of 5% APTES by volume. Silanization was performed at room temperature for 10 min. After silanization, probes were flushed with 95% ethanol, ultrasonicated for 3 min in 95% ethanol, followed by final rinsing in Milli-Q water. APTES-modified surfaces were activated with 1% glutaraldehyde (GA) in  $1 \times$  PBS for 60 min before immobilization. The modified QCM-D sensor crystals were placed in the Qsense E4 analyzer and  $1 \times$  PBS was injected at a flow rate of 150  $\mu$ L/min until a stable baseline was achieved. PG at a final concentration of 0.654  $\mu$ M in  $1 \times$  PBS was injected at the same flow rate until the  $\Delta f$  was stable (reached saturation), after which the crystal was washed again with  $1 \times$  PBS to remove unbound proteins. Any remaining active groups were deactivated after incubation for 15 min with a solution containing 0.1 M Tris and 50 mM ethanolamine (pH 9.0) followed by a blocking step (1 mg/mL bovine serum albumin, BSA, 10 min) to reduce non-specific binding. Humanized anti-HER2 monoclonal antibody trastuzumab was prepared at a final concentration of 1  $\mu$ g/mL in  $1 \times$  PBS and injected at a similar flow rate to achieve a stable response. Finally, the HER2 antigen at a concentration of 1  $\mu$ g/mL was injected until a stable  $\Delta f$  was obtained. Between each step, the crystals were thoroughly rinsed with  $1 \times$  PBS.

## 3. Results and Discussion

### 3.1. Effect of the Linker on the Structure and Stability of Protein G

Circular dichroism (CD) was used to determine if the presence of the linker affects the secondary structure of PG. The far-UV CD spectra of PG and LPG were measured at a concentration of 0.1 mg/mL (small variations in concentration were accounted for by scaling the CD signal based on the absorbance measured between 180 nm and 350 nm). As can be seen in Figure 1, both proteins display a positive peak at  $\sim 190$  nm and negative peaks at  $\sim 208$  and 222 nm, consistent with a significant  $\alpha$ -helical folded structure. Furthermore, CD secondary structure fitting of this data was performed using Dichroweb [22], using the SELCON3 algorithm [23] and the reference Set 3 [24,25] (which is optimized for a wavelength range of 185–240 nm). The proportion of  $\alpha$ -helix is estimated to be  $\sim 36\%$  for PG and  $\sim 22\%$  for LPG, respectively. As the PG module (185 amino acids) accounts for only  $\sim 2/3$  of the total LPG protein (276 amino acids), assuming the linker itself does not adopt any additional helical structure, this result is consistent with the PG module in PG and LPG maintaining the same fold. These results are also similar to those obtained by Goward et al. whose calculated secondary structure gives  $\sim 29\%$   $\alpha$ -helix for PG [26]. The LPG linker has been previously predicted by homology modeling to be unfolded [16]. Interestingly, using the SELCON3 algorithm and reference Set 3 (as well as many other combinations of fitting algorithm and reference set available on Dichroweb), the proportion of  $\beta$ -sheet was estimated to be  $\sim 17\%$  for PG and  $\sim 27\%$  for LPG, respectively. Taken at face value, this result would suggest that the linker assumes  $\beta$ -sheet structure in the presence of PG. However, it should be noted that random coil and  $\beta_{II}$  structure are, unfortunately, indistinguishable by CD. The reference sets used for CD secondary structure deconvolution typically consist of globular proteins



where  $\beta_{II}$  structures are often generically assigned as  $\beta$ -sheet. Hence, CD secondary structure fitting methods can have trouble distinguishing between unstructured regions and  $\beta_{II}$  structures, particularly in proteins that contain large disordered regions [27]. While it is tempting to suggest that the greater proportion of  $\beta$ -sheet estimated for LPG in comparison to PG may be consistent with the linker lying along the surface of the PG module in a  $\beta$ -sheet conformation, we cannot unequivocally conclude whether the linker truly adopts  $\beta$ -sheet structure in the presence of PG or remains unstructured.

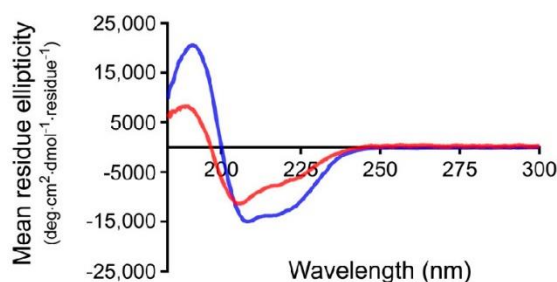


**Figure 1.** Far-UV spectra of *Streptococcus* protein G (PG) (blue) and linker-protein G (LPG) (red) in water at a concentration of 0.1 mg/mL.

PG is stable at high temperatures (melting temperature  $>80^{\circ}\text{C}$ ) [26]. Hence, performing thermal unfolding studies to compare the stability of PG and LPG would, in practice, be challenging if not impossible. Instead, we used fluorescence spectroscopy to compare the relative stability of PG and LPG to chemical denaturant, namely, GdnHCl. PG contains eight tyrosine and three tryptophan residues, whereas the linker itself lacks any of these aromatic amino acids. Our fluorescence experiments were conducted using an excitation of 295 nm to minimize excitation of the tyrosine residues, which generally occurs between 280 and 290 nm [26]. The linker sequence does not have any aromatic residues, so the overall fluorescence of LPG and PG with and without the linker can be attributed to the tryptophan residues of PG. Tryptophan fluorescence is environmentally sensitive, with the wavelength of maximum fluorescence emission correlating to the folding state of the protein, that is, hydrophilic environment fluorescence occurs at longer wavelengths. Unfolding of LPG and PG without the linker was monitored by the shift in maximum tryptophan fluorescence emission to longer wavelength with increasing GdnHCl concentration. The ratio of fluorescence emission intensity at 330 nm and 360 nm (330/360) was plotted against GdnHCl concentration and the data were non-linearly fitted, assuming a two-state denaturation, using GraphPad Prism 7.0 software (Figure 2).

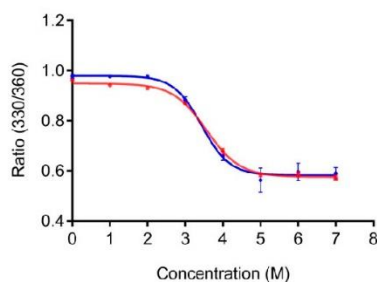


**Figure 2.** Unfolding of PG (blue) and LPG (red) in guanidinium hydrochloride (GdnHCl). Both PG and LPG were diluted to a final concentration of 2  $\mu\text{M}$  in  $1 \times \text{PBS}$ , pH 7.4, containing various concentrations of GdnHCl.



The GdnHCl denaturation curves for PG and LPG are shown in Figure 2. The relative fluorescence intensities at 330 nm and 360 nm (330/360) was used to monitor the shift in fluorescence emission maxima after excitation at 295 nm. No change in tryptophan fluorescence is seen until approximately 2 M GdnHCl for both LPG and PG. Similarly, both proteins were maximally unfolded after approximately 5 M GdnHCl. Based on the non-linear, two-state fitting of the denaturation curves, the concentration of GdnHCl required to induce 50% unfolding was determined to be  $3.4 \pm 0.2$  M (95% CI) for PG and  $3.6 \pm 0.1$  M (95% CI) for LPG. These results indicate that both PG and LPG have similar chemical stabilities, and thus, the linker region of LPG does not significantly affect the structural stability of PG.

### 3.2. Effect of the Linker on the Antibody-Binding Function of Protein G

SPR measurements were performed to analyze whether the linker had any effect on the antibody-binding function of the *Streptococcus* PG. For this purpose, the binding kinetics of PG with the linker (LPG) and PG without the linker were studied with two antibodies—trastuzumab and G203 (IgG1). Trastuzumab, a humanized IgG1 monoclonal antibody, targets the HER2 receptor that plays an important role in normal cell growth and differentiation, whereas G203 is a murine monoclonal antibody, also IgG1, which targets *Giardia lamblia*, a microscopic parasite, present on the cyst walls of the small intestine. The basic purpose of using these two different antibodies was to study whether the two proteins under study show similar binding interactions, irrespective of the source and target of the antibody. Figure 3; Figure 4 represent the SPR sensorgrams for the specific binding interactions of PG and LPG to trastuzumab and G203 (IgG1) using a 1:1 Langmuir approach. The Langmuir approach is based on the fact that a monolayer has been formed on a homogeneous surface, and thus, equivalent binding sites are available, meaning one antibody binds to one protein and that it is independent of the interactions from the occupancy of the nearby binding sites [28]. Since our SPR data fit the 1:1 Langmuir model, we assumed a monolayer adsorption of proteins to antibodies and, hence, a well-defined covering. The chi-squared ( $\chi^2$ ) value (a measure of fitting reliability) was less than 5 for each of the kinetic fitted results. According to the BIAevaluation handbook, a  $\chi^2$  value of less than 10 represents an excellent-fit model [6].

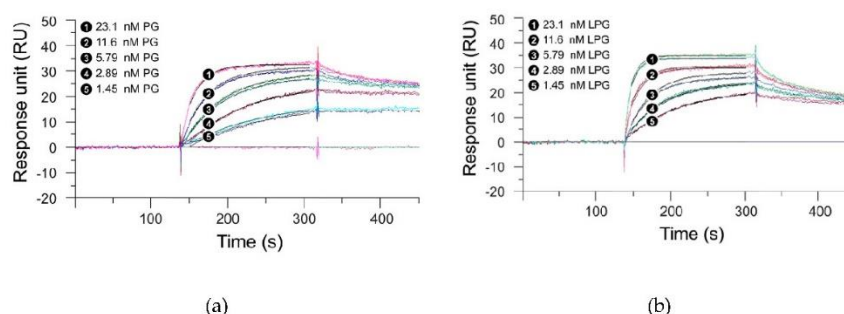


**Figure 3.** Global fit of 1:1 Langmuir binding model with trastuzumab for (a) PG and (b) LPG. Black lines constitute two repeat injections of PG and LPG over trastuzumab immobilized on a surface. The concentrations of each analyte (PG and LPG) injected were 23.1, 11.6, 5.79, 2.89, and 1.45 nM. Experiments were performed over a 700 s period, but for graphical display only the first 450 s are shown. Dissociation was performed for a total of 5 min.

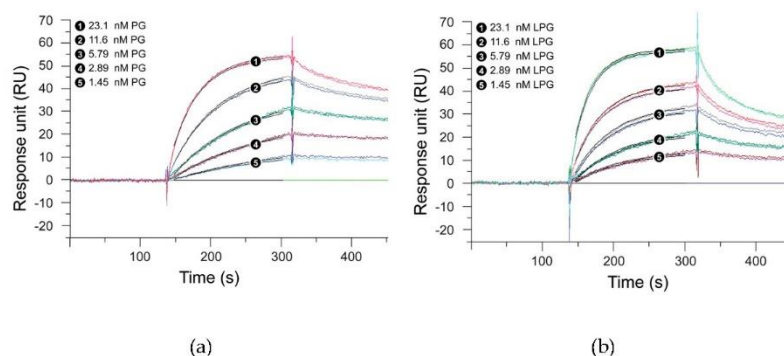


**Figure 4.** Global fit of 1:1 Langmuir binding model with G203 (IgG1) for (a) PG and (b) LPG. Black lines constitute two repeat injections of PG and LPG over G203 (IgG1) immobilized on a surface. The concentrations of each analyte (PG and LPG) injected were 23.1, 11.6, 5.79, 2.89, and 1.45 nM. Experiments were performed over a 700 s period, but for graphical display only the first 450 s are shown. Dissociation was performed for a total of 5 min.

Table 1 presents the association and dissociation rates derived from the SPR measurements for the binding of PG and LPG to trastuzumab and G203 (IgG1), respectively, using a 1:1 Langmuir binding model. Figures 3 and 4 indicate that PG had a faster association but a slower dissociation for both the antibodies when compared to LPG, which displayed fast association with an equally fast dissociation. However, quantitative data from Table 1 suggest that both proteins (PG and LPG) associate and dissociate at similar rates (i.e., all the  $k_a$  and  $k_d$  have a magnitude of  $10^6 \text{ M}^{-1}\text{s}^{-1}$  and  $10^{-3} \text{ s}^{-1}$ , respectively). The different trends for the qualitative and quantitative data can be attributed to random orientation of the antibodies conjugated to the gold surface of the SPR chip. In addition, PG and LPG displayed strong and similar binding affinities to both the antibodies in the nM range ( $K_D = 10^{-9} \text{ M}$ ).

**Table 1.** Kinetic rate constants ( $k_a$  and  $k_d$ ) and equilibrium dissociation constants ( $K_D$ ) for the binding interactions of PG and LPG with trastuzumab and G203 (IgG1). Data were fitted with the BIAevaluation software 4.1 using a 1:1 Langmuir binding model for three replicates of sample injection.

Protein-Antibody Complex	Rate of Association $k_a$ ( $\text{M}^{-1}\text{s}^{-1}$ )	Rate of Dissociation $k_d$ ( $\text{s}^{-1}$ )	Equilibrium Dissociation Constant $K_D$ (M)	Half-Life $t_{1/2}$ (s)
PG + trastuzumab	$1.79 \pm 0.10 \times 10^6$	$8.24 \pm 0.92 \times 10^{-3}$	$4.62 \pm 0.79 \times 10^{-9}$	83.7
LPG + trastuzumab	$3.88 \pm 1.20 \times 10^6$	$7.48 \pm 0.38 \times 10^{-3}$	$2.07 \pm 0.71 \times 10^{-9}$	92.2
PG + G203 (IgG1)	$0.84 \pm 0.02 \times 10^6$	$5.32 \pm 0.29 \times 10^{-3}$	$6.30 \pm 0.32 \times 10^{-9}$	129.7
LPG + G203 (IgG1)	$1.23 \pm 0.06 \times 10^6$	$9.50 \pm 0.30 \times 10^{-3}$	$7.77 \pm 0.58 \times 10^{-9}$	72.6

The lack of measurable SPR signal response for the linker alone (Figure S1, Supplementary Materials) suggests that non-specific binding interactions do not occur between the linker and the antibody. From the SPR experiments, we conclude that the linker has minimal influence on the overall binding function of PG and that only the PG part of LPG is responsible for antibody binding. Moreover, the presence of the linker does not appear to significantly affect the stability of the PG-antibody complex as indicated by the similar half-lives measured for both proteins, LPG and PG (Table 1). The half-life values also suggest that the proteins will not diffuse too far and will not be involved in an unintended process that will reduce the crosstalk between the adjacent protein molecules.

### 3.3. Binding Kinetics of LPG

The binding affinity of LPG to silica was calculated using QCM-D measurements (Figure 5a,b). The Langmuir fitted data (Figure 5c) gave an apparent dissociation constant/binding affinity ( $K_D$ ) of  $34.77 \pm 11.8$  nM, which is comparable to the binding affinity reported for other silica-binding peptides [29–31]. When PG was used at the same molar concentrations as LPG, no measurable  $\Delta f$  was observed in the QCM-D sensorgram (Figure S2, Supplementary Materials). Accordingly, no measurable binding affinity was calculated. Initial qualitative binding assays using SDS-PAGE implied that PG without the linker sequences was unable to bind to silica [13].

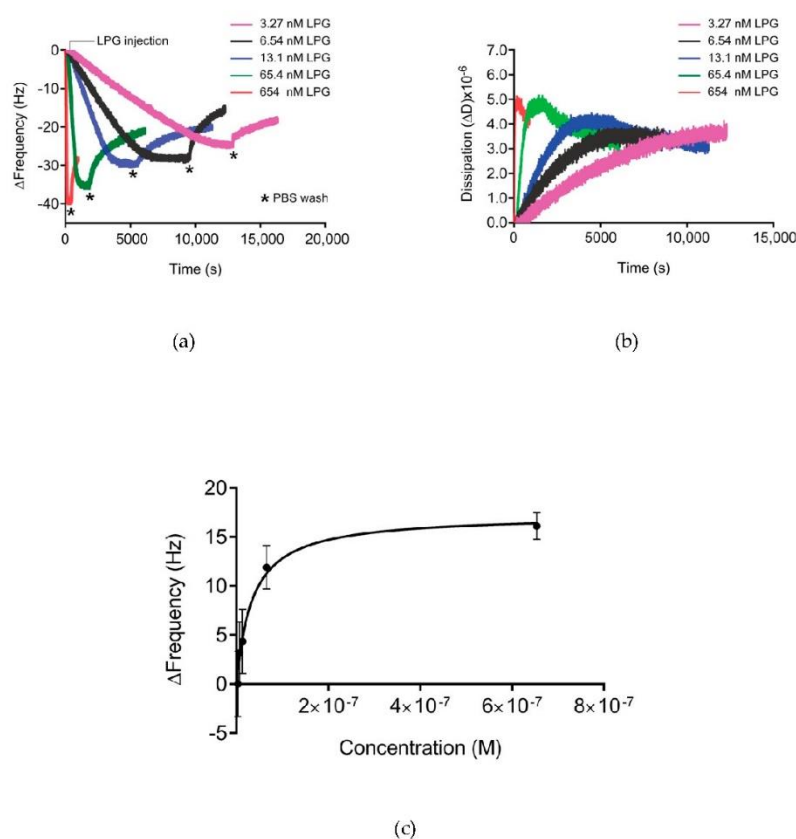


**Figure 5.** (a)  $\Delta f$  and (b)  $\Delta D$  for the 3rd overtone of the absorbed LPG on silica-coated QCM-D crystals at various concentrations (3.27–654 nM). The measurement consists of three steps with flow rates of 150  $\mu\text{L}/\text{mL}$ —baseline formation (PBS buffer), adsorption (LPG in PBS buffer, flow until saturation is achieved), and washing (PBS buffer) to remove unbound LPG. Three independent measurements were performed for each concentration. (c) Langmuir adsorption isotherm for the adsorption of LPG to silica. The data were fitted using the single-site-specific binding model.

Presentation of the QCM-D data in Figure 5 as  $\Delta D$  versus  $\Delta f$  ( $Df$  plots) enabled the comparison of adsorption behavior for different concentrations of LPG (Figure 6).  $Df$  plots depend dynamically on the effective deposited mass, its viscoelastic properties, the structure of the protein, and how these

features evolve over time during interactions. The region between the dotted lines in the  $Df$  plot represents the viscoelastic region between a pure elastic mass response where  $\Delta D = 0$  and a pure liquid viscosity–density change in the fluid above the crystal in the absence of surface binding [19,32,33]. The binding interactions between different LPG concentrations and silica surface resulted in a  $Df$  plot that fits within the viscoelastic region. Over the concentrations of LPG tested, the dynamic adsorption behavior was the same as shown by the similarly shaped profile for each concentration, with higher concentrations resulting in higher deposited mass, as shown by the larger  $\Delta f$  values at the end of the adsorption phase. These data demonstrate the stability of the LPG binding over the concentrations tested. Other globular proteins display similar stability of binding to surfaces over a range of concentrations, such as albumin binding to platinum [34]. However, it should be noted that the shape and magnitude of the  $\Delta f$  and  $\Delta D$  values are different due to different protein properties such as size and isoelectric point that govern the kinetics of interfacial interactions.

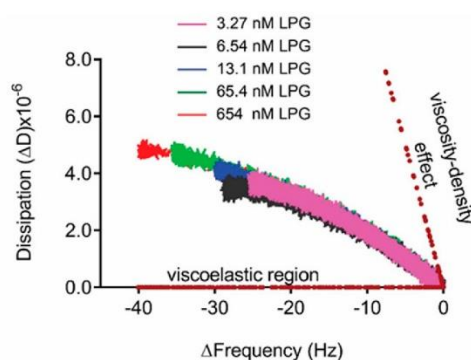


**Figure 6.**  $Df$  plot (3rd overtone) for the binding interactions between LPG and silica surface. The dotted lines indicate the pure elastic mass and viscosity–density responses.

The  $\Delta D$  measurements obtained (Figures 5b and 6) were greater than  $1 \times 10^{-6}$  per 10 Hz, indicating that the adsorbed layer was viscoelastic necessitating the use of the Kelvin–Voigt viscoelastic model to estimate adsorbed mass, thickness, and layer viscosity (Table 2). This model is based on the hypothesis that the adsorbed layer is of uniform density and thickness, does not flow, and maintains its shape. The raw data for the LPG interaction with silica displayed variation in the  $\Delta D$  values between different overtones, with the third overtone ( $n = 3$ ) displaying higher  $\Delta D$  values in comparison to the fifth ( $n = 5$ ), seventh ( $n = 7$ ), and eleventh ( $n = 11$ ) overtones (Figure S3, Supplementary Materials). Table 2 presents the various viscoelastic parameters for the binding interactions between LPG and the silica-coated QCM-D crystal at the association and dissociation phases obtained from modelling the data by applying the Kelvin–Voigt model using the 3rd overtone.

**Table 2.** Viscoelastic parameters for LPG and silica-binding interactions obtained by fitting the raw QCM-D data using the Kelvin–Voigt model for three sample replicates.

	Thickness (@ $R_{eq}$ ) <sup>a</sup> nm	Thickness (@ $k_d$ ) <sup>b</sup> nm	Mass Deposited (@ $R_{eq}$ ) ng/cm <sup>2</sup>	Mass Deposited (@ $k_d$ ) ng/cm <sup>2</sup>	Viscosity (@ $R_{eq}$ ) $\times 10^{-4}$ kg/ms	Viscosity (@ $k_d$ ) $\times 10^{-4}$ kg/ms
LPG/SiO <sub>2</sub>	7.84 $\pm$ 0.22	5.59 $\pm$ 0.22	862.95 $\pm$ 42.43	615.13 $\pm$ 58.06	24.70 $\pm$ 0.50	20.57 $\pm$ 0.45

<sup>a</sup> @ $R_{eq}$ , frequency shift at equilibrium; <sup>b</sup> @ $k_d$ , equilibrium achieved after dissociation.



The maximum thickness of the peptide layer calculated by the Kelvin–Voigt model was 7 nm, and the raw data for both the thickness and viscosity (Figure S4, Supplementary Materials) correlate with each other. This observation further supports the formation of a viscous multilayer of peptides on the surface of the silica. The viscous nature of the peptide layers can also be explained by the system response observed upon introduction of the washing buffer (PBS). The soft and viscous layer formed was reduced in size upon rinsing, suggesting the removal of a loosely bound peptide. This can be explained by the fact that the silica-binding peptide sequence used for our studies has a considerable number of hydrophobic amino acid residues (26 residues out of a total of 91 residues). The PBS washing step reduced the  $\Delta f$  and  $\Delta D$  consistent with the removal of loosely bound peptides via disruptions of the hydrophobic bonds to form a stable multilayer structure. In a similar study, a purely hydrophobic silica-binding peptide was reported to form a multilayer on silica via hydrophobic binding [35]. The authors found a multilayer formation on silica for a purely hydrophobic silica-binding peptide and concluded that it was not only the nature of the peptide itself, but also the hydrophobicity/hydrophilicity of the surface which governed the binding interaction between the two [35]. A monolayer of LPG (30.4 kDa) was approximated to 350 ng/cm<sup>2</sup> for an end-on orientation and 190 ng/cm<sup>2</sup> for a side-on orientation on a dry mass basis when assuming LPG to be a globular protein approximately half the size of albumin (66 kDa) due to its molecular weight being approximately half. The 7 nm thick layer of immobilized LPG equates to approximately 770 ng/cm<sup>2</sup> that was hydrated and viscoelastic in nature. Adsorbed mass estimates from QCM-D include the bound water associated with the proteins and, for globular proteins, the hydration is reported to account for approximately 50% of the mass [36]. This together with the relatively low dissipation values observed during LPG adsorption to silica suggested that LPG adsorbed to silica predominantly in an end-on orientation. The end-on-end peptide orientation is an advantage for immobilizing proteins on the surface since the PG part of the LPG is free and oriented towards the solution phase, enabling maximal interaction with the antibody and, thus, reducing the chances of non-specific binding. The maximum amount of LPG bound to the surface of the silica-coated QCM-D crystal was determined to be 863 ng/cm<sup>2</sup> for 20 µg/mL LPG as this is the maximum concentration of LPG sufficient to saturate the entire surface of the silica crystal. Considering the molecular mass of LPG (30.4 kDa) and the mass of one LPG molecule ( $5.05 \times 10^{-11}$  ng), there are  $1.7 \times 10^{13}$  LPG molecules bound per cm<sup>2</sup> of silica.

An orientation on the surface which makes the binding site available is essential to preserve the bioactivity of immobilized biomolecules. The QCM-D results indicated that LPG binds strongly to silica and forms viscoelastic multilayers with an end-to-end conformation. Further studies were performed to support this finding using an antibody–antigen binding assay. The interaction between silica-immobilized LPG and trastuzumab was determined in various biological fluids (i.e., human serum, mouse serum, and FBS) spiked with the HER2 antigen (Figure 7a). These experiments also provided information about the binding efficiency of the system in the presence of common and more complex biological environments used for clinical biosensing.

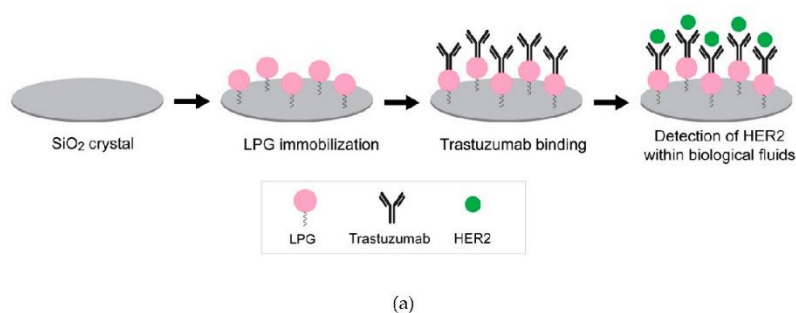
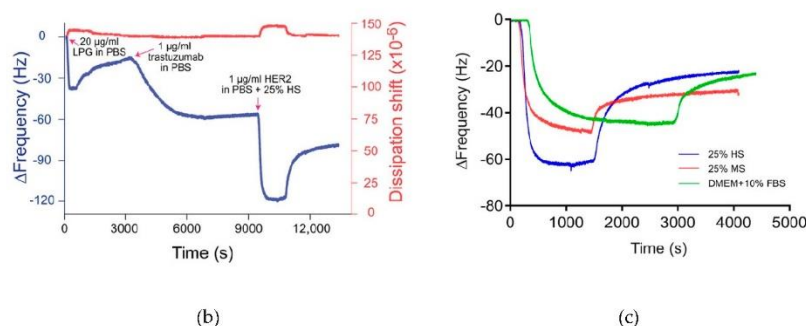


Figure 7. Cont.



**Figure 7.** (a) Experimental workflow to determine the interaction of antibody (trastuzumab) to silica-immobilized LPG. (b) QCM-D response for the binding interactions of trastuzumab to silica-immobilized LPG and subsequent detection of HER2 antigen spiked in 25% human serum. The arrows indicate the time points for the injection of LPG, trastuzumab, and HER2. (c) Frequency shifts for binding interactions between trastuzumab and HER2 spiked in various biological fluids. Extensive PBS washing was performed between each sample injection.

The binding interactions between the immobilized LPG and trastuzumab are shown in Figure 7b. The binding of trastuzumab to LPG is represented by the decrease in  $\Delta f$ . The binding interaction between both molecules was strong since only a negligible  $\Delta f$  was observed after the unbound antibody was washed off. HER2 can bind to the immobilized trastuzumab in buffer which acts as a positive control. Relative binding to this positive control can then be established when HER2 is presented in more complex mixtures including serum. The interaction between trastuzumab and HER2 spiked in 25% human serum and mouse serum as well as DMEM + 10% FBS is shown in Figure 7b and Figure S5, Supplementary Materials. In both the figures, a strong drop in the  $\Delta f$  was observed when HER2 spiked in different serums was injected in the QCM-D, indicating a strong binding of HER2 to trastuzumab. Figure 7c represents the  $\Delta f$  for the binding interactions between trastuzumab and HER2 spiked in different biological fluids. HER2 binds to trastuzumab irrespective of the buffer, with the highest  $\Delta f$  observed in human serum, followed by mouse serum and FBS. The minimum binding interaction in the case of FBS is probably due to the unstable composition of the serum media which may interfere in the efficient detection of HER2. Moreover, there may be some non-specific interactions due to the presence of foreign proteins (e.g., antigens) in FBS. The advantage of human serum over FBS has also been demonstrated in cell culture studies by Heger et al. [37], where human serum remarkably enhanced the invasion and spheroid formation when compared to FBS. In conclusion, with respect to our studies and irrespective of the buffer media, the responses indicate that the HER2 was bound to LPG in such an orientation that its antigen-binding fragments (Fab) were exposed to the surrounding environment.

### 3.4. Linker and Covalent Functionalization of Silica Surface

The efficiency of the LPG-mediated functionalization was compared to the traditional amine coupling method used to covalently bind PG onto the silica-coated QCM-D crystal. Covalent attachment of PG was required for these studies as PG alone did not bind to silica (Figure S2). A glutaraldehyde (GA) linker was used to chemically immobilize PG to an aminated silica surface. Prior to PG conjugation, an amino reactive aldehyde layer was formed on the silica-coated QCM-D crystal by first treating it with oxygen plasma followed by reaction with 3-aminopropyltriethoxysilane (APTES), and finally derivatizing with GA. The length and conditions of the reaction can be altered to control the thickness of the silane layer. After the chemical coupling of PG, a small amount of ethanolamine (in Tris buffer) was added to deactivate the unreacted aldehyde groups, followed by the addition of BSA to block non-specific binding sites. Each of the above-mentioned steps included a thorough washing

step with Milli-Q water. The same experimental procedure was used to calculate the viscoelastic parameters for the binding of antibodies to PG. The QCM-D sensorgrams for the  $\Delta f$  and  $\Delta D$  for three independent measurements are shown in Figure S6, Supplementary Materials, and they revealed that the chemical immobilization of PG resulted in a smaller change in both  $f$  and  $D$ . Modelling these measurements in the Kelvin–Voigt model indicated that chemically immobilized PG formed a thinner layer than physisorbed LPG (Table 3). In addition, the chemically immobilized PG layer supported approximately 38% of the amount of antibody that the LPG layer supported (Table 3), which in turn bound approximately 36% of the amount of antigen as the LPG layer. These data suggest that LPG immobilization on silica was a more efficient method of antibody and antigen capture than chemically immobilized PG. The linker-mediated immobilization was experimentally easy and only took ~6 min. On the contrary, the chemical conjugation had longer experimental time (~3 h) and involved the handling of harsh chemicals.

**Table 3.** Comparison of the viscoelastic parameters for PG immobilization mediated by linker and through chemical conjugation and their subsequent effect on antibody and antigen binding. Each parameter is an average of three independent measurements.

Immobilization	Thickness of Bound Protein (nm)	Mass of Protein Deposited (ng/cm <sup>2</sup> )	Thickness of Bound Antibody (nm)	Mass Deposited for Bound Antibody (ng/cm <sup>2</sup> )	Thickness of Bound Antigen (nm)	Mass Deposited for Bound Antigen (ng/cm <sup>2</sup> )
LPG physisorbed	7.84 ± 0.22	862.95	20 ± 0.05	1200.14	27.84 ± 0.74	1600.47
PG chemically immobilized	2.89 ± 0.18	256.76	7.43 ± 0.15	450.79	12.76 ± 0.22	578.43

#### 4. Conclusions

The binding interaction experiments conducted with LPG and PG on silica provided new quantitative data that support previous observations reported by Sunna et al. [13] based on qualitative data. The binding of the LPG to the silica surface is purely mediated by the silica-specific linker region and was determined to be in the nM range. The results from QCM-D suggest that the linker orientates on the surface to present PG to the soluble phase, thus enabling antibody binding. Furthermore, results obtained from various biophysical characterization techniques showed that the linker has no effect on the overall structure, chemical stability, and hence antibody-binding function of PG. Moreover, when compared to traditional chemical conjugation of biomolecules, the linker-mediated system represents a facile and rapid technology to immobilize protein on a solid surface without compromising its biological function.

**Supplementary Materials:** The following are available online at <http://www.mdpi.com/2218-273X/10/1/4/s1>, Figure S1: Global fit of 1:1 Langmuir binding model with trastuzumab for a 21-single peptide, LP1, Figure S2: Frequency shift for the adsorbed PG on silica coated QCM-D crystal for various concentrations (3.27–654 nM) performed on QCM-D, Figure S3: QCM-D signal from different overtones for LPG binding to silica coated quartz crystal, Figure S4: Overlay of the Kelvin–Voigt fitted raw data for thickness and viscosity for the adsorption of LPG to silica coated crystal,  $n = 3$  overtone, Figure S5: QCM-D response for the binding interactions of trastuzumab to LPG and subsequent detection of HER2 and Figure S6: CM-D response for the binding interactions of trastuzumab to PG and subsequent detection of HER2 spiked in PBS.

**Author Contributions:** Conceptualization, R.B., A.C., and A.S.; methodology, R.B., A.C., S.C.G., Z.E., M.S.L., A.R., and A.S.; data collection, R.B., Z.E., and S.C.G.; data analysis, R.B., S.C.G., Z.E., M.S.L., and A.R.; writing—original draft preparation, R.B. and A.S.; writing—review and editing, R.B., A.C., S.C.G., Z.E., M.S.L., A.R., and A.S.; project administration, A.S. All authors have read and agreed to the published version of the manuscript.

**Funding:** R.B. is supported by an international Macquarie University Research Excellence Scholarship (iMQRES). A.C. is supported by a Cancer Institute New South Wales Early Career Fellowship (Project Number: ECF171114). This work was supported by the Australian Research Council (CE140100003).

**Acknowledgments:** The authors would like to thank Dennis Diaz Rincon for her expertise and assistance with the ÄKTA start protein purification system.



**Conflicts of Interest:** The authors declare no conflict of interest. The funders had no role in the design of the study; in the collection, analyses, or interpretation of data; in the writing of the manuscript; or in the decision to publish the results.

## References

1. Liu, G.Y.; Amro, N.A. Positioning protein molecules on surfaces: A nanoengineering approach to supramolecular chemistry. *Proc. Natl. Acad. Sci. USA* **2002**, *99*, 5165–5170. [\[CrossRef\]](#)
2. Chan, W.C.W.; Nie, S. Quantum dot bioconjugates for ultrasensitive nonisotopic detection. *Science* **1998**, *281*, 2016–2018. [\[CrossRef\]](#) [\[PubMed\]](#)
3. Phizicky, E.; Bastiaens, P.I.; Zhu, H.; Snyder, M.; Fields, S. Protein analysis on a proteomic scale. *Nature* **2003**, *422*, 208–215. [\[CrossRef\]](#) [\[PubMed\]](#)
4. Matsuno, H.; Sekine, J.; Yajima, H.; Serizawa, T. Biological selection of peptides for poly (l-lactide) substrates. *Langmuir* **2008**, *24*, 6399–6403. [\[CrossRef\]](#) [\[PubMed\]](#)
5. Hnilova, M.; Oren, E.E.; Seker, U.O.S.; Wilson, B.R.; Collino, S.; Evans, J.S. Effect of molecular conformations on the adsorption behavior of gold-binding peptides. *Langmuir* **2008**, *24*, 12440–12445. [\[CrossRef\]](#) [\[PubMed\]](#)
6. Serizawa, T.; Sawada, T.; Matsuno, H. Highly specific affinities of short peptides against synthetic polymers. *Langmuir* **2007**, *23*, 11127–11133. [\[CrossRef\]](#) [\[PubMed\]](#)
7. Bansal, R.; Care, A.; Lord, M.S.; Walsh, T.R.; Sunna, A. Experimental and theoretical tools to elucidate the binding mechanisms of solid-binding peptides. *N. Biotechnol.* **2019**, *52*, 9–18. [\[CrossRef\]](#)
8. Naik, R.R.; Stringer, S.J.; Agarwal, G.; Jones, S.E.; Stone, M.O. Biomimetic synthesis and patterning of silver nanoparticles. *Nat. Mater.* **2002**, *1*, 169–172. [\[CrossRef\]](#)
9. Nel, A.E.; Madler, L.; Velegol, D.; Xia, T.; Hoek, E.M.V.; Somasundaran, P. Understanding biophysicochemical interactions at the nano-bio interface. *Nat. Mater.* **2009**, *8*, 543–557. [\[CrossRef\]](#)
10. Seker, U.O.S.; Wilson, B.; Dincer, S.; Kim, I.W.; Oren, E.E.; Evans, J.S.; Tamerler, C.; Sarikaya, M. Adsorption behaviour of linear and cyclic genetically engineered platinum binding peptides. *Langmuir* **2007**, *23*, 7895–7900. [\[CrossRef\]](#)
11. Sultan, A.M.; Westcott, Z.C.; Hughes, Z.E.; Palafox-Hernandez, J.P.; Giesa, T.; Puddu, V. Aqueous peptide–TiO<sub>2</sub> interfaces: Isoenergetic binding via either entropically or enthalpically driven mechanisms. *ACS Appl. Mater. Interface* **2016**, *8*, 18620–18630. [\[CrossRef\]](#) [\[PubMed\]](#)
12. Sawada, T.; Okeya, Y.; Hashizume, M.; Serizawa, T. Screening of peptides recognizing simple polycyclic aromatic hydrocarbons. *Chem. Commun. (Camb. U.K.)* **2013**, *49*, 5088–5090. [\[CrossRef\]](#) [\[PubMed\]](#)
13. Sunna, A.; Chi, F.; Bergquist, P.L. A linker peptide with high affinity towards silica-containing materials. *N. Biotechnol.* **2013**, *30*, 485–492. [\[CrossRef\]](#) [\[PubMed\]](#)
14. Liang, L.; Care, A.; Zhang, R.; Lu, Y.; Packer, N.H.; Sunna, A.; Qian, Y.; Zvyagin, A.V. Facile assembly of functional upconversion nanoparticles for targeted cancer imaging and photodynamic therapy. *ACS Appl. Mater. Interfaces* **2016**, *8*, 11945–11953. [\[CrossRef\]](#) [\[PubMed\]](#)
15. Care, A.; Petroll, K.; Gibson, E.S.Y.; Bergquist, P.L.; Sunna, A. Solid-binding peptides for immobilisation of thermostable enzymes to hydrolyse biomass polysaccharides. *Biotechnol. Biofuels* **2017**, *10*, 1–16. [\[CrossRef\]](#) [\[PubMed\]](#)
16. Sayyadi, N.; Care, A.; Connally, R.E.; Try, A.C.; Bergquist, P.L.; Sunna, A. A novel universal detection agent for time-gated luminescence bioimaging. *Sci. Rep.* **2016**, *6*, 1–9. [\[CrossRef\]](#) [\[PubMed\]](#)
17. Shipunova, V.O.; Zelepukin, I.V.; Stremovskiy, O.A.; Nikitin, M.P.; Care, A.; Sunna, A.; Zvyagin, A.V.; Deyev, S.M. Versatile platform for nanoparticle surface bioengineering based on SiO<sub>2</sub>-binding peptide and proteinaceous Barnase\*Barstar interface. *ACS Appl. Mater. Interfaces* **2018**, *10*, 17437–17447. [\[CrossRef\]](#) [\[PubMed\]](#)
18. Voinova, M.B.; Jonson, M.; Kasemo, B. ‘Missing mass’ effect in biosensor’s QCM applications. *Biosens. Bioelectron.* **2002**, *17*, 835–841. [\[CrossRef\]](#)
19. Lord, M.S.; Whitelock, J.M.; Simmons, A.; Williams, R.L.; Milthorpe, B.K. Fibrinogen adsorption and platelet adhesion to silica surfaces with stochastic nanopopography. *Biointerphases* **2014**, *9*, 041002. [\[CrossRef\]](#)
20. Liu, S.X.; Kim, J.T. Application of Kevin-Voigt model in quantifying whey protein adsorption on Polyethersulfone using QCM-D. *JALA* **2009**, *14*, 213–220. [\[CrossRef\]](#)



21. Hovgaard, M.B.; Dong, M.; Otzen, D.E.; Besenbacher, F. Quartz Crystal Microbalance studies of multilayer glucagon fibrillation at the solid-liquid interface. *Biophys. J.* **2007**, *93*, 2162–2169. [[CrossRef](#)] [[PubMed](#)]
22. Whitmore, L.; Wallace, B.A. DICHROWEB: An online server for protein secondary structure analyses from circular dichroism spectroscopic data. *Nucleic Acids Res.* **2004**, *32*, W668–W673. [[CrossRef](#)] [[PubMed](#)]
23. Sreerama, N.; Venyaminov, S.Y.; Woody, R.W. Estimation of the number of helical and strand segments in proteins using CD spectroscopy. *Protein Sci.* **1999**, *8*, 370–380. [[CrossRef](#)] [[PubMed](#)]
24. Sreerama, N.; Woody, R.W. Estimation of protein secondary structure from CD spectra: Comparison of CONTIN, SELCON and CDSSTR methods with an expanded reference set. *Anal. Biochem.* **2000**, *287*, 252–260. [[CrossRef](#)] [[PubMed](#)]
25. Sreerama, N.; Venyaminov, S.Y.; Woody, R.W. Estimation of protein secondary structure from CD spectra: Inclusion of denatured proteins with native protein in the analysis. *Anal. Biochem.* **2000**, *287*, 243–251. [[CrossRef](#)]
26. Goward, C.R.; Irons, L.I.; Murphy, J.P.; Atkinson, T. The secondary structure of Protein G', a robust molecule. *Biochem. J.* **1991**, *274*, 503–507. [[CrossRef](#)]
27. Khrapunov, S. Circular dichroism spectroscopy has intrinsic limitations for protein secondary structure analysis. *Anal. Biochem.* **2009**, *389*, 174–176. [[CrossRef](#)]
28. Atkins, P.W. *Physikalische Chemie*; Wiley-VCH: Weinheim, Germany, 2001.
29. Seker, U.O.S.; Wilson, B.; Sahin, D.; Tamerler, C.; Sarikaya, M. Quantitative affinity of genetically engineered repeating polypeptides to inorganic surfaces. *Biomacromolecules* **2009**, *10*, 250–257. [[CrossRef](#)]
30. Hnilova, M.; So, C.R.; Oren, E.E.; Wilson, B.R.; Kacar, T.; Tamerler, C.; Sarikaya, M. Peptide-directed co-assembly of nanopores on multimeral patterned solid surfaces. *Soft Matter* **2012**, *8*, 4327–4334. [[CrossRef](#)]
31. Seker, U.O.S.; Sharma, V.K.; Akhavan, S.; Demir, H.V. Engineered peptides for nanohybrid assemblies. *Langmuir* **2014**, *30*, 2137–2143. [[CrossRef](#)]
32. Marx, K.A. Quartz crystal microbalance: A useful tool for studying thin polymer films and complex biomolecular systems at the solution-surface interface. *Biomacromolecules* **2003**, *4*, 1099–1120. [[CrossRef](#)] [[PubMed](#)]
33. Zhou, T.; Marx, K.A.; Warren, M.; Schulze, H.; Braunhut, S.J. The quartz crystal microbalance as a continuous monitoring tool for the study of endothelial cell surface attachment and growth. *Biotechnol. Prog.* **2000**, *16*, 268–277. [[CrossRef](#)] [[PubMed](#)]
34. Palmer, J.C.; Green, R.A.; Boscher, F.; Poole-Warren, L.A.; Carter, P.M.; Enke, Y.L.; Lovell, N.H.; Lord, M.S. Development and performance of a biomimetic artificial perilymph for in vitro testing of medical devices. *J. Neural Eng.* **2019**, *16*, 026006. [[CrossRef](#)] [[PubMed](#)]
35. Puddu, V.; Perry, C.C. Peptide adsorption on silica nanoparticles: Evidence of hydrophobic interactions. *ACS Nano* **2012**, *6*, 6356–6363. [[CrossRef](#)]
36. Höök, F.; Vörös, J.; Rodahl, M.; Kurrat, R.; Böni, P.; Ramsden, J.J.; Textor, M.; Spencer, N.D.; Tengvall, P.; Gold, J.; et al. A comparative study of protein adsorption on titanium oxide surfaces using in situ ellipsometry, optical waveguide lightmode spectroscopy, and quartz crystal microbalance/dissipation. *Colloids Surf. B Biointerfaces* **2002**, *24*, 155–170. [[CrossRef](#)]
37. Heger, J.I.; Froehlich, K.; Pastuszek, J.; Schmidt, A.; Baer, C.; Mrowka, R.; Backsh, C.; Schleußner, E.; Markert, U.R.; Schmidt, A. Human serum alters cell culture behavior and improves spheroid formation in comparison to fetal bovine serum. *Exp. Cell Res.* **2018**, *365*, 57–65. [[CrossRef](#)]



© 2019 by the authors. Licensee MDPI, Basel, Switzerland. This article is an open access article distributed under the terms and conditions of the Creative Commons Attribution (CC BY) license (<http://creativecommons.org/licenses/by/4.0/>).

## Supplementary information

**biomolecules***Supplementary Material*

### Elucidating the binding mechanism of a novel silica-binding peptide

Rachit Bansal <sup>1,2</sup>, Zehra Elgundi <sup>3</sup>, Andrew Care <sup>1,2</sup>, Sophia C. Goodchild <sup>1</sup>, Megan S. Lord <sup>3</sup>,

Alison Rodger <sup>1</sup>, and Anwar Sunna <sup>1,2,4</sup> \*

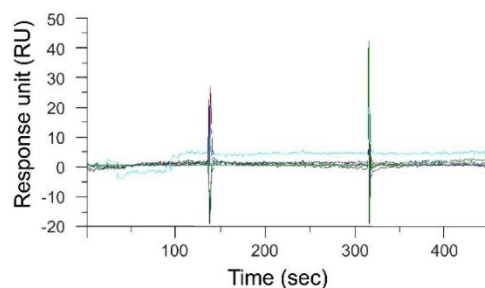
<sup>1</sup> Department of Molecular Sciences, Macquarie University, Sydney, NSW 2109, Australia ; rachit.bansal@hdr.mq.edu.au (R.B) ; andrew.care@mq.edu.au (A.C); sophia.goodchild@mq.edu.au (S.G); alison.rodger@mq.edu.au (A.R); anwar.sunna@mq.edu.au (A.S)

<sup>2</sup> ARC Centre of Excellence for Nanoscale Biophotonics, Macquarie University, Sydney, NSW 2109, Australia

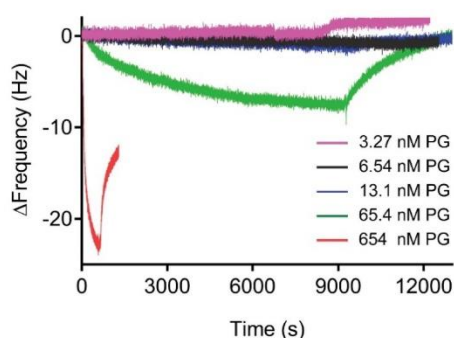
<sup>3</sup> Graduate School of Biomedical Engineering, University of New South Wales, Sydney, NSW 2052, Australia ; z.elgundi@unsw.edu.au (Z.E) ; m.lord@unsw.edu.au (M.L)

<sup>4</sup> Biomolecular Discovery and Design Research Centre, Macquarie University, Sydney, NSW 2109, Australia

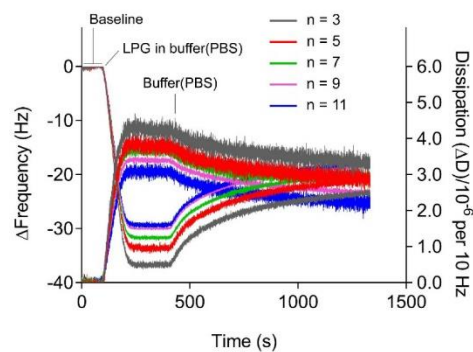
\* Correspondence: anwar.sunna@mq.edu.au; Tel.: +612-9850-4220



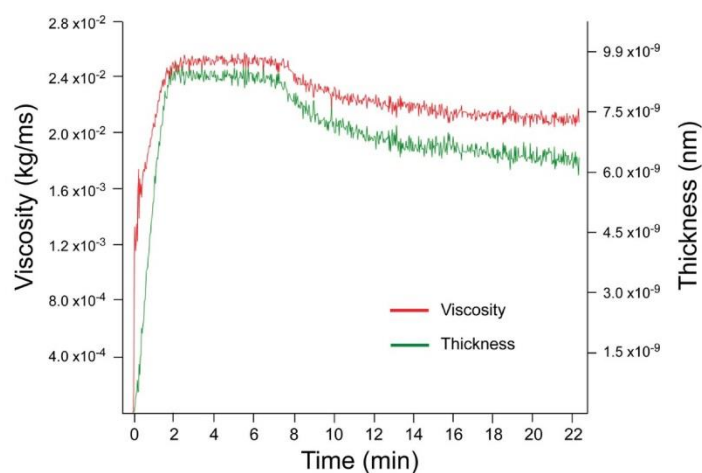
**Figure S1.** Global fit of 1:1 Langmuir binding model with trastuzumab for a 21-single peptide, LP1 (VKTQATSREEPPRLPSKHPG). Black lines constitute two repeat injections of the LP1 peptide over trastuzumab immobilized on a surface. The concentrations of LP1 peptide injected were 23.1, 11.6, 5.79, 2.89 and 1.45 nM.



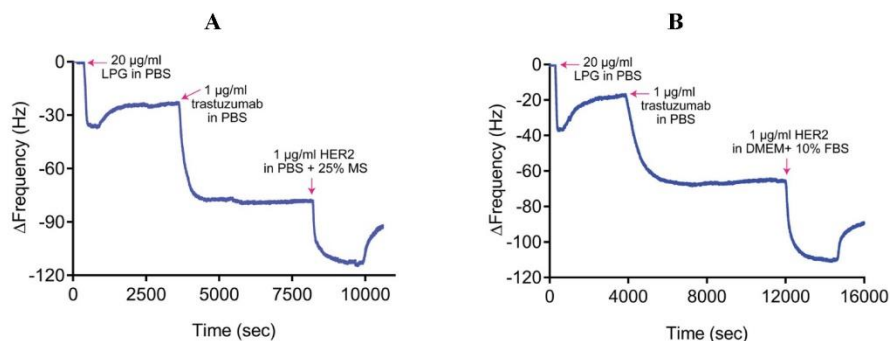
**Figure S2.** Frequency shift for the absorbed PG on silica coated QCM-D crystal for various concentrations (3.27-654 nM) performed on QCM-D,  $n=3$ . The measurement consists of three steps: baseline formation (PBS buffer, flow rate= 150  $\mu\text{L}/\text{min}$ ), adsorption (PG in PBS buffer, flow rate= 150  $\mu\text{L}/\text{min}$ , flow till a saturation is achieved and then stop injection), and washing (PBS buffer, flow rate= 150  $\mu\text{L}/\text{min}$ ) to get rid of unbound PG. The graph showed almost all PG was dissociated after washing with PBS buffer. Three independent measurements were performed for each concentration and the graph presented in this figure is for clarification.



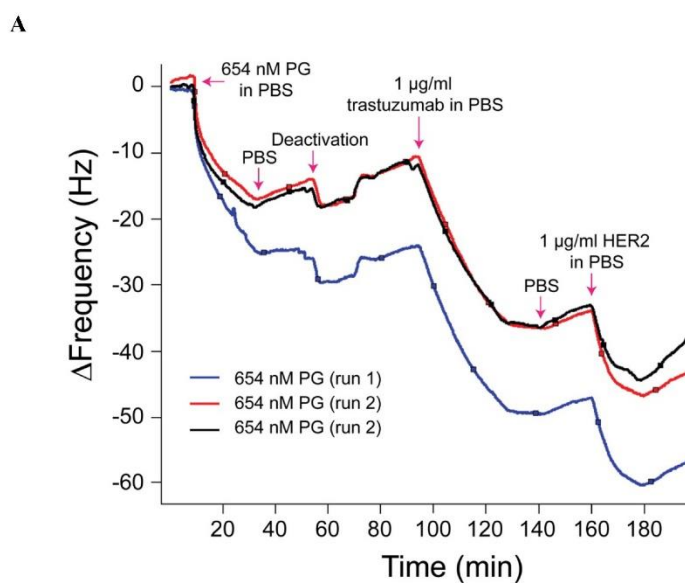
**Figure S3.** QCM-D signal from different overtones for LPG binding to silica coated quartz crystal. As displayed in the figure, the baseline is first established by injecting PBS buffer followed by 654 nM of LPG solution (in PBS), and finally washing with PBS buffer again. A decrease in the frequency shift is a result of LPG adsorption onto silica coated crystal. Since the signals from different overtones does not overlap and are not close to each other, with a significant dissipation response, the adsorbed LPG layer is viscous and multilayered.



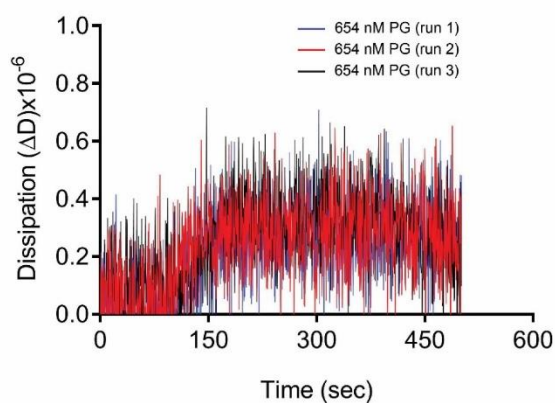
**Figure S4.** Overlay of the Kelvin-Voigt fitted raw data for thickness and viscosity for the adsorption of LPG to silica coated crystal,  $n=3$  overtone. The frequency and dissipation signal for both the parameters follow each other, showing the formation of a viscous peptide layer.



**Figure S5.** QCM-D response for the binding interactions of trastuzumab to LPG and subsequent detection of HER2 spiked in (A) PBS+25% mouse serum (MS) and (B) DMEM+10% fetal bovine serum (FBS). 20  $\mu$ g/ml LPG (654 nM) in PBS was immobilized to silica surface and the non-specific binding was avoided using a solution of 1 mg/ml BSA in PBS. The arrows indicate the time points for the injection of LPG, trastuzumab and HER2, with PBS washing between each sample injection.





**B**

**Figure S6.** (A) QCM-D response for the binding interactions of trastuzumab to PG and subsequent detection of HER2 spiked in PBS. 654 nM of PG (in PBS) was immobilized to amine activated silica surface. Deactivation of the unused groups was carried by injecting 0.1 M Tris, 50 mM ethanolamine (pH 9.0), followed by blocking with 1 mg/ml BSA to avoid non-specific binding interactions. The arrows indicate the time points for the injection of PG, trastuzumab and HER2, with a PBS washing between each sample injection. (B)  $\Delta D$  for the 3<sup>rd</sup> overtone of the chemisorbed PG on silica coated QCM-D crystals for three independent measurements at a final PG concentration of 654 nM.

## **Chapter 3**

Effect of solid-binding peptide  
multimerization on its binding  
to silica-based materials

### 3.1 Introduction

The previous chapter highlighted the binding mechanism of a silica-binding peptide, Linker Protein G (LPG) and how the linker enhances the binding of PG to silica surface without affecting its structural and chemical properties. In this chapter, we studied the effect of multimerization on the binding affinity of LPG. Among several molecule design methods, multimerization can be used to tune the overall binding and physical and chemical properties of an SBP by applying simple tandem repeat of the original SBP sequence. Various truncated derivatives of 4xLPG (LPG) were constructed and analysed using the same biophysical characterization techniques as used in the previous chapter. It was found that the degree of silica-binding is proportional to the linker repeats, i.e. truncated derivative with single sequence showed no measurable binding while the one with two sequence repeats displayed moderate binding to silica. The binding was found to increase with the number of repeats where the three repeats showed a  $K_D=53.23 \pm 4.5$  nM, which is 1.5 lower than the 4xLPG. Also, the spectroscopic techniques revealed that the linker repeats don't have any effect on the overall structure or chemical stability of parent, PG. The effect of overall linker length on silica binding was also studied, where the three repeat sequence was replaced by a glycine-rich spacer to form the fusion protein, 1X-(GGGS)<sub>12</sub>-PG. Surprisingly, this fusion protein binds with comparable affinity to silica (qualitatively). This overall study demonstrated that not the peptide repeats but the peptide length mediates a strong silica-binding owing to increased flexibility and plasticity of the peptide.

This chapter has been prepared as a manuscript for submission to *ACS Biomacromolecules*.

### 3.2 Contribution to manuscript 3

The concept of this publication was developed together with my main supervisor A/Prof Anwar Sunna and my co-supervisor Dr. Andrew Care. They were also involved in experimental designing and troubleshooting. I designed and performed all the experimental work including data collection and analysis. The initial draft of the manuscript was written by me and was reviewed by all authors. The contributions of each author are given in Table 3.1

Table 3.1 Author contributions for manuscript 3

	Conceptualization	Methodology	Data collection	Data analysis	Manuscript
Rachit Bansal	✓	✓	✓	✓	✓
Zehra Elgundi		✓	✓	✓	✓
Sophia C. Goodchild	✓	✓			✓
Andrew Care		✓	✓	✓	✓
Megan S. Lord		✓		✓	✓
Alison Rodger		✓		✓	✓
Anwar Sunna	✓	✓			✓

### 3.3 Manuscript 3

#### **Effect of solid-binding peptide multimerization on its binding to silica-based materials**

Rachit Bansal <sup>a,b</sup>, Zehra Elgundi <sup>c</sup>, Sophia C. Goodchild <sup>a</sup>, Andrew Care <sup>a,b</sup>, Megan S. Lord <sup>c</sup>, Alison Rodger <sup>a</sup>, Anwar Sunna <sup>a,b,d\*</sup>

<sup>a</sup> Department of Molecular Sciences, Macquarie University, Sydney, NSW 2109, Australia

<sup>b</sup> ARC Centre of Excellence for Nanoscale Biophotonics, Macquarie University, Sydney, NSW 2109, Australia

<sup>c</sup> Graduate School of Biomedical Engineering, University of New South Wales, Sydney, NSW 2052, Australia

<sup>d</sup> Biomolecular Discovery and Design Research Centre, Macquarie University, Sydney, NSW 2109, Australia

\*Corresponding author

Anwar Sunna  
Department of Molecular Sciences  
Macquarie University  
North Ryde, NSW 2109  
Australia

Phone: +61 2 9850 4220

Fax: +61 2 9850 8313

Email: [anwar.sunna@mq.edu.au](mailto:anwar.sunna@mq.edu.au)



## Abstract

The bifunctional linker-protein G (LPG) fusion protein is comprised of a peptide (linker) sequence and a truncated form of *Streptococcus* strain G148 protein G (protein G'). The linker represents a multimeric solid-binding peptide (SBP) comprised of  $4 \times 21$ -amino acid sequence repeat that displayed high binding affinity towards silica-based materials. In this study, several truncated derivatives were investigated to determine the effect of the SBP multimerization on the silica binding function of LPG (for the sake of clarity, LPG will be referred from here on as 4xLPG). Various biophysical characterization techniques were used to quantify and compare the truncated derivatives against 4xLPG and protein G' without linker. The derivative containing two sequence repeats (2xLPG) showed minimal binding to silica while the truncated derivative with only a single sequence (1xLPG) displayed no binding. The derivative containing three sequence repeats (3xLPG) was able to bind to silica but with a binding affinity of  $K_D = 53.23 \pm 4.5$  nM. This value represents a 1.5 times lower binding affinity than that obtained for 4xLPG under similar experimental conditions. Circular dichroism (CD) spectroscopy and fluorescence spectroscopy studies indicated that the SBP degree of multimerization has no effect on the secondary structure and chemical stability of the parent protein G. However, based on quartz crystal microbalance with dissipation monitoring (QCM-D) multimerization was an important parameter for a strong and stable binding to silica. The replacement of 3 sequence repeats by a (GGGGS)<sub>12</sub> glycine-rich spacer indicated that the overall length rather than the SBP multimerization mediated the effective binding to silica.

## Keywords

Linker-protein G; multimerization; solid-binding peptide (SBP); silica-binding peptide; silica-based materials; quartz crystal microbalance with dissipation monitoring (QCM-D).

## Introduction

Solid-binding peptides (SBPs) are a group of short amino acid sequences that specially bind to the surfaces of various inorganic materials including minerals, semiconductors and polymers. In doing so, they are able to mediate the simple and controlled attachment of biomolecules onto solid surfaces, conferring biological functionality. SBPs can also act as functionalizing agents for binding and linking biomolecules to solid nanostructures (1,2). Molecular biology protocols further allow tailoring of the selected peptides to tune their

binding and material selectivity properties so that they can be used in bionanotechnological applications. Some of these SBPs have already been used in the development of multifunctional hybrid materials and for the oriented immobilization of biomolecules (3-5). For example, Coyle et al. demonstrated the use of a silica-binding dodecapeptide (Car9), having micromolar affinity to silica gel, for the purpose of a rapid and inexpensive affinity purification technique (6). Two polystyrene-binding peptides screened by Kumada et al. (5) were shown to mediate an effective site-specific immobilization of proteins onto polystyrene surfaces without considerable conformational change, using an enzyme linked immunosorbent assay (ELISA). To improve hospital sanitation and reduce biohazard exposure, Mansoor et al. developed a graphene wireless nanosensor based on a bifunctional peptide system, where a graphene-binding peptide (GrBP) was fused with an antimicrobial peptide (AMP) to recognize and capture pathogens such as *Staphylococcus aureus* and *Helicobacter pylori* (7). The bifunctional peptide approach was also used by Cui et al. (8) to develop a graphene field effect transistor (GFET)-based sensor device for efficient vapor phase detection of trinitrotoluene (TNT), where a TNT-binding peptide domain was fused to a GrBP. SPBs have initiated and regulated the synthesis of composite materials, such as biosynthesis of silver nanoparticles using combinatorially-selected silver-binding peptides (9).

Proper orientation is crucial to preserve the bioactivity as well as the avidity of biomolecules. Care et al. demonstrated the oriented immobilization of antibodies onto silica-coated magnetic particles using a bifunctional linker-protein G (LPG) fusion protein which contains a silica-

binding peptide and an antibody-binding region (10). Other applications of SBPs include the design of medical biomaterials via surface modification. One such case has been reported for the use of a bispecific material-binding peptide, TBP-NHBP, which was designed as a fusion of a titanium-binding peptide (TBP) and single walled carbon nanohorn-binding peptide (NHBP) connected via a GG linker (11). TBP-NHBP displayed binding affinity to both titanium and single walled carbon nanohorn (SWNH). TBP-NHBP was applied for the efficient loading and controlled release of drugs such as dexamethasone (DEX), necessary for bone regeneration and osteogenesis. Similarly, a titanium-binding peptide fused to an antimicrobial peptide was shown to reduce bacterial growth on titanium-made dental implants (12).

The binding of SBPs to their corresponding materials is governed by several non-covalent

interactions (e.g. electrostatic, polar, hydrophobic, hydrogen bonds) and these interactions can result in equilibrium binding constants in the nM to sub-mM range (2,13). However, due to the complexity (14,15) displayed at the SBP–material interface (9) many of the mechanisms involved in these interactions remain poorly understood. At present, a collection of experimental and theoretical tools is available to investigate these interactions. For example, surface plasmon resonance (SPR) (16), quartz crystal microbalance with dissipation monitoring (QCM-D) (17), and isothermal titration calorimetry (18) can be used to investigate the selectivity, binding kinetics, thermodynamics, stoichiometry, orientation, and viscoelastic properties of these interactions. Circular dichroism (CD) spectroscopy (19), nuclear magnetic resonance (NMR) spectroscopy (20) and Fourier-transform infrared (FTIR) spectroscopy (21) provide information about dynamics, structure and conformation of SBPs. Computational approaches such as *in silico* molecular modelling and simulation (22) with the development of artificial intelligence (23,24) provides in depth knowledge of these interfaces at atomic level (25).

The interactions between SBPs and their substrates relies on the affinity that particular chemical groups within amino acid residues have for solid surfaces. For example, SBPs that bind to metals predominantly contain hydrophobic and hydroxyl-containing polar residues (13) while those that bind to carbon-based materials are high in aromatic residues (26). Various molecular-tailoring strategies can be applied to tune the affinity and selectivity of SBPs, the most common being site-specific mutagenesis. Another method used to tune the binding and structural features of an SBP is by increasing the number of repeats of the original SBP sequence, also known as multimerization (27,28). Multimerization can be achieved by the sequential attachment of the original sequence (i.e. simple tandem repeat of the peptide sequence). For example, Seker et al (29) reported the improved affinity and selectivity of a gold-binding peptide (GBP) as a function of polypeptide sequence repeats. Using SPR, they showed that a 3-repeat GBP (3R-GBP) was able to bind 5 times more strongly to gold when compared to 1-repeat GBP (1R-GBP). In another case, Cho et al. (30) used ITC analysis to show that a zinc oxide-binding peptide (ZBP) with triplicate tandem repeats (3xZBP) displayed nearly two-fold higher binding affinity ( $K_D = 0.69 \mu\text{M}$ ) to zinc oxide nanoparticles when compared to the single peptide domain (1xZBP,  $K_D = 1.5 \mu\text{M}$ ). These findings implied that there might be a direct relationship between the binding activity and the number of repeated sequences for some SBPs.

LPG (for the sake of clarity, LPG will be referred from here on as 4xLPG) was initially reported by Sunna et al. (1) and was designed as a bifunctional fusion protein for the rapid and oriented biofunctionalization of silica-based materials (31-33). 4xLPG connects a recombinant form of *Streptococcus* protein G' antibody-binding protein to a multimeric linker made of a  $4 \times 21$ -amino acid sequence repeat that display high binding affinity towards silica-based materials. Here, we used various biophysical characterization techniques to examine several truncated derivatives of 4xLPG and to determine the effect of the linker multimerization on the stability of the parental protein G. The study also provides insights into the general effect of SBP multimerization on the binding affinity to silica substrate. We also show the potential effect played by the overall length of the SBP on the effective binding to the silica surface.

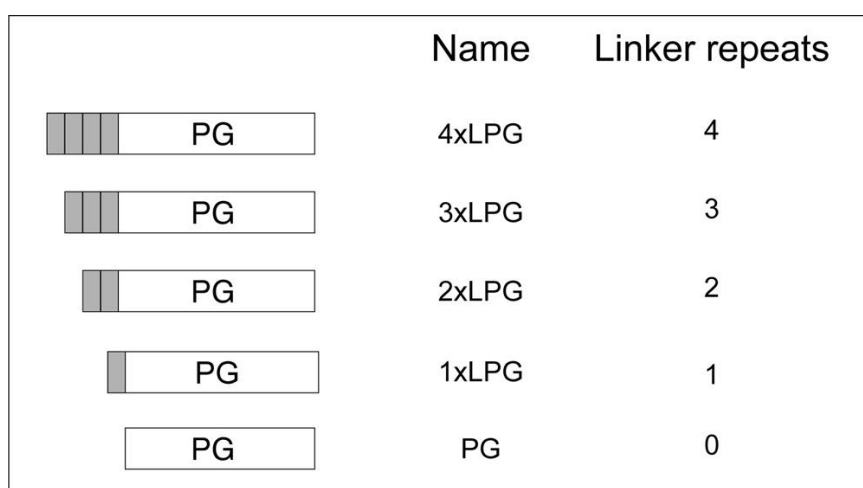


**Figure 1.** Truncated derivatives used in this study.

## Materials and Methods

The silica binding studies were performed using silica coated quartz crystals purchased from ATA Scientific (Australia). Pefabloc, lysozyme and Benzonase nuclease were purchased from Sigma-Aldrich. Human serum was obtained from Sigma-Aldrich while the humanized anti-HER2 monoclonal antibody trastuzumab was purchased from Jomar Life Research. The human HER2/ErbB2 protein (His-Tag) was purchased from Sino Biological Inc. (China). All biological assays were performed at room temperature with standard phosphate-buffered saline (1×PBS) buffer at pH 7.4.

### *Production and purification of truncated derivatives*

The expression plasmids (pLink1xpET22b, pLink2xpET22b and pLink3xpET22b) used to produce the recombinant proteins were previously reported by (1). The production of each of the truncated derivatives (1xLPG, 2xLPG and 3xLPG) was as follows. 1 litre Luria Bertani (LB) medium supplemented with 50 µg/ml carbenicillin was inoculated with 10 mL of an overnight culture of *E. coli* Tuner (DE3) cells (Novagen) harbouring the expression plasmid. The culture was incubated at 37 °C with continuous shaking (250 rpm) until the  $A_{600}$  was approximately 0.7–1.0. The incubation temperature was reduced to 20 °C and protein synthesis was induced by the addition of 0.2 mM isopropyl β-D-thiogalactoside (IPTG). Cells were harvested after 3–4 h induction by centrifugation for 15 min at 10,000 x g and 4 °C and were stored at -20 °C.

The cells were resuspended in ice-cold lysis buffer (25 mM Tris-HCl, pH 8.0, 100 mM NaCl, 1.25 mM EDTA and 0.05% Tween 20), supplemented with 4 mM of the Pefabloc serine protease inhibitor and 1.5 mg lysozyme. They were ruptured by three passages through a French pressure cell. After cell rupture, 50 units of Benzonase nuclease and 4 mM Pefabloc were added. The sample was incubated on ice for 20 min. The debris was removed by centrifugation for 30 min at 20,000 x g and 4 °C. The supernatant obtained was first filtered through a 0.45 µm and then through a 0.22 µm sterile filter and stored at 4 °C.

All purifications were performed using the Äkta™ start chromatography system (GE Healthcare, USA). For purification, each truncated derivative soluble extract (1xLPG, 2xLPG and 3xLPG) was loaded onto a 5 ml HiTrap Q anion exchanger column (GE Healthcare) previously equilibrated with 25 mM Tris-HCl, pH 8.0, supplemented with 100 mM NaCl. The column was washed extensively with the same buffer. Under these conditions all truncated derivatives eluted at 200 mM NaCl. The eluted protein samples were concentrated using an Amicon Ultra-15 centrifugal filter (10 kDa cut-off, Millipore) followed by buffer exchange with a PD-10 desalting column (GE Healthcare). 1xLPG was buffered exchanged into 20 mM Bis-Tris (bis-(2-hydroxyethyl)-amino-tris(hydroxymethyl)-methane) buffer pH 6.0. This fraction was applied again the 5 ml HiTrap Q column previously equilibrated with 20 mM Bis-Tris buffer pH 6.0. The column was washed extensively with the same buffer and the 1xLPG recombinant protein was eluted at 200 mM NaCl. 2xLPG and 3xLPG were buffer exchanged into 50 mM HEPES (4-(2-hydroxyethyl)-1-piperazineethanesulfonic acid) buffer pH 8.0. The fractions were applied to a 5 ml HiTrap SP cation exchanger column (GE Healthcare) previously equilibrated with 50 mM HEPES buffer pH 8.0. The column was washed



extensively with the same buffer. Under these conditions 2xLPG eluted at 50 mM NaCl while 3xLPG eluted at 100 mM NaCl.

Fractions containing the truncated derivatives were identified on 4–15% Mini-PROTEAN® TGX™ Precast Protein Gels (Bio-Rad laboratories) by SDS-PAGE and staining with Coomassie Brilliant Blue. Individual fractions were concentrated using an Amicon Ultra-15 centrifugal filter and all final samples were stored in 1xPBS buffer (after fresh addition of Pefabloc) at -80 °C. The final protein concentration was measured using Micro BCA protein assay kit (ThermoFisher Scientific) according to the manufacturer's instructions.

#### *Construction, production and purification of a synthetic linker derivative*

Three sequence repeats from the 4xLPG peptide linker were replaced by a synthetic (GGGGS)<sub>n</sub> linker sequence. This replacement was important to determine whether the multimerization or the overall SBP length was required for efficient binding to silica. The protein G sequence was ligated into plasmid pET44a (+) via NheI/BamHI restriction sites to obtain the plasmid pET44-PG. A gene sequence containing one original SBP sequence from LPG followed by the synthetic linker sequence (GGGGS)<sub>12</sub> was synthesized by Invitrogen GeneArt Gene Synthesis (ThermoFisher Scientific) and ligated into plasmid pET44-PG via NdeI/NheI restriction sites to assemble the expression plasmid pLink1x-(GGGGS)<sub>12</sub>-PG (Figure 8). *E. coli* α-Select (Bioline) was used as a host for general gene cloning and vector storage and *E. coli* Tuner (DE3) cells were used for recombinant protein expression.

Link1x-(GGGGS)<sub>12</sub>-PG was produced and the soluble protein fraction obtained as described for the truncated derivatives. For purification of Link1x-(GGGGS)<sub>12</sub>-PG, the soluble extract was loaded onto a 5 mL HiTrap Q anion exchanger column previously equilibrated with 25 mM Tris-HCl, pH 8.0, supplemented with 100 mM NaCl. The column was washed extensively with the same buffer. Under these conditions the Link1x-(GGGGS)<sub>12</sub>-PG did not bind to the column and was found in the unbound fraction. The Link1x-(GGGGS)<sub>12</sub>-PG was concentrated using an Amicon Ultra-15 centrifugal filter (10 kDa cut-off) followed by buffer exchange with PD-10 desalting column and 50 mM MES (2-(N-morpholino) ethanesulfonic acid) buffer pH 6.0. This fraction was applied to a 5 mL HiTrap SP cation exchanger column previously equilibrated with 50 mM MES buffer pH

6.0. The column was washed extensively with the same buffer and the Link1x-(GGGS)<sub>12</sub>-PG was eluted at 300 mM NaCl. Fractions containing the Link1x-(GGGS)<sub>12</sub>-PG were identified by SDS-PAGE as described above. Fractions containing the purified Link1x-(GGGS)<sub>12</sub>-PG were pooled and concentrated using an Amicon Ultra-15 centrifugal filter. Samples were stored in 50 mM MES buffer pH 6.0 at -20°C after sterile filtration through a 0.22 µm filter.

#### *Silica binding assay*

The binding of purified recombinant Link1x-(GGGS)<sub>12</sub>-PG to silica was determined as follows; 5 mg silica (BDH Ltd) was washed three times with washing buffer (10 mM Tris-HCl, pH 7.5, 100 mM NaCl and 1% Triton-X100). Soluble protein in a final volume of 100 µl was mixed with silica and incubated by rotation at room temperature for 1 h. The unbound fraction was removed after centrifugation at 14,000 x g for 20 s. The silica pellet was washed three times by vortexing with 100 µl of 100 mM Tris-HCl buffer, pH 8.0. Finally, the silica-bound protein was eluted after addition of 100 µl of SDS PAGE-loading buffer and incubation at 99°C for 10 min (with short mixing every 2 min). Fractions containing the Link1x-(GGGS)<sub>12</sub>-PG protein were identified by SDS-PAGE as described above.

The percentage of protein in the different fractions was semi-quantified by analyzing the intensity of bands of digital images from SDS-PAGE with ImageJ software (<http://rsb.info.nih.gov/ij/index.html>).

#### *Circular Dichroism (CD) spectroscopy*

CD spectra were collected at room temperature (approximately 25°C) on a JASCO J-1500 spectrophotometer (JASCO Corporation, Japan). CD data was collected in water in order to avoid any interference or noise below 200 nm since PBS absorbs strongly at wavelengths below approximately 200 nm. All protein samples were buffer exchanged to Milli-Q water using Amicon Ultra-10K 0.5 mL centrifugal filters and then were further diluted in Milli-Q water to a final concentration of 0.1 mg/mL. Wavelength scans were performed between 180 and 350 nm in a rectangular, 1 mm pathlength quartz cuvette (Starna Scientific Ltd., Ilford, UK). For each sample, 3 accumulations were recorded using a 2 nm bandwidth, a scan speed of 100 nm/min and digital integration time (D.I.T.) of 2 sec. The data is reported in terms of mean residue ellipticity [ $\theta_M$ ], expressed in deg.cm<sup>2</sup>.dmol<sup>-1</sup>. residue<sup>-1</sup>.

### *Fluorescence Spectroscopy*

Protein samples were dissolved to a final concentration of 2  $\mu\text{M}$  in 1xPBS containing various concentrations (0–7 M) of guanidinium hydrochloride (GdnHCl). All measurements were recorded at room temperature (approximately 25°C) in a micro-volume fluorescence cuvette with 3 mm pathlength (Starna Scientific Ltd., Ilford, UK) using a JASCO FP-8500 Spectrofluorometer (JASCO Corporation, Japan). Fluorescence emission spectra were collected between 300 and 550 nm using a 295 nm excitation wavelength, 2.5 nm excitation bandwidth, 5 nm emission bandwidth and scan speed of 100 nm/min.

### *Quartz crystal microbalance with dissipation monitoring (QCM-D)*

The adsorption of the proteins onto silica surface was monitored on a Q-sense E4 system (Biolin Scientific AB, Sweden) using AT-cut  $\text{SiO}_2$  coated QCM-D quartz crystal sensors. The viscoelastic properties of the adsorbing layers were studied by simultaneously measuring the dissipation changes (33). The frequency and dissipation changes were measured at a fundamental frequency of 5 MHz and at 3<sup>rd</sup> overtone (n). All the samples were prepared in

1xPBS buffer pH 7.4 at room temperature. The adsorbed mass is proportional to frequency change via the Sauerbrey equation only when the adsorbed layer is rigid, uniformly distributed on the sensor surface and the adsorbed mass is small compared to the mass of the crystal (35-36). However, in the case of most proteins these assumptions are not valid as the adsorbed layer is viscoelastic as there is a dissipation change greater than  $1 \times 10^{-6}/10$  Hz requiring the use of the Voigt viscoelastic model to estimate adsorbed mass and thickness of the adsorbed protein layer from frequency and dissipation measurements at multiple harmonics and assuming an adsorbed layer density of  $1000 \text{ g/m}^3$ . All QCM-D experiments were repeated three times under a constant flow rate of 150  $\mu\text{L}/\text{min}$  at room temperature (22°C).

### *Orientation and viscoelastic properties of bound 3xLPG truncated derivative*

The  $\text{SiO}_2$  coated crystals were placed in the respective chambers provided in the QSense E4 analyzer and 1xPBS was injected at a flow rate of 150  $\mu\text{L}/\text{min}$  until a stable baseline was reached. Samples of 3xLPG, prepared in 1xPBS, were then injected into the system at a concentration range of 3.27-654 nM and a flow rate of 150  $\mu\text{L}/\text{min}$ . As soon as a stable baseline was achieved for each sample concentration, the unbound fractions were washed off by injecting 1xPBS. To eliminate the risk of non-specific binding, the free binding sites

on the crystal surface were blocked by injecting 1 mg/mL BSA (in 1xPBS). Humanized anti-HER2 monoclonal antibody, trastuzumab, was injected into the system at a final concentration of 1  $\mu$ g/mL until a stable response was observed. The final step included the injection of HER2 antigen at a concentration of 1  $\mu$ g/mL until equilibrium was reached. Each of the above steps included an additional crystal rinsing with 1xPBS.

## Results and Discussion

### *Effect of linker multimerization on the secondary structure and chemical stability of PG*

The bioactivity of a biomolecule is dependent on its secondary structure. Circular dichroism (CD) spectroscopy was used to determine the effect of different truncations of the linker sequence on the overall secondary structure of protein G (PG). A concentration of 0.1 mg/mL (the absorbance for the CD signals measured between 180 nm and 350 nm were normalized to account for the small variations in concentration) was used to measure the far-UV spectra of the truncated derivatives (1xLPG, 2xLP and 3xLPG). Figure 2 shows an overlay of CD spectra obtained for PG alone and the respective linkers. A significant  $\alpha$ -helical folded component can be seen in all the proteins which is evident by the presence of a positive peak at  $\sim$ 190 nm and negative peaks at  $\sim$ 208 nm and  $\sim$ 222 nm. Further, Dichroweb was used to perform the CD secondary structure fitting of this data using SELCON3 algorithm and reference Set 3 (which is optimized for a wavelength range of 185-240 nm). Table 1 represents the various structural fitting parameters obtained for all the truncated derivatives.

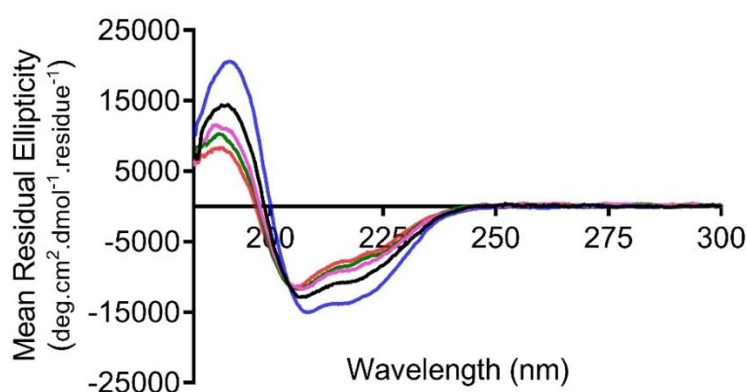


**Figure 2.** Far-UV spectra of PG (blue), 1xLPG (black), 2xLPG (pink), 3xLPG (green) and 4xLPG (red) in water at a concentration of 0.1 mg/ml.

**Table 1:** Structural composition of PG and various truncated derivatives as obtained from CD analysis

<b>Truncated Derivative</b>	<b>% PG in truncated derivative</b>	<b><math>\alpha</math> helix proportion</b>	<b><math>\beta</math> sheet proportion</b>
PG <sup>(34)</sup>	100	~36 %	~17 %
1xLPG	~90	~31 %	~19 %
2xLPG	~82	~25 %	~23 %
3xLPG <sup>(34)</sup>	~75	~24 %	~24 %
4xLPG	~67	~22 %	~27 %

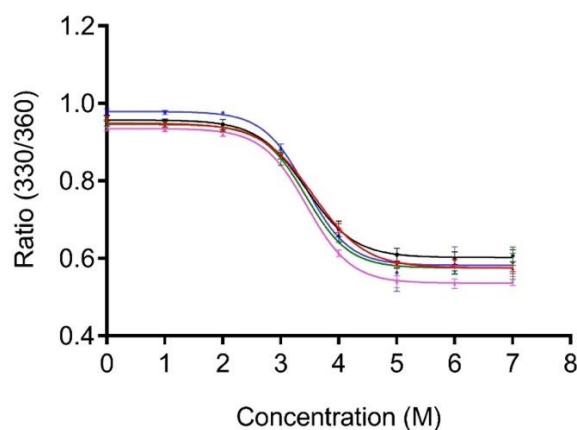
A comparison of this data to the one previously obtained for PG and 4xLPG (34), indicates that the percentage proportion of  $\alpha$ -helix decreases with an increasing multimerization of the linker region. Since the PG portion (185 amino acids) accounts for ~90% of the total 1xLPG (206 amino acids), ~82% of 2xLPG (227 amino acids) and only 75% of 3xLPG (248 amino acids), these results are consistent with maintenance of the native PG module structure, indicating that the PG is still folded and is not affected by its fusion to different truncations of the linker.

Contrary to the decreased  $\alpha$ -helix proportion with increasing linker length, the  $\beta$ -sheet component of the truncated derivatives was found to increase with an increased peptide (linker) multimerization. Using SELCON3 algorithm and reference Set3 (in addition to various other combinations of fitting algorithm and reference set available on Dichroweb) the  $\beta$ -sheet component was estimated to be ~17%, ~19%, ~23% and ~24% for PG, 1xLPG, 2xLPG and 3xLPG respectively (Table 1). Looking at the percentage composition of  $\alpha$ -helix and  $\beta$ -sheet content in PG and 1xLPG, we can say that 1xLPG followed the progression of increasing  $\beta$ -sheet and decreasing  $\alpha$ -helix in the overall structure with the addition of single peptide repeat. Also, similar to 4xLPG, the higher  $\beta$ -sheet components predicted for 2xLPG and 3xLPG might be a result of an artefact of the secondary structure fitting approach. This might have occurred due to the poor ability of the reference sets to efficiently distinguish between  $\beta$ -sheet ( $\beta_H$ ) structure and random coils, especially in case of proteins consisting of highly disordered regions. Hence, the CD spectra suggest that



multimerization of the linker peptide sequence only contributed an additional unstructured component (possibly with some additional  $\beta$ -sheet-like structure) without distorting or affecting the overall secondary structure of its fusion protein partner, PG. This result is significant for understanding the binding efficiency of the different linker lengths as the binding of SBPs to their solid substrates in some cases is not only determined by their amino acid sequences but may also be controlled on their secondary structure conformation (35). For example, the linear and constrained forms of a platinum-binding peptide (PtBP) displayed different platinum binding behaviour that were attributed to molecular their structural differences (35).

The relative stability of all truncated derivatives was compared in the presence of the chemical denaturant GdnHCl using fluorescence spectroscopy. PG consists of eight tyrosine and three tryptophan residues. Accordingly, intrinsic tryptophan fluorescence (ITF) experiments were performed at an excitation of 295 nm so as to minimize the excitation between 280-290 nm which corresponds to tyrosine residues. In addition, the linker sequence does not contain any aromatic residues, so it does not contribute to the overall fluorescence which is solely due to tryptophan residues in PG. The unfolding of 1xLPG, 2xLPG and 3xLPG was monitored by measuring the shift in the maximum tryptophan fluorescence emission with an increasing concentration of GdnHCl. Assuming the protein denaturation to be two-state process, the (330/360) fluorescence intensity ratio at 330 nm and 360 nm was plotted against increasing denaturant concentrations and finally the GraphPad Prism 7.0 software was used to non-linearly fit the data.

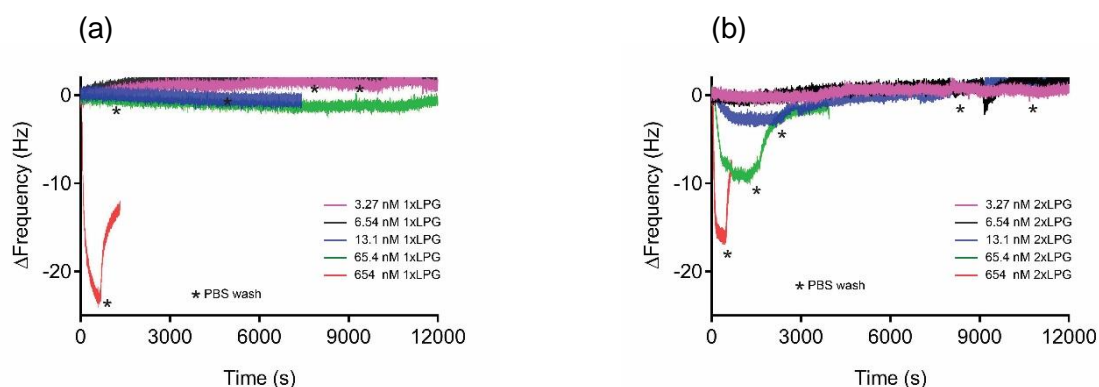


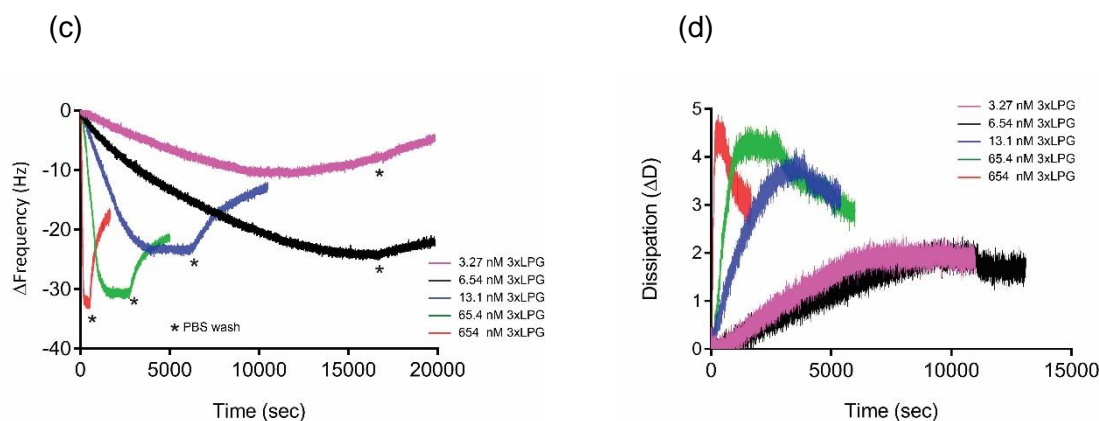
**Figure 3.** Unfolding of PG (blue), 1xLPG (black), 2xLPG (pink), 3xLPG (green) and 4xLPG (red) in GdnHCl. All protein samples were diluted to a final concentration of 2  $\mu$ M in 1xPBS, pH 7.4, containing various molar concentrations of GdnHCl. The ratio of relative fluorescence intensity at 330 nm and 360 nm (330/360) was monitored after excitation at 295 nm.

Figure 3 represents the GdnHCl denaturation curves for PG, 4xLPG and each truncated derivative. For all three derivatives (1xLPG, 2xLPG and 3xLPG), no change was observed in the tryptophan fluorescence until exposure to  $\sim 2$  M GdnHCl. Also, the truncated derivatives showed maximum foldability at  $\sim 5$  M GdnHCl. On the basis of the 2-state non-linear fitting of the denaturation curves, the concentration of GdnHCl required for 50% unfolding was determined to be  $3.4 \pm 0.2$  M (95% CI),  $3.4 \pm 0.1$  (95% CI) and  $3.4 \pm 0.2$  (95% CI) for 1xLPG, 2xLPG and 3xLPG, respectively. These results are consistent with the ones obtained for the original polypeptide (four linker repeats) in 4xLPG ( $3.6 \pm 0.1$  M) and the model antibody-binding protein, PG ( $3.4 \pm 0.2$  M) (34). Based on the above results, the chemical stability of the PG portion of the 4xLPG fusion protein is unaffected by truncations of the linker sequence. Apart from adding an extra random coil component, the SBP multimerization has no remarkable effect on the overall structural stability of PG.

#### *Minimal number of repeats required for silica binding*

The binding affinity of the various truncated derivatives to silica surface was calculated using QCM-D at comparable protein molar concentrations (3.27 – 654 nM). The binding affinity of 1xLPG was not possible to calculate since only the highest concentration amongst the selected set of five concentrations showed some binding but the adsorbed peptide gets dissociated from the surface after subsequent washing with 1xPBS (Figure 4a). The other four concentrations, especially the lowest two concentrations did not show any change in frequency or dissipation response (Supplementary Figure S1a) and these responses remained stable all throughout the experiment.





**Figure 4.**  $\Delta f$  vs time (a) 1xLPG, (b) 2xLPG, and (c) 3xLPG, and  $\Delta D$  vs time (d) 3xLPG for the 3<sup>rd</sup> overtone of the absorbed truncated derivatives on silica coated QCM-D crystals at various concentrations (3.27–654 nM). The measurement was performed in three steps at a flow rates of 150  $\mu\text{L/mL}$ : establishment of baseline (PBS buffer), adsorption of protein samples until saturation, and washing (PBS buffer) to remove unbound protein. Three independent measurements were performed for each concentration.

The sensorgram for frequency shift vs time sensorgram for the binding interactions of 2xLPG to silica surface is shown in Figure 4b. Only the three highest concentrations (654, 65.4 and 13.1 nM) showed measurable binding response for silica binding. 2xLPG at the lowest two concentrations (6.54 and 3.27 nM) appeared to bind to the surface but with minimum adsorption and the resulting frequency response appeared as just noise because of the crystal oscillation (considering the maximum mass sensitivity of the system in liquid to be 0.5  $\text{ng/cm}^2$ ). Since Langmuir isotherm fitting requires a minimum of five concentrations, it was not possible to calculate the binding affinity for 2xLPG. However, looking at the frequency shift for the highest 2xLPG concentration, it seems that the adsorption of the protein to the silica surface is almost half ( $\sim 16.5$  Hz) that observed for 4xLPG (34). On this basis, it could be said that 2xLPG binds moderately to silica surface when compared to 4xLPG. The experiment performed on QCM-D for 3xLPG (Figure 4c) using the same concentration set as the other protein samples gave a binding affinity ( $K_D$ ) of  $53.23 \pm 4.5$  nM, when fitted using Langmuir isotherm (Figure 5). This  $K_D$  value is 1.5 times higher than the one obtained for 4xLPG under similar experimental conditions ( $K_D = 34.77 \pm 11.8$  nM) and indicated an overall lower binding affinity of the 3xLPG truncated derivative. Based on these data, a general trend of increased binding to the silica surface was observed with linker multimerization.

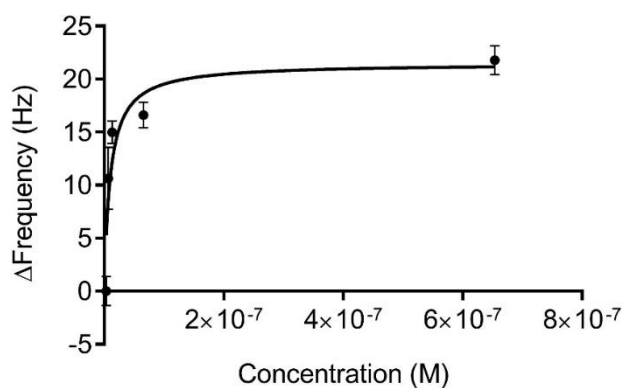


**Figure 5.** Langmuir adsorption isotherm for the adsorption of 3xLPG to silica surface. The data was fitted as per single-site specific binding model, giving a binding affinity/equilibrium dissociation constant ( $K_D$ ) =  $53.23 \pm 4.5$  nM.

Figure 6 represents the  $Df$  plot for the interaction of 3xL-PG to silica measured by QCM-D. The binding interactions between different 3xLPG concentrations and silica resulted in a  $Df$  plot that fits within the viscoelastic region. This indicates that the interactions act as viscoelastic materials and is further supported by the fact that the dissipation is greater than 2 units of magnitude which suggests that the protein layer formed is not rigid but viscous (Figure 4d).

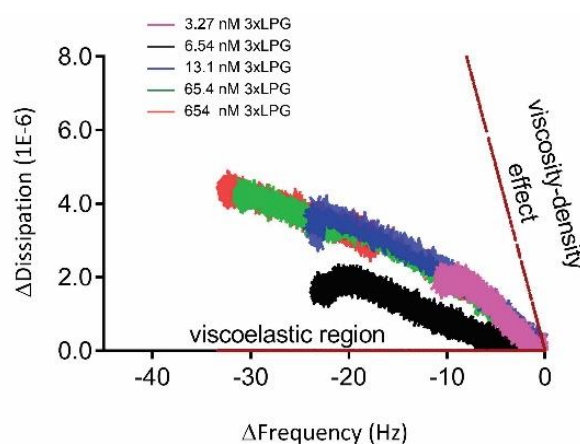


**Figure 6.**  $Df$  plot for the binding interactions between 3xL-PG and silica surface. The dotted lines indicate the pure elastic mass and viscosity-density responses.

Because of the constraint that the adsorbed peptide layer is viscoelastic rather than rigid, the Voigt model over Sauerbrey protocol was preferred. Table 2 represents the various viscoelastic parameters for the binding interactions between 3xLPG and silica at the association and dissociation phases.

**Table 2:** Viscoelastic parameters for 3xLPG and silica binding interactions obtained by fitting the raw QCM-D data using Voigt model.

	Thickness (@R <sub>eq</sub> ) <sup>a</sup> (nm)	Thickness (@k <sub>d</sub> ) <sup>b</sup> (nm)	Mass deposited (@R <sub>eq</sub> ) (kg/m <sup>2</sup> )	Mass deposited (@k <sub>d</sub> ) (kg/m <sup>2</sup> )	Viscosity (@R <sub>eq</sub> ) x10 <sup>-4</sup> (kg/ms)	Viscosity (@R <sub>eq</sub> ) x10 <sup>-4</sup> (kg/ms)
3xLPG/SiO <sub>2</sub>	5.76 ± 0.15	4.36 ± 0.05	680.67 ± 34.63	589.13 ± 23.56	19.67 ± 0.36	17.56 ± 0.15

<sup>a</sup> @Req, frequency shift at equilibrium; <sup>b</sup> @k<sub>d</sub>, saturation achieved after dissociation

The maximum thickness of the peptide layer calculated by Voigt model was 6 nm. The viscous nature of the peptide layers can also be explained by the system's response observed upon the introduction of washing buffer (1xPBS). Figure 6a represents the plot of dissipation vs time for 3xLPG. The dissipation for the binding interactions was more than 2 units, which indicates the formation of a viscoelastic and soft layer. This might be due to the entrapment of water between the peptide layers owing to the hydrophilic nature of the protein. Although the dissipation exceeds 2 units for both 1xLPG and 2xLPG (Supplementary Figure S1), the binding was not strong enough to keep the peptides intact on the surface. In case of 1xLPG, the sample was removed from the surface after the PBS wash step, while for 2xLPG only half of the initial bound protein remained on the surface after the washing step. The formation of viscous layer is likely due to the entrapment of water. For an end-on orientation, a monolayer of 3xLPG (28.2 kDa) was approximated to be 324 ng/cm<sup>2</sup> while it is just 88 ng/cm<sup>2</sup> for a side-on orientation. This is assumed for 3xLPG being a globular protein and approximately 0.4 times the size of albumin (66 kDa), since its molecular weight is half to that of albumin. The ~6 nm thick layer of immobilized 3xLPG equates to ~700 ng/cm<sup>2</sup> which is stabilized via hydrophobic interactions and is hydrated and viscous, being oriented in an end-on bilayer configuration. The maximum amount of 3xLPG bound to the surface of silica crystal was calculated to be 681 ng/cm<sup>2</sup> (Table 2). Considering the molecular mass of 3xLPG (28.2 kDa) and the mass of one 3xLPG molecule to be 5.05x10<sup>-11</sup> ng, there are 0.79x10<sup>13</sup> 3xLPG molecules bound per cm<sup>2</sup> on to the silica surface, which is almost 0.5-fold less than the one calculated for 4xLPG (1.7x10<sup>13</sup> molecules/cm<sup>2</sup>) (34). Based on these results it appears that the three repeats of the linker (3xLPG) support to a similar extent the parent PG binding to silica surface as that of the 4 repeats (4xLPG) but with comparatively weaker binding affinity.



Initial work by Brown highlighted the possible dependence of a gold-binding peptide binding multimerization and the avidity towards its inorganic substrate (36). In this case the binding affinity of a gold-binding peptide and alkaline phosphatase fusion protein to gold was directly dependent on the numbers of repeating gold-binding polypeptides. Seker et al. (35) studied the effect of SBP multimerization on the binding affinity to their solid substrate. An increase in the binding affinity of a gold-binding peptide (GBP1) was observed with the increasing number of tandem repeats (3-repeats). Similarly, increased binding affinity to the surface of ZnO-coated nanoparticles was observed after the multimerization of a zinc-binding peptide (ZBP). In this case, the trimeric (3xZBP) variant displayed a binding to the ZnO-coated nanoparticles nearly twice as strong as that observed with the monomeric (1xZBP) variant (30). Interestingly, the binding stoichiometry of each ZBP per ZnO-coated nanoparticle followed a reverse pattern where it was lower for 3xZBP (~2.3 molecules) as compared to 1xZBP (~3.9 molecules). This can be attributed to the fact that the small tethered length of 1xZBP supported a denser packing of the peptide molecules onto the ZnO surface due to the availability of comparatively more free binding sites. The silica-binding peptides QBP1 and QBP2 displayed equilibrium binding constants of  $0.12 \times 10^6$  and  $1.2 \times 10^6$ , respectively (26). However, only the tandem 3-repeats derivative of QBP1 (3l-QBP1) showed increased affinity to silica but not the QBP2 derivative (3l-QBP2).

The complexity of the peptide-material interface makes it difficult to properly understand the mechanisms behind SBP recognition, selectivity, and binding affinity. The peptide exists in variety of conformations, structures, chemistries, polarities, electrostatic charges, or binding affinities. Similarly, the material surface can have a variety of facets, oxidation states, surface charges, crystallographic orientations, or defects. Further complexity arises from the dynamic nature of the assembled peptide-material surface interface in which peptides are in constant motion, tending to diffuse, reorient, and adapt themselves to the lowest-energy structures. Based on the current data available, there is no general trend for increased binding strength as a result of SBP multimerization. While in some cases multimerization increased binding affinity, in others the affinity was reduced, and this was attributed to the conformational changes between the single and the multiple peptide repeats (29,35).

### *Binding orientation of truncated derivative 3xLPG*

In order to assess whether 3xLPG also binds to silica surface in an oriented manner to present its antibody-binding region, we studied the binding interaction between silica-bound 3xLPG and the trastuzumab antibody followed by the ability of the 3xLPG – trastuzumab complex to detect the HER2 antigen in complex biological fluids. Figure 7 represents the sensorgram for the binding interactions of trastuzumab with silica-bound 3xLPG and subsequently HER2 interaction with the 3xLPG immobilized trastuzumab. The sensorgram indicated that 3xLPG mediated a properly oriented immobilization of trastuzumab to the silica surface and mediated the binding and detection of the HER2 antigen spiked into human serum. The quantitative analysis for the various viscoelastic properties involved in the above binding interactions are summarized in Table 3.

**Table 3.** Viscoelastic parameters for the interaction between silica-bound 3xLPG and trastuzumab followed by HER2 binding and detection

<b>Immobilized truncated derivative</b>	<b>Thickness of bound protein (nm)</b>	<b>Mass of protein deposited (ng/cm<sup>2</sup>)</b>	<b>Thickness of bound trastuzumab (nm)</b>	<b>Mass deposited for bound trastuzumab (ng/cm<sup>2</sup>)</b>	<b>Thickness of bound HER2 (nm)</b>	<b>Mass deposited for bound HER2 (ng/cm<sup>2</sup>)</b>
3xLPG	5.76 ± 0.22	680.67	15 ± 0.20	1000.14	20 ± 0.36	1250.65

The thickness and mass deposited for antibody (trastuzumab) and antigen (HER2) with the truncated derivative 3xLPG are quantitatively lesser than that obtained for 4xLPG, for which the calculated thickness and mass for the bound trastuzumab were 20 nm and 1200 ng/cm<sup>2</sup>, respectively (34). These results are in accordance with the stoichiometric data presented above where as many as twice 4xLPG molecules were bound on the silica surface per cm<sup>2</sup> as compared to 3xLPG.

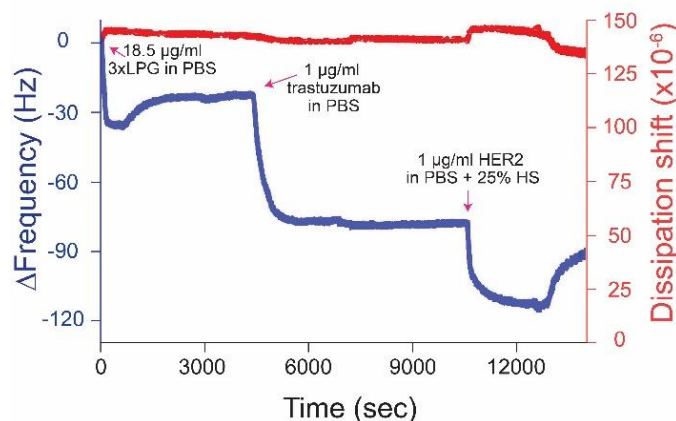


**Figure 7.** QCM-D response for the binding interactions of trastuzumab to silica-immobilized 3xLPG and subsequent detection of HER2 antigen spiked in 25% human serum (HS).

Although the results obtained from all these biophysical characterization techniques showed that multimerization of the linker peptide enhanced the silica-binding mechanism, it is also important to study the various interactions forces driving this binding process. Table 4 summarizes the physicochemical properties (molecular weight, charge, hydrophobicity and isoelectric point) of the 4xLPG derivatives and the different linker repeats.

**Table 4.** Truncated derivatives of 4xLPG with different linker repeats and their Physicochemical Properties

	Mw (kDa) <sup>a</sup>	pI <sup>b</sup>	Charge <sup>c</sup>	GRAVY <sup>d</sup>
<i>Derivative</i>				
PG	21.363	4.58	-14.0	-0.56
1xLPG	23.443	4.69	-13.8	-0.69
2xLPG	25.797	4.94	-10.5	-0.78
3xLPG	28.151	5.25	-7.3	-0.85
4xLPG	30.504	5.80	-4.1	-0.91
<i>Linker repeat</i>				
1xL	3.232	10.94	3.2	-1.27
2xL	5.586	11.38	6.4	-1.43
3xL	7.939	11.50	9.6	-1.50
4xL	10.293	11.57	12.9	-1.54

<sup>a</sup> Theoretical molecular weight (Mw)<sup>\*</sup>

<sup>b</sup> Theoretical isoelectric point (pI)<sup>\*</sup>

<sup>c</sup> Theoretical charge at pH 7.0<sup>\*</sup>

<sup>d</sup> Theoretical grand average hydropathicity (GRAVY)<sup>†</sup>

<sup>\*</sup> Values calculated using Protein calculator v3.4 (<http://protpcalc.sourceforge.net/>)

<sup>†</sup> Values calculated using Protein GRAVY

([https://www.bioinformatics.org/sms2/protein\\_gravy.html](https://www.bioinformatics.org/sms2/protein_gravy.html))

An increase in linker multimerization resulted in an associated increase in isoelectric point (pI), overall charge at pH 7.0 and hydrophilicity of all fusion protein derivatives (Table 4). The surface of silica is negative and adsorption of proteins to its surface is influenced by the sum of attraction and repulsion electrostatic forces. Adsorption of proteins will be driven mainly by Coulomb's electrostatic attractions at pH values below the pI (proteins will carry an overall positive charge). However, absorption will be driven by the sum of the Columbic repulsion and attractive forces (e.g., hydrophobic interactions) at pH's above the pI since proteins and silica will be negatively charged. At pH 7.0 (above pI) PG, and all the derivatives (Table 4) carry an overall negative charge. Considering the charge contribution by the linker region alone, the positive charge increases with multimerization. Accordingly, 4xL is highly positively charged at pH 7.0 (charge of 12.9) when compared to PG (charge of -14). Silica has a negatively charged surface for the interaction of positively charged molecules and this may indicate the linker multimerization and the concomitant increase in positive charge is the main drive for a strong binding to silica through electrostatic attraction forces. Taniguchi et al (37) reported that the binding of a silica-binding tag (Si-Tag) was pH dependent. Due to the presence of 63 positively charged amino acid residues, the peptide displayed a pI of 10.9 and maximum binding to the silica surface was obtained at pH 8.0, when Si-tag carried a net positive charge. Sarikaya et al. (38) found that the high affinity of polypeptides to inorganic surfaces was the result of a net high charge and a large proportion of basic amino acid residues.




#### *Introduction of a (GGGS)<sub>n</sub> linker*

Although the above results provide a plausible explanation for the increase of binding strength of 4xLPG, it remains unclear whether the linker sequence multimerization or the space it occupies (length) is the important factor for silica binding. Poly-glycine and glycine-rich flexible sequences (GGGS)<sub>n</sub> (usually  $n \leq 6$ ) have been by far the most

frequently used linkers that acts as bridges to join two or more individual peptide sequences because they enhance solubility, are thought to be resistant to proteolysis, and presumably confer conformational flexibility to the overall peptide sequence (39). A model fusion protein was designed in which a 12-repeat glycine rich spacer (GGGGS)<sub>12</sub> was fused between the single linker sequence and PG to create a 4xLPG analogue fusion protein (Figure 8a).

The analogue fusion protein Link1X-(GGGGS)<sub>12</sub>-PG was recombinantly-expressed in *E. coli* and purified. Link1X-(GGGGS)<sub>12</sub>-PG displayed identical pI (4.69), overall charge at pH 7.0 (-13.8) and similar grand average hydropathicity (-0.21) as the 1xLPG truncated derivative (Table 4). Silica binding assays (Figure 8b) indicated that the space occupied by the repeat sequence is an important factor for solid binding. The introduction of the synthetic (GGGGS)<sub>12</sub> sequence into Link1x-PG dramatically increases the binding affinity from <5% to >80%. These qualitative initial results seems to indicate an important role for the length of the peptide (distance from the repeats) in an efficient binding to silica.

a

	Name	Linker <sup>a</sup>	Binding <sup>b</sup>
 PG	4xLPG	4	100
 PG	1xLPG	1	<5
 PG	Link1X-(GGGGS) <sub>12</sub> -PG	1	>80

<sup>a</sup> Number of original linker or linker repeats.

<sup>b</sup> Percentage of purified protein found in the bound fraction. Binding assays were performed with silica as described in the binding assay section.

b

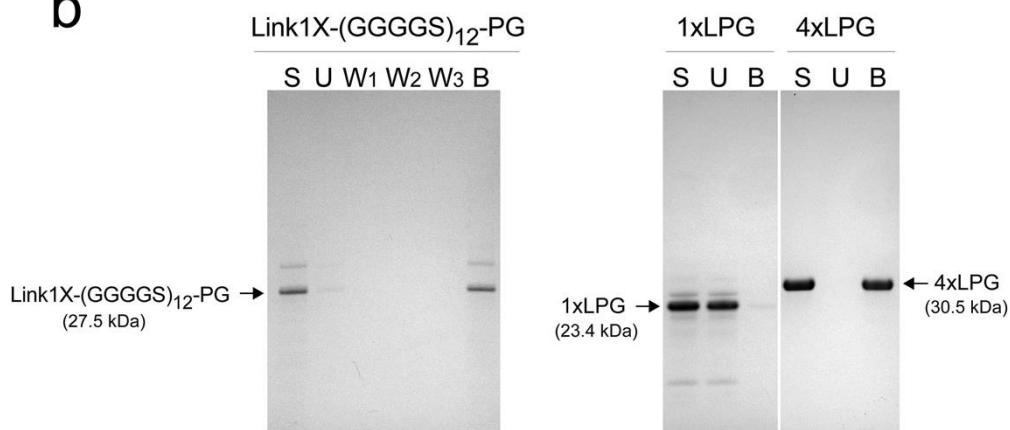




**Figure 8.** (a) Architecture of the fusion protein with and without the glycine-rich spacer and their subsequent zeolite-binding assays. (b) SDS-PAGE of silica binding assays. Arrows indicate position of Link1X-(GGGGS)<sub>12</sub>-PG, 1xLPG and 4xLPG on the gel. 1xLPG and 4xLPG SDS-PAGE were from (1).

The introduction of (GGGGS)<sub>12</sub> to Link1x-PG, results in Link1X-(GGGGS)<sub>12</sub>-PG which seems to function as an analogue of 4xLPG but carries only a single sequence of the silica-binding peptide rather than four repeats. This (GGGGS)<sub>12</sub> spacer addition was enough to convert 1xLPG, which display negligible binding to silica, into fusion protein displaying at least qualitatively comparable binding affinity to silica as 4xLPG. In terms of linker multimerization, the additional three tandem repeats of the linker may just act as spacer regions that allow the single linker sequence to interact with the silica surface. Although, it is not always necessary that the addition of a long glycine-rich peptide sequence will enhance the binding. Care et al (40) have mentioned the effect of surrounding medium on the overall binding of the sequence. They found that a sequence ManA-(GGGGS)<sub>16</sub> showed binding to zeolites at pH 5 (acidic media) but no significant binding was observed in case of pH 7 (neutral) or basic environment (pH 9). The pH of the binding experiments performed in this project was 7.4, at which (GGGGS)<sub>16</sub> linker showed no binding according to Care et al (40). On other hand, Shan et al (41) found that out of three peptide constructs GS1, (GGGGS)<sub>1</sub>; GS2, (GGGGS)<sub>2</sub> and GS3, (GGGGS)<sub>3</sub>, the short linker peptide of ~5 aa (GS1) is the best with a higher binding affinity to CD20. SBPs are usually present in an unfolded state and adsorption and conformational adaptation to the substrate binding interface are fast and simultaneous events (40). Over 76% of the amino acid residues of 4xLPG have the tendency to promote structural disorder (39) and confer low overall hydrophobicity and high net charge which has reported for other polypeptide sequences exhibiting affinity to inorganic materials (38). Thus, the sequence repeats may provide enhanced flexibility and plasticity to adopt an optimal conformation for binding substrates with differently shaped topologies or surfaces. Due to the time constraints of this PhD project, it was not possible to perform a detailed biophysical characterization of Link1X-(GGGGS)<sub>12</sub>-PG to determine its silica-binding mechanism in a more quantitative manner.

## Conclusion

SBPs have been used increasingly as molecular building blocks in several nanobiotechnological applications and have become key molecules for the engineering of biomimetic and bioinspired materials. More biophysical and quantitate analysis of the

interaction between SBPs and their inorganic substrates are required to understand their fundamental binding mechanism and expand their range of practical applications. The bifunctional fusion protein 4xLPG contains a linker made of a  $4 \times 21$ -amino acid sequence repeat that display high binding affinity towards silica. CD and fluorescence spectroscopy studies indicated no apparent negative effect to the secondary structure and chemical stability of the partner PG upon truncation of the associated linker sequence repeats. However, QCM-D analysis suggest that a linker multimerization is an important parameter for a strong and stable binding to the silica. Removal of the linker sequence below three repeats drastically reduced (2xLPG) or completely abolished (1xLPG) the silica-binding property of the 4xLPG. A 12-repeat glycine rich spacer (GGGGS)<sub>12</sub> was fused between the single linker sequence and PG (1xLPG) to create a 4xLPG analogue fusion protein, Link1X-(GGGGS)<sub>12</sub>-PG. The analogue fusion protein Link1X-(GGGGS)<sub>12</sub>-PG was able to restore the silica binding property of the truncated derivative 1xLPG. This preliminary qualitative data provides further motivation to investigate not only multimerization but also the length of the linker as potentially important parameters for strong silica binding. The results presented here also suggest SBPs multimerization or incorporation of flexible interdomain linkers like (GGGGS)<sub>n</sub> can be used to tailor the adsorption and affinity of a given sequence to a solid material. This provides an additional manipulation tool for future applications requiring surface specific SBPs that acting as molecular linkers and assemblers.

## References

1. Sunna, A.; Chi, F.; Bergquist, P.L. A linker peptide with high affinity towards silica-containing materials. *N. Biotechnol.* **2013**,*30*,485-492.
2. Care, A.; Bergquist, P.L.; Sunna, A. Solid-binding peptides: smart tools for nanobiotechnology. *Trends Biotechnol.* **2015**,*33*,259-268.
3. Rothenstein, D.; Claasen, B.; Omiecienski, B.; Lammel, P.; Bill, J. Isolation of ZnO-binding 12-mer peptides and determination of their binding epitopes by NMR spectroscopy. *J. Am. Chem. Soc.* **2012**,*134*,12547-12556.
4. Heinz, H.; Farmer, B.L.; Pandey, R.B.; Slocik, J.M.; Patnaik, S.S.; Pachter, R.; Naik, R.R. Nature of molecular interactions of peptides with gold, palladium and Pd-Au bimetal surfaces in aqueous solution. *J. Am. Chem. Soc.* **2009**,*131*,9704-9714.

5. Kumada, Y.; Tokunaga, Y.; Imanaka, H.; Imamura, K.; Sakiyama, T.; Katoh, S.; Nakanishi, K. Screening and characterization of affinity peptide tags specific to polystyrene supports for the orientated immobilization of proteins. *Biotechnol. Prog.* **2006**, *22*, 401-405.
6. Coyle, B.L.; Baneyx, F. A cleavable silica-binding affinity tag for rapid and inexpensive protein purification. *Biotechnol. Bioeng.* **2014**, *111*, 2019-2026.
7. Mannoor, M.S.; Tao, H.; Clayton, J.D.; Sengupta, A.; Kaplan, D.L.; Naik, R.R.; Verma, N.; Omenetto, F.G.; McAlpine, M.C. Graphene-based wireless bacteria detection on tooth enamel. *Nat. Comm.* **2012**, *3*, 763.
8. Cui, Y.; Kim, S.N.; Jones, S.E.; Wissler, L.L.; Naik, R.R.; McAlpine, M.C. Chemical functionalization of graphene enabled by phage displayed peptides. *Nano Lett.* **2010**, *10*, 4559-4565.
9. Naik, R.R.; Stringer, S.J.; Agarwal, G.; Jones, S.E.; Stone, M.O. Biomimetic synthesis and patterning of silver nanoparticles. *Nat. Mater.* **2002**, *1*, 169-72.
10. Care, A.; Chi, F.; Bergquist, P.L.; Sunna, A. Biofunctionalization of silica-coated magnetic particles mediated by a peptide. *J. Nanopart. Res.* **2014**, *16*, 2543.
11. Kokubun, K.; Matsumura, S.; Yudasaka, M.; Iijima, S.; Shiba, K. Immobilization of a carbon nanomaterial-based localized drug-release system using a bispecific material-binding peptide. *Int. J. Nanomed.* **2018**, *13*, 1643-1652.
12. Yazici, H.; O'Neill, M.B.; Kacar, T.; Wilson, B.R.; Oren, E.E.; Sarikaya, M.; Tamerler, C. Engineered chimeric peptides as antimicrobial surface coating agents toward infection-free implants. *ACS Appl. Mater. Interfaces* **2016**, *8*, 5070-5081.
13. Tang, Z.; Palafox-Hernandez, J.P.; Law, W.C.; Hughes, Z.E.; Swihart, M.T.; Prasad, P.N.; Knecht, M.R.; Walsh, T.R. Biomolecular recognition principles for bionanocombinatorics: an integrated approach to elucidate enthalpic and entropic factors. *ACS Nano* **2013**, *7*, 9632-9646.
14. Sapsford, K.E.; Algar, W.S.; Berti, L.; Gemmill, K.B.; Casey, B.J.; Oh, E.; Stewart, M.H.; Medintz, I.L. Functionalizing nanoparticles with biological molecules: developing chemistries that facilitate nanotechnology. *Chem. Rev.* **2013**, *113*, 1904-2074.
15. Nel, A.E.; Madler, L.; Velegol, D.; Xia, T.; Hoek, E.M.V.; Somasundaran, P.; Klaessig, F.; Castranova, V.; Thompson, M. Understanding biophysicochemical interactions at the nano-bio interface. *Nat. Mater.* **2009**, *8*, 543-557.

16. Yamaguchi, A.; Isozaki, K.; Nakamura, M.; Takaya, H.; Watanabe, T. Discovery of 12-mer peptides that bind to wood lignin. *Sci. Rep.* **2016**,*6*,21833.
17. Sultan, A.M.; Westcott, Z.C.; Hughes, Z.E.; Palafox-Hernandez, J.P.; Giesa, T.; Puddu, V.; Buehler, M.J.; Perry, C.C.; Walsh, T.R. Aqueous peptide–TiO<sub>2</sub> interfaces: isoenergetic binding via either entropically or enthalpically driven mechanisms. *ACS Appl. Mater. Interfaces* **2016**,*8*,18620-18630.
18. Jaworski, J.W.; Raorane, D.; Huh, J.H.; Majumdar, A.; Lee, S-W. Evolutionary screening of biomimetic coatings for selective detection of explosives. *Langmuir* **2008**, *24*,4938-4943.
19. Sawada, T.; Okeya, Y.; Hashizume, M.; Serizawa, T. Screening of peptides recognizing simple polycyclic aromatic hydrocarbons. *Chem. Commun. (Cambridge, U.K.)* **2013**,*49*,5088-5090.
20. Suzuki, Y.; Shindo, H. Binding sites and structure of peptides bound to SiO<sub>2</sub> nanoparticles studied by solution NMR spectroscopy. *Polym. J.* **2018**,*50*,989-996.
21. Gwak, Y.; J-i, Park.; Kim, M.; Kim, H.S.; Kwon, M.J.; Oh, S.J.; Kim, Y.P.; Jin, E. Creating anti-icing surfaces via the direct immobilization of antifreeze proteins on aluminum. *Sci. Rep.* **2015**,*5*,12019.
22. Yu, J.; Becker, M.L.; Carri, G.A. The influence of amino acid sequence and functionality on the binding process of peptides onto gold surfaces. *Langmuir* **2012**,*28*,1408-1417.
23. Heffernan, R.; Paliwal, K.; Lyons, J.; Dehzangi, A.; Sharma, A.; Wang, J.; Sattar, A.; Yang, Y.; Zhou, Y. Improving prediction of secondary structure, local backbone angles, and solvent accessible surface area of proteins by iterative deep learning. *Sci. Rep.* **2015**,*5*,11476.
24. Sun, T.; Zhou, B.; Lai, L.; Pei, J. Sequence-based prediction of protein-protein interaction using a deep-learning algorithm. *BMC Bioinformatics* **2017**,*18*,277.
25. Walsh, T.R.; Knecht, M.R. Biointerface structural effects on the properties and applications of bioinspired peptide-based nanomaterials. *Chem. Rev.* **2017**,*117*,12641-12704.
26. Kuang, Z.; Kim, S.N.; Crookes-Goodson, W.J.; Farmer, B.L.; Naik, R.R. Biomimetic chemosensor: Designing peptide recognition elements for surface functionalisation of carbon nanotube field effect transistors. *ACS Nano*. **2010**,*1*,452-458.

27. Brown, S.; Sarikaya, M.; Johnson, E. A genetic analysis of crystal growth. *J. Mol. Biol.* **2000**, *299*, 725-735.
28. Seker, O.U.S.; Wilson, B.; Dincer, S.; Kim, I.W.; Oren, E.E.; Evans, J.S.; Tamerler, C.; Sarikaya, M. Adsorption behaviour of linear and cyclic genetically engineered platinum binding peptides. *Langmuir* **2007**, *23*, 7895-7900.
29. Seker, O.U.S.; Wilson, B.; Kulp, J.L.; Evans, J.S.; Tamerler, C.; Sarikaya, M. Thermodynamics of Engineered Gold Binding Peptides: Establishing the Structure–Activity Relationships. *Biomacromolecules* **2014**, *15*, 2369-2377.
30. Cho, N.; Cheong, T.; Min, J.H.; Wu, J.H.; Lee S.J.; Kim, D.; Yang, J.; Kim, S.; Kim, Y.K.; Seong, S. A multifunctional core-shell nanoparticle for dendritic cell-based cancer immunotherapy. *Nat. Nanotechnol.* **2011**, *6*, 675-682.
31. Lu, Y.; Zhao, J.; Zhang, R.; Liu, Y.; Liu, D.; Goldys, E.M.; Yang, X.; Xi, P.; Sunna, A.; Lu, J.; Shi, Y.; Leif, R.C.; Huo, Y.; Shen, J.; Piper, J.A.; Robinson, J.P.; Jin, D. Tunable lifetime multiplexing using luminescent nanocrystals. *Nat. Photonics* **2014**, *8*, 32-36.
32. Liang, L.; Care, A.; Zhang, R.; Lu, Y.; Packer, N.H.; Sunna, A.; Qian, Y.; Zvyagin, A.V. Facile assembly of functional upconversion nanoparticles for targeted cancer imaging and photodynamic therapy. *ACS Appl. Mater. Interfaces* **2016**, *8*, 11945-11953.
33. Polikarpov, D.; Liang, L.; Care, A.; Sunna, A.; Campbell, D.; Walsh, B.; Balalaeva, I.; Zvyagin, A.; Gillatt, D.; Guryev, E. Functionalized Upconversion Nanoparticles for Targeted Labelling of Bladder Cancer Cells. *Biomolecules* **2019**, *9*, 820.
34. Bansal, R.; Elgundi, Z.; Care, A.; Goodchild, S. C.; Lord, M. S.; Rodger, A.; Sunna, A. Elucidating the binding mechanism of a novel silica-binding peptide. *Biomolecules*, **2019** (accepted).
35. Seker, U.O.S.; Wilson, B.; Sahin, D.; Tamerler, C.; Sarikaya, M. Quantitative affinity of genetically engineered repeating polypeptides to inorganic surfaces. *Biomacromolecules* **2009**, *10*, 250-257.
36. Brown, S. Metal-recognition by repeating polypeptides. *Nat. Biotechnol.* **1997**, *15*, 269-272.
37. Taniguchi, K.; Nomura, K.; Hata, Y.; Nishimura, T.; Asami, Y.; Kuroda A. The Si-tag for immobilizing proteins on a silica surface. *Biotechnol. Bioeng.* **2007**, *96*, 1023-1029.

38. Sarikaya, M.; Tamerler, C.; Jen, A. K.; Schulten, K.; Baneyx, F. Molecular biomimetics: nanotechnology through biology. *Nat. Mater.* **2003**,2,577-585.
39. Campen, A.; Williams, R.M.; Brown, C.J.; Meng, J.; Uversky, V.N.; Dunker, A.K. TOP-IDP-Scale: A new amino acid scale measuring propensity for intrinsic disorder. *Protein Pept Lett.* **2008**,15,956-963.
40. Care, A; Nevalainen, H; Bergquist, P.L; Sunna, A. Effect of *Trichoderma reesei* Proteinases on the Affinity of an Inorganic-Binding Peptide. *Appl Biochem Biotech* **2014**,173,2225-2240.
41. Shan, D; Press, O.W; Tsu, T.T; Hayden, M.S; Ledbetter, J.A. Characterization of scFv-Ig constructs generated from the Anti-CD20 mAb 1F5 using linker peptides of varying lengths. *J Immunol* **1999**,162,6589-6595.
42. Ikeda, T.; Kuroda, A. Why does the silica-binding protein Si-tag bind strongly to silica surfaces? Implications of conformational adaptation of the intrinsically disordered polypeptide to solid surfaces. *Colloids Surf B Biointerfaces* **2011**;86:359-363.



## Supplementary Information

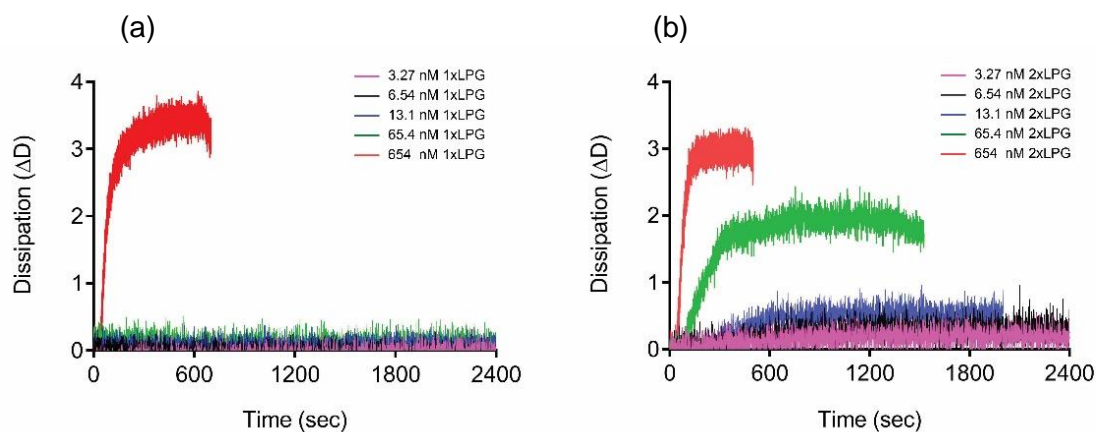


**Figure S1:**  $\Delta D$  vs time for the 3<sup>rd</sup> overtone of the absorbed (a) 1xLPG and (b) 2xLPG on silica coated QCM-D crystals at various concentrations (3.27–654 nM). The measurement was performed in three steps at a flow rate of 150  $\mu\text{L/mL}$ : baseline formation (PBS buffer), adsorption of protein samples until saturation, and washing (PBS buffer) to remove of unbound protein. Three independent measurements were performed for each concentration.

## **Chapter 4**

A solid-binding peptide-based detection of HER2 biomarker

## Introduction

The development of drug delivery systems that can selectively reach and accumulate at specific target cells or tissues is of widespread interest (1-3). Accordingly, the use of selective targeting molecules (e.g., antibodies, aptamers, peptides) as strategy to functionalize drug carrier systems has been used extensively. Nanoparticles are currently used as carrier systems for targeted drug delivery in cancer nanomedicine (4). These nanoparticles have the potential to improve the physicochemical properties of chemotherapeutics, improve pharmacokinetic profile of the drug and bio-distribution and improve the clinical outcome of the treatment (5). Although several nanoparticle-based drug delivery systems have been reported, only less than 2% have advanced to clinical trials (6). More facile and controllable nanoparticle functionalization strategies may help overcome biological and physical barriers to target delivery that may have hampered the translation of nanoparticles into clinical applications.

Another potential nanomedicine area of interest is the efficient detection of molecular recognition events which has played an important role in drug discovery and molecular biology (7). Recently, it has been applied to monitor and detect diseases, including various types of cancers. This has been achieved by detecting biomarkers in patient's blood and as well as tissues. A biomarker is defined as "a characteristic objectively measured and evaluated as an indicator of normal biological processes, pathogenic processes or pharmacological responses to a therapeutic intervention" (8). For clinical diagnosis, it is important to accurately detect and monitor cancer by means of reliable, cost-effective and powerful strategies in order to start an appropriate treatment of the patient and also to monitor the progression, regression and recurrence of the disease. In the past few decades, there has been a promising and significant progress in the field of biomarker detection and various detection methods have been developed. Some of these includes surface plasmon resonance (SPR) (9), enzyme-linked immunosorbent assay (ELISA) (10), polymerase chain reaction (PCR) (11), electrophoresis (12), microcantilevers (13), electrochemical assay (14), surface enhanced Raman spectroscopy (SERS) (15), calorimetric assay (16), fluorescence-based methods (17) and quartz crystal microbalance (QCM) (18), to name a few. However, these techniques still lack accuracy, sensitivity and specificity for use in

clinical diagnostics. The detection is also limited by the presence of secondary proteins in serum or tissue samples.

Human epidermal growth factor receptor 2 (HER2) is a transmembrane tyrosine kinase receptor that is overexpressed in HER2-positive cancer cells (19). The overexpression of HER2 has been reported in at least 15-25% of cases of breast cancer. In these patients HER2 reached 15-75 ng/mL (in serum) as opposed to 4-15 ng/mL observed in a normal person (13-17). This abnormality has been used as a molecular diagnosis and monitoring tool of breast cancer (20). Several techniques are currently available to detect HER2 in breast cancer cells including immunohistochemistry (IHC), Western blotting, ELISA and fluorescence in situ hybridization (FISH) (21).

Nanoparticles-based biosensors have been modelled by chemical and physicochemical functionalization of biomolecules for effective detection of HER2. For example, Poturnayová et al (22) demonstrated the successful use of gold nanoparticles modified with aptamers specific to HER2 receptors for the amplification and detection of cancer cells. Direct detection of the cancer cells with the nanoparticles-based amplification improved the limit of detection (LOD) by 2.8-fold to 550 cells/mL compared to the same detection without amplification. The streptavidin gold particles were functionalized using biotinylated aptamers. Adolphi et al (23) used carboxyl-functionalized nanoparticles to chemically conjugate anti-HER2/neu antibody using the carbodiimide method. The biofunctionalized nanoparticles were used to target HER2-expressing MCF7/Her2-18 breast cancer cells. Magnetic relaxometry and magnetic resonance imaging (MRI) were used to detect and locate the nanoparticles in the target cancer cells. Similarly, Hathaway et al (24) showed that antibody-conjugated magnetic nanoparticles are promising reagents for *in vivo* cancer cell detection. They conjugated Anti-HER2 antibody to superparamagnetic iron oxide nanoparticles using the carbodiimide method. The biofunctionalized nanoparticles were incubated with breast cancer cell lines and visualized by several techniques including confocal microscopy, Prussian blue histochemistry, and magnetic relaxometry. Arkan et al. (25) deposited HER2 antibody biofunctionalized gold nanoparticles on a multiwall carbon nanotube (MWCNT)-ionic liquid electrode. The detection system achieved linear dynamic range and LOD of 10–110 ng mL<sup>-1</sup> and 7.4 ng mL<sup>-1</sup>, respectively, using electrochemical impedance spectroscopy (EIS).

Most of these functionalization methods use covalent attachment of proteins to the reactive

groups of nanoparticles via the protein's primary amines and carboxylic acids (26,27). However, one of the major drawbacks of this coupling method is the potential attachment of biomolecules in a random orientation, which might limit or cause complete loss of the protein's biological function (28).

In this chapter, we performed a preliminary investigation to assess the linker-protein G (LPG) as a suitable system for potential use in nanomedicine applications. We take advantage of the ability of the LPG bifunctional fusion protein to bind in an end-on-end orientation on the silica surface. Thus, LPG mediates the facile oriented immobilization of antibodies faster and under milder conditions. The sensitive, selective and efficient detection of the HER2 biomarker was also investigated in the presence of biological fluids.

### **Materials and methods**

Commercial silica-coated magnetic nanoparticles (1  $\mu\text{m}$ ) were purchased from Kisker Biotech (Steinfurt, Germany). Recombinant LPG was expressed in *E. coli* and purified using ion exchange chromatography as described previously by Sunna et al (29). Trastuzumab, a humanized anti-HER2 monoclonal antibody, was purchased from Jomar Life Research and a FITC-labeled human HER2/ErbB2 protein (His-Tag) was obtained from Acro Biosystems. All other materials unless specified otherwise were from Sigma-Aldrich. Assays were performed at room temperature and with standard phosphate-buffered saline (1xPBS) buffer pH 7.4.

#### *Functionalization of silica-coated magnetic nanoparticles with LPG*

Figure 1 shows a schematic representation of the overall functionalization of silica-coated magnetic nanoparticles with LPG. 0.2 mg (200  $\mu\text{g}$ ) of the silica-coated magnetic nanoparticles were washed three times with a washing solution containing 1xPBS supplemented with 0.075% Triton X100. The washed particles were mixed with 3  $\mu\text{g}$  LPG (0.81 mg/ml) to a final volume of 100  $\mu\text{L}$ . The particle/LPG mixture was incubated at room temperature (RT) for 15 min on an Intelli-Mixer RM-2, with continuous rotation and shaking. This was followed by a short and quick centrifugation of the particles after which they were collected magnetically, and the unbound LPG removed. These particles were additionally washed magnetically three times with 1xPBS. The LPG functionalized silica-coated nanoparticles were blocked with 1% bovine serum albumin (BSA) in 1xPBS buffer and incubated at RT for 15 min. The particles were washed three times, centrifuged and

collected magnetically. Then, the particles were incubated with 6  $\mu\text{g}$  of trastuzumab antibody in a final volume of 100  $\mu\text{L}$  1xPBS buffer and incubated at RT for 15 min. After short centrifugation, the unbound antibody was removed by collecting the particles using magnetic separation. The resulting trastuzumab functionalized silica-coated nanoparticles were finally dispersed in 1xPBS.

#### *Detection of HER2 in biological fluids*

Trastuzumab functionalized silica-coated nanoparticles were incubated with 100  $\mu\text{l}$  of either 1xPBS buffer, human serum or human urine. Each sample was spiked with 0.039-20  $\text{ng}/\mu\text{L}$  of FITC-labeled human HER2/ErbB2 protein (FITC-HER2) and incubated for 15 min at RT in the dark. Any unbound FITC-HER2 was removed by washing the particles 3 times and after which the nanoparticles were collected magnetically and finally dispersed in 50  $\mu\text{L}$  1xPBS. Samples were transferred to a Greiner CELLSTAR 96 well plate with micro-clear flat bottom. The fluorescence measurements were performed on a PHERAstar FSX microplate reader (BMG Labtech) at an excitation wavelength of 495 nm and the emission was measured at 519 nm with an optical gain function of 1000 (Figure 1). The performance characteristics of the assay was validated by measuring limit of detection (LOD) and limit of quantification (LOQ). LOD, also called detection limit, is the smallest amount or concentration of analyte in the test sample that can be reliably distinguished from the blank sample, whereas LOQ is the lowest concentration of the analyte that can be determined with an acceptable repeatability and trueness. LOD and LOQ were calculated using the formulas:

$$\text{LOD} = 3.3 * (\text{SD}/m) \text{ and } \text{LOQ} = 10 * (\text{SD}/m)$$

where, SD = standard deviation of the linear regression

m = slope of the regression line

LOD and LOQ values were verified by analyzing a number of samples within a range of FITC-HER2 concentrations. The factor 3.3 and 10 represents the signal to noise ratio (S/N) for LOD and LOQ, respectively. All experiments were performed in triplicates.



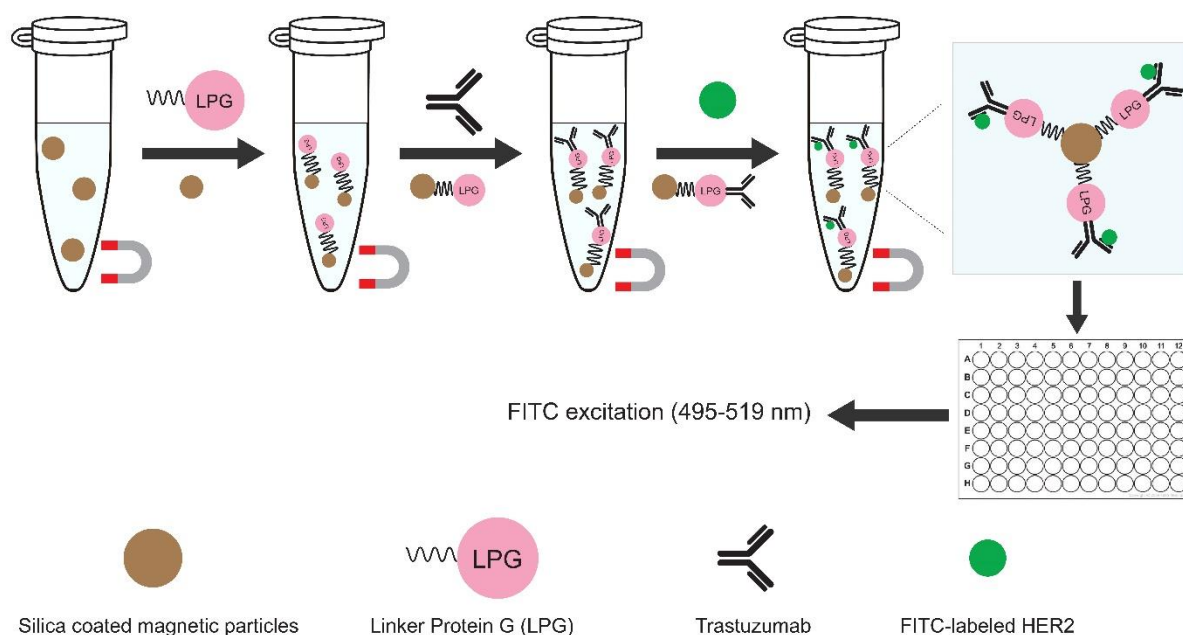


**Figure 1.** The schematic represents the detection of FITC-labeled HER2, in various biological fluids, using silica-coated magnetic particles conjugated with LPG. The particles were conjugated with trastuzumab using LPG and used to detect FITC-labeled HER2.

## Results and Discussion

### *Determining optimum concentration range of HER2*

The LPG-functionalized silica-coated nanoparticles were conjugated with trastuzumab and then incubated with FITC-HER2 in a concentration range of 0.039-20 ng/ $\mu$ L. After incubation and subsequent washing, the particles were dispersed into 50  $\mu$ L of 1xPBS buffer for fluorescence measurements. Figure 2 shows the calibration curve for the fluorescence intensity (FI) measured for each FITC-HER2 concentration.

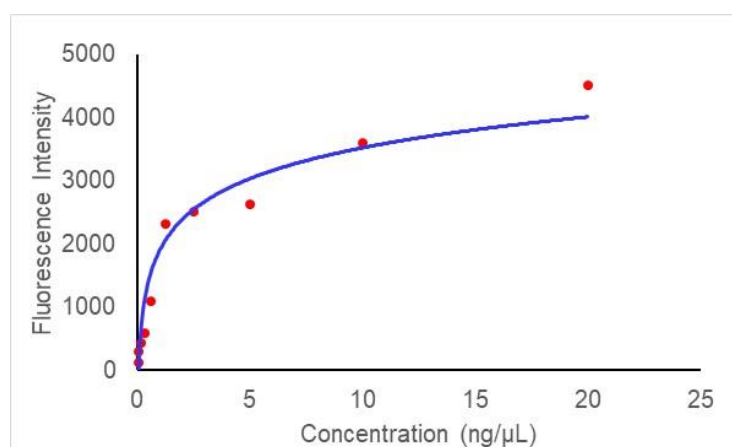


**Figure 2.** Calibration curve for the fluorescence intensity (FI) vs concentration of FITC-HER2 spiked in 1xPBS. The measurement was performed at RT. The emission was measured at 519 nm.

The data was fitted using the logarithmic fitting in Microsoft excel. The fluorescence signal increased with increasing FITC-HER2 concentration until it reached saturation at approximately 2.5 ng/ $\mu$ L. Accordingly, all further experiments were conducted at concentrations which falls in the area of linearity (0.039-1.25 ng/ $\mu$ L).

#### *Detection of HER2 in buffer and biological fluids*

Silica-coated nanoparticles conjugated with LPG and trastuzumab were incubated with different concentrations (0.039-1.25 ng/ $\mu$ L) of FITC-HER2 spiked into 1xPBS buffer, human serum and urine. The fluorescence reading for all three samples were measured separately and the representative fitting curves for fluorescence intensity (FI) versus FITC-HER2 are shown in Figure 3.

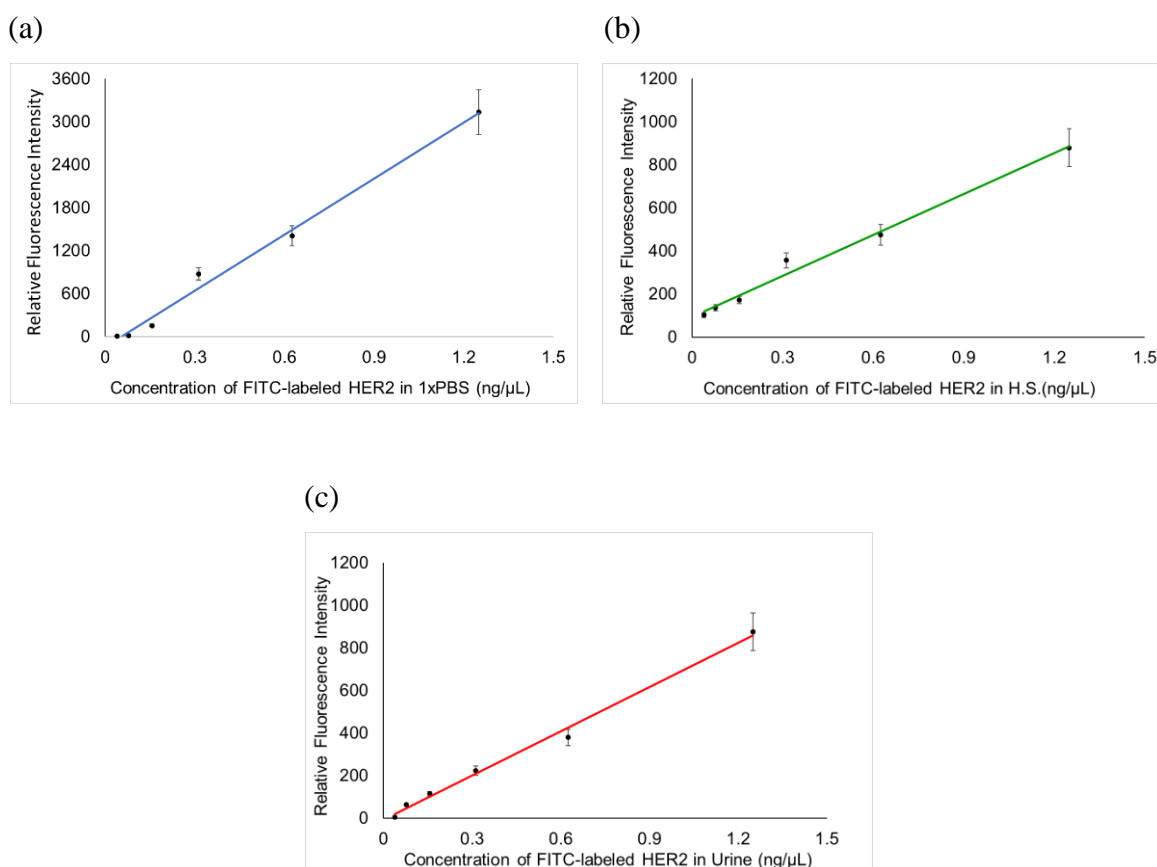


Figure 3. Fluorescence intensity vs concentration of FITC-HER2 spiked into (a) 1xPBS; (b) human serum; and (c) urine. All the graphs were fitted using linear fitting algorithm.  $R^2$  for (a) and (b) is 0.99 while for (c) is 0.98. The emission was measured at 519 nm.

The data showed a linear fluorescence signal during the concentration range (0.039-1.25

ng/ $\mu$ L). From each fitted graph, the slope and the standard deviation were calculated. The standard deviation was used to calculate LOD and LOQ and are summarized in Table 1.

**Table 1.** LOD and LOQ values for FITC-HER2 detection spiked in different biological samples.

Sample	Limit of Detection (LOD) (ng/ $\mu$ L)	Limit of Quantification (LOQ) (ng/ $\mu$ L)
1xPBS	0.29	0.89
Human serum	0.19	0.59
Human urine	0.28	0.85

Considering the LOD and LOQ values, both 1xPBS and human urine have similar detection limits of 0.29 ng/ $\mu$ L and 0.89 ng/ $\mu$ L, respectively. However, the values for both LOD (0.19 ng/ $\mu$ L) and LOQ (0.59 ng/ $\mu$ L) are comparatively lower for human serum. Silica-coated magnetic particles conjugated with LPG-trastuzumab were used as controls and 1xPBS was used as blank. There was no measurable fluorescence from these two samples. The lower value of detection for human serum can be attributed to the fact that human serum is known to have high background fluorescence. Although the samples with serum were washed three times before taking the reading, some serum molecules might have attached to the particles. Secondly, instead of taking human serum as control, 1xPBS was used, which could have undermined the background fluorescence. The system has a LOD and LOQ in the order of ng/ $\mu$ L. Although preliminary, these results are better than the one reported by others using other detection techniques. An electrochemical biosensor based on the screen printing of gold electrode (30), detected HER2 biomarker, spiked into human serum sample with a detection limit of as low as  $1.6 \times 10^{-6}$  ng/ $\mu$ L, with an LOQ of  $5.6 \times 10^{-6}$  ng/ $\mu$ L. An aptamer-based detection system based on aptamer-peptide conjugated probe uses liquid chromatography and mass spectroscopy to detect HER2 with a detection limit 25 pmol/L (31). Similarly, HER2 spiked into serum was detected at 0.0013 ng/ $\mu$ L using an opto-fluidic ring resonator-based system (32).

Also, as compared to other HER2 detection systems which rely on longer and more complex chemical coupling to conjugate antibodies, the LPG mediated conjugation of antibody to nanoparticles was simple, quick (15-20 min) and performed in milder conditions without the need for harsh chemicals.

## Conclusion

This preliminary work showed that LPG mediates the functionalization silica-coated nanoparticles with anti-HER2 antibody trastuzumab easily and under mild conditions. The system was able to detect the HER2 biomarker in the presence of biological fluids demonstrating its potential suitability in nanomedicine applications e. g., nanoparticle-based drug delivery systems and efficient detection of disease biomarkers.

## References

1. Accardo, A.; Tesauro, D.; Morelli, G. Peptide-Based Targeting Strategies for Simultaneous Imaging and Therapy with Nanovectors. *Polym. J.* **2013**, *45*, 481-493.
2. Schroeder, A.; Heller, D. A.; Winslow, M. M.; Dahlman, J. E.; Pratt, G. W.; Langer, R.; Jacks, T.; Anderson, D. G. Treating Metastatic Cancer with Nanotechnology. *Nat. Rev. Cancer* **2012**, *12*, 39-50.
3. Rajendran, L.; Knolker, H. J.; Simons, K. Subcellular Targeting Strategies for Drug Design and Delivery. *Nat. Rev. Drug Discovery* **2010**, *9*, 29-42.
4. Shi, J.; Kantoff, P.W.; Wooster, R.; Farokhzad, O.C. Cancer nanomedicine: progress, challenges and opportunities. *Nat. Rev. Cancer* **2017**, *17*, 20-37.
5. Sandra, F.; Khaliq, N.U.; Sunna, A.; Care, A. Developing protein-based nanoparticles as versatile delivery systems for cancer therapy and imaging. *Nanomaterials*, **2019**, *9*, 1329.
6. Wicki, A.; Witzigmann, D.; Balasubramanian, V.; Huwyler, J. Nanomedicine in cancer therapy: challenges, opportunities, and clinical applications. *J. Controlled Release* **2015**, *200*, 138-157.
7. Yalow, R.S.; Berson, S.A. Immunoassay of endogenous plasma insulin in man. *J. Clin. Invest.* **1960**, *39*, 1157-1175 .

8. Biomarkers Definitions Working Group. Biomarkers and surrogate endpoints: preferred definitions and conceptual framework. *Clin. Pharmacol. Ther.* **2001**,69,89-95.
9. Law, W-C.; Yong, K-T.; Baev, A.; Prasad, P.N. Sensitivity Improved Surface Plasmon Resonance Biosensor for Cancer Biomarker Detection Based on Plasmonic Enhancement. *ACS Nano* **2011**,5,4858-4864.
10. de la Rica, R.; Stevens, M.M. Plasmonic ELISA for the ultrasensitive detection of disease biomarkers with the naked eye. *Nat. Nanotechnol.* **2012**,7,821-824.
11. Pfitzner, C.; Schroeder, I.; Scheungraber, C.; Dogan, A.; Runnebaum, I.B.; Duerst, M.; Haefner, N. Digital-Direct-RT-PCR: a sensitive and specific method for quantification of CTC in patients with cervical carcinoma. *Sci. Rep.* **2014**,4,3970.
12. Lee, H.; Park, J-E.; Nam, J-M. Bio-barcode gel assay for microRNA. *Nat. Commun.* **2014**,5,3367.
13. Loo, L.; Capobianco, J.A.; Wu, W.; Gao, X.; Shih, W.Y.; Shih, W.H.; Pourrezaei, K.; Robinson, M.K.; Adams, G.P. Adams Highly sensitive detection of HER2 extracellular domain (ECD) in the serum of breast cancer patients by piezoelectric microcantilevers (PEMS). *Anal. Chem.* **2011**,83,3392-3397.
14. Labib, M.; Khan, N.; Ghobadloo, S.M.; Cheng, J.; Pezacki, J.P.; Berezovski, M.V. Three-mode electrochemical sensing of ultralow microRNA levels. *J. Am. Chem. Soc.* **2013**,135,3027-3038.
15. Li, M.; Cushing, S.K.; Zhang, J.; Suri, S.; Evans, R.; Petros, W.P.; Gibson, L.F.; Ma, D.; Liu, Y.; Wu, N. Three-dimensional hierarchical plasmonic nano-architecture enhanced surface-enhanced Raman scattering immunosensor for cancer biomarker detection in blood plasma. *ACS Nano* **2013**,7,4967-4976.
16. Wang, J.; Wu, L.; Ren, J.; Qu, X. Visualizing human telomerase activity with primer-modified Au nanoparticles. *Small* **2012**,8,259-264.
17. Mizusawa, K.; Takaoka, Y.; Hamachi, I. Specific Cell Surface Protein Imaging by Extended Self-Assembling Fluorescent Turn-on Nanoprobes. *J. Am. Chem. Soc.* **2012**,134,13386-13395.
18. Di Natale, C.; Macagnano, A.; Martinelli, E.; Paolesse, R.; D'Arcangelo, G.; Roscioni, C.; Finazzi-Agro, A.; D'Amico, A. Lung cancer identification by the analysis of breath by means of an array of non-selective gas sensors. *Biosens. Bioelectron.* **2003**,18,1209-1218.
19. Yarden Y, Sliwkowski MX. Untangling the ErbB signalling network. *Nat. Rev. Mol. Cell Biol.* **2001**,2,127-137.

20. G. Ferretti, A. Felici, P. Papaldo, A. Fabi and F. HER2/neu role in breast cancer: from a prognostic foe to a predictive friend. *Curr. Opin. Obstet. Gynecol.* **2007**,19,56-62.
21. Furrer, D.; Sanschagrín, F.; Jacob, S.; Diorio, C. Advantages and Disadvantages of Technologies for HER2 Testing in Breast Cancer Specimens. *Am. J. Clin. Pathol.* **2015**,144,686-703.
22. Poturnayová, A.; Dzubinova, L.; Burikova, M.; Bizik, Jozef.; Hianik, T. Detection of Breast Cancer Cells Using Acoustics Aptasensor Specific to HER2 Receptors. *Biosensors* **2019**, 9,72.
23. Adolphi, N.L.; Butler, K.; Lovato, D.M.; Tessier, T.E. Imaging of Her2-Targeted Magnetic Nanoparticles for Breast Cancer Detection: Comparison of SQUID-detected Magnetic Relaxometry and MRI. *Contrast Med. Mol. I.* **2012**,7,308-319.
24. Hathaway, H.J.; Butler, K.S.; Adolphi, N.L.; Lovato, D.M.; Belfon, R.; Fegan, D.; Monson, T.C.; Trujillo, J.E.; Bryant, H.C.; Huber, D.L.; Larson, R.S.; Flynn, E.R. Detection of breast cancer cells using targeted magnetic nanoparticles and ultra-sensitive magnetic field sensors. *Breast Cancer Res.* **2011**,13,R108.
25. Arkan, E.; Saber, R.; Karimi, Z.; Shamsipur, M. A novel antibody-antigen based impedimetric immunosensor for low level detection of HER2 in serum samples of breast cancer patients via modification of a gold nanoparticles decorated multiwall carbon nanotube-ionic liquid electrode. *Anal. Chim. Acta* **2015**,874,66-74.
26. Liu, G.Y.; Amro, N.A. Positioning protein molecules on surfaces: a nanoengineering approach to supramolecular chemistry. *Proc. Natl. Acad. Sci. U.S.A.* **2002**,99,5165-5170.
27. Chan, W.C.W.; Nie, S. Quantum dot bioconjugates for ultrasensitive nonisotopic detection. *Science* **1998**,281,2016-2018.
28. Phizicky, E.; Bastiaens, P.I.; Zhu, H.; Snyder, M.; Fields, S. Protein analysis on a proteomic scale. *Nature* **2003**,422,208-215.
29. Sunna, A.; Chi, F.; Bergquist, P.L. A linker peptide with high affinity towards silica-containing materials. *N. Biotechnol.* **2013**,30,485-492.
30. Pacheco, J.P.G.; Rebelo, P.; Freitas, M.; Nouws, H.P.A.; Delerue-Matos, C. Breast Cancer Biomarker (Her2-Ecd) Detection Using a Molecularly Imprinted Electrochemical Sensor. *Sens. Actuators B Chem.* **2018**,273,1008-1014.



31. Zhou, W.; Xu, F.; Li, D.; Chen, Y. Improved Detection of HER2 by a Quasi-Targeted Proteomics Approach Using Aptamer–Peptide Probe and Liquid Chromatography–Tandem Mass Spectrometry. *Clin. Chem.* **2018**, *64*, 526-535.
32. Dale, P.S.; Gohring, J.T.; Fan, X. (2010). Detection of the HER2/neu Protein in Serological Samples Using a Novel Optofluidic Ring Resonator Biosensor. *J. Sur. Res.* **2009**, *158*, 379-380.

## **Chapter 5**

### Summary and future perspectives

In this thesis, a comprehensive study of the binding mechanism of the bifunctional fusion protein linker-protein G (LPG) is presented for the first time. The study involved the use of several biophysical techniques to quantify the binding of LPG to a silica-based substrate. These techniques were also used to investigate the effect of the linker portion of the fusion protein (LPG) on the antibody-binding function and stability of the parent protein G (PG). The contribution of linker multimerization was studied using several truncated derivatives of LPG. Further investigation to determine the contribution of the linker length rather than its multimerization was conducted after partial replacement of the linker region with a synthetic glycine-rich sequence.

The study mentioned in the thesis can only be applied to silica-based materials, since SBPs that bind to a similar class of materials usually display similar amino acid compositions. This is based on the fact that the chemical groups present in the amino acid sequence of an SBP mediates its binding to a particular material surface. However, the exact amino acid sequence is more important than the amino acid composition in defining the binding avidity of an entire peptide to a particular material.

**Chapter 1** sets the scene by providing an up-to-date review of existing experimental and theoretical tools as well as strategies for the in-depth analysis of solid-binding peptides (SBPs) and their binding interactions. The review first introduces the various non-covalent interactions and structural conformations responsible for the strong binding of SBPs onto the solid surfaces. It also highlights the ineffectiveness of screening methods towards giving information about binding interactions. A closer examination was provided of the different biophysical characterization techniques (experimental approach) currently available to study and SBP-surface interactions. Also, the use of molecular modelling and computer simulation (theoretical approach) to predict SBPs binding interaction was discussed. The advantages and the challenges faced by both experimental and theoretical approaches were highlighted. Lastly, the review presents selected functional applications of SBPs in the field of biosensing devices for the detection of pathogens and dangerous chemical analytes like explosives.

The orientation of a biomolecule is important in order to conserve its bioactivity. In **Chapter 2**, we studied the binding mechanism of the bifunctional fusion protein linker-protein G (LPG). Several of the techniques introduced in **Chapter 1** were applied to

characterize the binding mechanism of LPG to silica. The results obtained highlighted the advantage of LPG-mediated affinity conjugation over traditional chemical conjugation of antibodies onto solid surfaces. The results also confirmed an end-on orientation of LPG onto silica surface which provides an efficient antibody orientation as opposed to chemisorption where the antibodies attain random orientation to the surface of silica. One of the major drawbacks of chemisorption of biomolecules, including antibodies, is the potential attachment of biomolecules in a random orientation, which might limit or cause complete loss of the protein's biological function (1). The biophysical studies also confirmed that the linker region of LPG had no effect on the chemical and structural integrity of the protein G partner fusion protein.

In **Chapter 3**, we aimed to study the effect of two individual structural parameters on the binding affinity and binding strength of LPG to silica. In several SBPs multimerization has been reported the improved affinity and selectivity of the SBP to its substrate (2,3). Multimerization can be achieved by the sequential attachment of the original sequence (i.e. simple tandem repeat of the peptide sequence). Using a set of truncated derivatives of LPG, initial results from quartz crystal microbalance with dissipation monitoring (QCM-D) indicated that linker multimerization resulted in a strong silica binding and that the binding increased with increase in the number of peptide-repeats. Although these results aligned well with some of the previous studies that showed improved binding upon SBP multimerization (2,3), it remained unclear whether the linker sequence multimerization or the space it occupies (length) was the important factor for silica binding. Accordingly, to answer this question, a derivative was designed in which three of the original linker repeats of LPG were substituted by a synthetic poly-glycine-rich spacer, (GGGGS)<sub>12</sub>. Data obtained with the Link1X-(GGGGS)<sub>12</sub>-PG derivative pointed towards the linker length rather than linker multimerization as the main structural factor affecting the binding strength of LPG to silica. Thus, based on the current data available and the results obtained in this study, there is no general trend for increased binding strength as a result of SBP multimerization. While in some reports multimerization increased binding affinity, in others the affinity was reduced. This effect was attributed to the conformational changes between the single and the multiple peptide repeats (2,4).

In both, **Chapter 2** and **Chapter 3**, SPR and QCM-D were the two most important techniques utilized to quantify the binding of LPG and its truncated derivatives to the silica-

surface. These techniques were also used to determine the binding orientation and the effects of the linker region on the antibody-binding function of the partner protein G. Interestingly, SPR has been repeatedly utilized to study SBP-solid interactions (5-11). Also, the Langmuir 1:1 binding model is the primary fitting algorithm used to extract kinetic parameters of binding (12). QCM-D measurements can be difficult when performed at low peptide concentration, as was in our case, the lower three concentrations for 1xLPG and 2xLPG did not give any measurable binding response.

Molecular conformation also plays an important role in solid-binding. The effect of molecular conformations (e.g., cyclic and linear) on the adsorption behavior of gold-binding peptides has showed that different molecular structures, lead to differences in their gold-binding affinities (13-15). Looking forward it would be interesting to assess whether cyclic and linear molecular conformation of 4- and linker repeats of LPG show similar effects.

Future work will require the proper characterization of Link1X(GGGGS)<sub>12</sub>-PG using the various biophysical techniques used during the course of this project. Unfortunately, this was not possible due to the time constraints of this 3-year PhD project. Qualitative data along with the structural analysis will provide a deeper insight into the relationship between silica-binding, linker multimerization and minimum linker length requirement. In this context, it would be also interesting to design and study a truncated derivative with a single original linker sequence positioned in the middle of two adjacent (GGGGS)<sub>6</sub> synthetic linkers [(GGGGS)<sub>6</sub>-Link1X-(GGGGS)<sub>6</sub>-PG].

While hydroxyl-containing residues, like serine are commonly found in zeolite-binding and other silica-binding peptides, both glycine and serine adsorb to zeolites (16,17). Because of their small size, glycine and serine help maintaining the linker's stability in aqueous solution by forming hydrogen bonds. Glycine has no side chain and thus, also contribute towards the increasing conformational flexibility of the main peptide chain (18). Based on these information, future experiments should aim at designing a derivative in which the complete 4- linker repeats of LPG are fully substitute by a synthetic (GGGGS)<sub>n</sub> linker. This full linker substitution by a (GGGGS)<sub>n</sub> linker will rule out any potential binding contribution from the glycine and serine. If no considerable binding contribution would be attributed to the (GGGGS)<sub>n</sub> linker, this will provide conclusive evidence that a minimum of one original linker sequence (in LPG) is required for efficient binding to silica as long as the final length of the deleted 3-repeats is covered by the (GGGGS)<sub>12</sub> linker substitute.

Theoretical approaches which include molecular modelling and computer simulation have been used to predict SBPs binding interaction. Although, we initially envisaged the use of this theoretical approach with our collaborator Prof. Tiffany Walsh at Deakin University, Geelong, Australia, this was not further pursued due to the computational challenge to run simulations with a longer peptide like ours. Usually the maximum peptide sequence which can be effectively modelled contains 12-14 amino acids.

In **Chapter 4**, we provide a preliminary proof-application for the potential use of the LPG technology for in nanomedicine applications. The fact that LPG mediated the proper orientation of antibodies on silica surface was used for the detection of HER2 cancer biomarker in different biological fluids. The preliminary data suggest the effective detection of the biomarker with minimal interference or effect on the stability of the immobilized LPG-antibody complex in the presence of urine and serum. This initial but promising results open the door for future studies towards the incorporation of the LPG technology in biosensors for disease biomarker detection or in the development of improved targeted drug delivery system.

Overall, this work shows the advantage of a solid-binding peptide approach for a fast, robust and facile immobilization of biomolecules onto solid surfaces without compromising their biological function and without the need for harsh chemicals and surface preparation technologies. In this work, we thoroughly investigated the binding mechanism LPG onto silica and compared its properties against the parent protein PG. Different biophysical techniques were used to quantitatively characterize the silica-binding mechanism and to show its advantages over the chemical-based protein conjugation. From our results, we concluded that: (a) the silica-specific linker region present in LPG is the sole factor responsible for a strong binding to silica; (b) the linker does not have any effect on the structural and chemical properties of PG, and thus preserves its antibody-binding function; (c) the linker region of LPG binds to silica in an oriented manner and thus effectively anchoring the antibody via the Fc region maximizing the available binding sites for the antigen; (d) the overall length rather than multimerization appears to be the prominent factor responsible for a strong binding of LPG to silica.

This work will provide further insights for the molecular tailoring of SBPs for a wide range of applications in the ever-growing field of nanobiotechnology and biomedicine.



## References

1. Phizicky, E.; Bastiaens, P.I.; Zhu, H.; Snyder, M.; Fields, S. Protein Analysis on a proteomic scale. *Nature* **2003**, *422*, 208-215.
2. Seker, O.U.S.; Wilson, B.; Kulp, J.L.; Evans, J.S.; Tamerler, C.; Sarikaya, M. Thermodynamics of Engineered Gold Binding Peptides: Establishing the Structure–Activity Relationships. *Biomacromolecules* **2014**, *15*, 2369-2377.
3. Cho, N.; Cheong, T.; Min, J.H.; Wu, J.H.; Lee S.J.; Kim, D.; Yang, J.; Kim, S.; Kim, Y.K.; Seong, S. A multifunctional core-shell nanoparticle for dendritic cell-based cancer immunotherapy. *Nat. Nanotechnol.* **2011**, *6*, 675-682.
4. Seker, U.O.S.; Wilson, B.; Sahin, D.; Tamerler, C.; Sarikaya, M. Quantitative affinity of genetically engineered repeating polypeptides to inorganic surfaces. *Biomacromolecules* **2009**, *10*, 250-257.
5. Tamerler, C.; Oren, E. E.; Duman, M.; Venkatasubramanian, E.; Sarikaya, M. Adsorption kinetics of an engineered gold binding peptide by surface plasmon resonance spectroscopy and a quartz crystal microbalance. *Langmuir* **2006**, *22*, 7712-7718.
6. Hnilova, M.; Oren, E. E.; Seker, U. O. S.; Wilson, B. R.; Collino, S.; Evans, J. S.; Tamerler, C.; Sarikaya, M. Effect of molecular conformations on the adsorption behavior of gold-binding peptides. *Langmuir* **2008**, *24*, 12440-12445.
7. Seker, U. O. S.; Wilson, B.; Kulp, J. L.; Evans, J. S.; Tamerler, C.; Sarikaya, M. Thermodynamics of engineered gold binding peptides: Establishing the structure-activity relationships. *Biomacromolecules* **2014**, *15*, 2369-2377.
8. Seker, U. O. S.; Wilson, B.; Dincer, S.; Kim, I. W.; Oren, E. E.; Evans, J. S.; Tamerler, C.; Sarikaya, M. Adsorption behavior of linear and cyclic genetically engineered platinum binding peptides. *Langmuir* **2007**, *23*, 7895-7900.
9. Seker, U. O. S.; Wilson, B.; Sahin, D.; Tamerler, C.; Sarikaya, M. Quantitative affinity of genetically engineered repeating polypeptides to inorganic surfaces. *Biomacromolecules* **2009**, *10*, 250-257.
10. So, C. R.; Tamerler, C.; Sarikaya, M. Adsorption, diffusion, and self-assembly of an engineered gold-binding peptide on au(111) investigated by atomic force microscopy. *Angew. Chem., Int. Ed.* **2009**, *48*, 5174-5177.

11. Coyle, B. L.; Rolandi, M.; Baneyx, F. Carbon-binding designer proteins that discriminate between sp<sup>2</sup>- and sp<sup>3</sup>-hybridized carbon surfaces. *Langmuir* **2013**,*29*,4839-4846.
12. Karlsson, R.; Fält, A. Experimental design for kinetic analysis of protein-protein interactions with surface plasmon resonance biosensors. *J. Immunol. Methods* **1997**,*200*,121-133.
13. Hnilova, M.; Oren, E.E.; Seker, U.O.S.; Wilson, B.R.; Collino, S.; Evans, J.S.; Tamerler, C.; Sarikaya, M. Effect of molecular conformation on the adsorption behavior of gold-binding peptides. *Langmuir* **2008**,*24*,12440-12445.
14. So, C.R.; Tamerler, C.; Sarikaya, M. Adsorption, diffusion, and self-assembly of an engineered gold-binding peptide on Au (111) investigated by atomic force microscopy. *Angew. Chem. Int. Ed. Engl.* **2009**,*48*,5174-5177.
15. Corni, S.; Hnilova, M.; Tamerler, C.; Sarikaya, M. Conformational behaviour of genetically-engineered dodecapeptides as a determinant of binding affinity for gold. *J. Phys. Chem. C* **2013**,*117*,16990-17003.
16. Naik, R. R., Brott, L. L., Clarson, S. J., & Stone, M. O. Silica-precipitating peptides isolated from a combinatorial phage display peptide library. *J. Nanosci. Nanotechnol.* **2002**,*2*,95-100.
17. Sarikaya, M., Tamerler, C., Jen, A. K., Schulten, K., & Baneyx, F. Molecular biomimetics: nanotechnology through biology. *Nat. Mater.* **2003**,*2*,577-585.
18. Oren, E.E.; Tamerler, C.; Sahin, D.; Hnilova, M.; Seker, U.O.S.; Sarikaya, M.; Samudrala, M. A novel knowledge-based approach to design inorganic-binding peptides. *Bioinformatics* **2007**,*23*,2816-2822.

Pages 101-109 ("Biosafety Application") of this thesis have been removed as they contain sensitive material.

**OFFICE OF THE DEPUTY VICE-CHANCELLOR (RESEARCH)**  
**Research Office | Biosafety**



**MACQUARIE**  
**University**  
SYDNEY • AUSTRALIA

23/10/2019

Dear Anwar ,

**Re: " Stability of Antibody Binding Proteins" - 5201958279970**

Your notification application has been documented effective Biosafety Application Approval Date. The risk assessment portion of this project is valid for 5 years.

Please ensure a hard copy of this project is made available in your laboratory for reference.

A final report for this project will be due by 23/10/2024 .

Kind Regards  
Claudia Huang

Biosafety Secretariat - Research Services Level 3  
Research Hub, Building C5C East  
Macquarie University, NSW 2109 Australia  
T: +61 2 9850 4063  
E: biosafety@mq.edu.au  
W: mq.edu.au/research

Level 3, Research Hub T: +61 (2) 9850 4063  
Building C5C East  
Macquarie University  
NSW 2109 Australia

E: biosafety@mq.edu.au  
mq.edu.au/research

ABN 90 952 801 237 | CRICOS Provider 00002J